이 학 석 사 학 위 논 문

Design and Synthesis of New Benzimidazole-Based Fluorophores: Tunable Emission over a Wide Spectral Range in Solution and Solid States

용액과 고체상에서 다양한 범위의 발광성을 갖는

벤지미다졸 기반 형광체의 설계와 합성

2016년 8월

서울대학교 대학원

화학부 무기화학 전공

이 보 란

Design and Synthesis of New Benzimidazole-Based Fluorophores: Tunable Emission over a Wide Spectral Range in Solution and Solid States

By

Boran Lee

Supervisor: Prof. Dongwhan Lee

A Thesis for the M.S. Degree

in Inorganic Chemistry

Department of Chemistry

Graduate School

Seoul National University

August, 2016

Abstract

Design and Synthesis of New Benzimidazole-Based Fluorophores: Tunable Emission over a Wide Spectral Range in Solution and Solid States

Boran Lee

Inorganic Chemistry in Department of Chemistry

The Graduate School

Seoul National University

A new class of fluorophores have been developed that cover a wide spectral range in emission and display solid-state fluorescence. As light-emitters and signal-transducing components, fluorescent molecules are finding useful applications in various fields including materials science and biomedical science. Therefore, the development of fluorescent materials having tunable emissive and physical properties is a task of significant importance. In this Thesis is described the design and development of new "T-shaped" benzimidazole fluorophores. In this system, a benzimidazole core is functionalized with two π-conjugated motifs that profoundly impact the photophysical property of the fluorophore. Specifically, one "π-strand" is embedded with chelating motifs for sequential binding of $\{BF_2\}^+$ units, whereas the other π-strand serves as an electronic controller group. Systematic structural variations of those components result in changes in the emission wavelength and quantum yield. Since such structural modifications are designed to take place at the very last steps of synthesis, one could

readily broaden the substrate scope from common synthetic intermediates. We found that the emission spectra of select compounds cover a full range of visible light in both solution and solid state. Intriguingly, most of the compounds are fluorescent even in the solid state despite their nearly planar structures, which is crucial for applications in electroluminescent devices such as OLEDs. These appealing features, including ease of synthesis, emission wavelength tuning, and solid-state fluorescence, promise the use of this modularly accessible fluorophores in various areas, ranging from chemical sensors to light-emitting devices.

Keywords: fluorescent benzimidazole derivatives • tunable emission • wide spectral range • modular synthesis • structure–property relationship • solid-state fluorescence

***Student Number*:** 2014-20309

Table of Contents

I. Introduction

Fluorescent dyes re-emit part of the energies that they have absorbed. Certain fluorophores have drawn a great attention for decades since they usually provide high sensitivity optical response, thereby lowering the detection limit.[1] Consequently, fluorescent molecules are utilized extensively as bioprobes,[2] indicators for metal ions,[3] pH sensors,[2c, 4] or materials for thin layer displays.[5] As summarized in Scheme 1, typical fluorophores have extended π-conjugation supported by rigid molecular backbone. Structural rigidity often contributes to high fluorescence quantum yields (Φ_F). Conformationally rigid molecules are less likely to dissipate the excitation energy by internal vibration/rotation, which is one the most dominant pathways for non-radiative decay.

Scheme 1. Chemical structures of representative fluorophores.

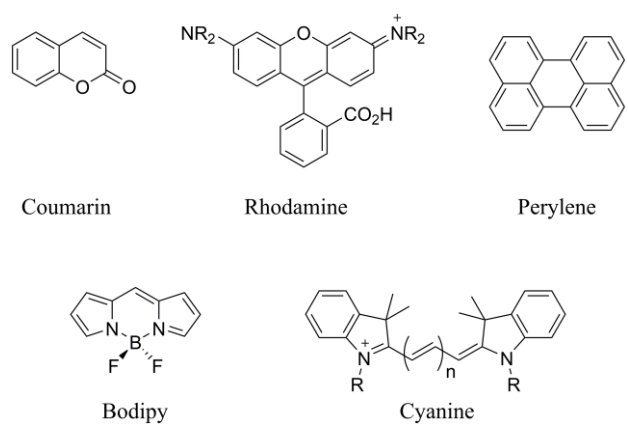

This interpretation is widely accepted, and *structural rigidification* has been exploited to produce brighter materials and/or to realize fluorescence "turn-on" sensors. For example, Das *et al*. reported an azine-based receptor **L1** which selectively

binds Hg^{2+} ion to elicit a turn-on fluorescence response (Scheme 2(a)).[6] This remarkable change in fluorescence might arise from the inhibition of two non-radiative decay processes, i.e. C=N isomerization in the excited state, and photo-induced electron transfer (PET). In a similar manner, two analogues of green fluorescent protein (GFP) chromophores were synthesized from non-fluorescent compounds, **L2** and **L3** (Scheme 2(b)).[7] As shown in Scheme 2, compounds that are either reversibly (**L2-Zn**) or irreversibly (**L3-BF_2**) locked exhibit intense fluorescence and high photo-acidity. In both cases, chelating units were employed to restrict molecular motions. In fact, chelation of difluoroboryl (= BF_2) units is one of the most straightforward strategies to transform non-fluorescent or weakly fluorescent *N*,*N*-, *N*,*O*-bidentate ligands into highly emissive adducts.

In addition to the brightness, emission wavelength is another essential consideration for fluorophores. For biological applications such as *in vivo* analysis and imaging, fluorophores that emit red or near-infrared (NIR) light are preferred because of their minimal photodamage.[8] For organic light emitting devices (OLEDs), however, emission at various wavelengths from deep blue to near-infrared is desired.[5] In this regard, fluorophores having tunable and predictable emission wavelengths are important functional components in molecular devices and materials. For designer fluorophores, a detailed understanding of structure–property relationships should form the basis of rational design to control emissive properties. For example, BODIPY[9] is one of the most extensively studied class of fluorophores displaying rich structure-dependent photophysics, but their synthetic modifications are often time-consuming and cumbersome. This is because substituents to control the electronic/structural properties are introduced at early stages of the synthesis, so that

each derivative needs to be produced in essentially parallel fashion by following lengthy linear synthetic sequences. As such, there is a growing need to invent new fluorogenic motifs that are amenable for last-stage synthetic modifications for diversity-oriented synthesis.

Scheme 2. Select examples of structural rigidification strategies to achieve high efficiency in fluorescence emission.

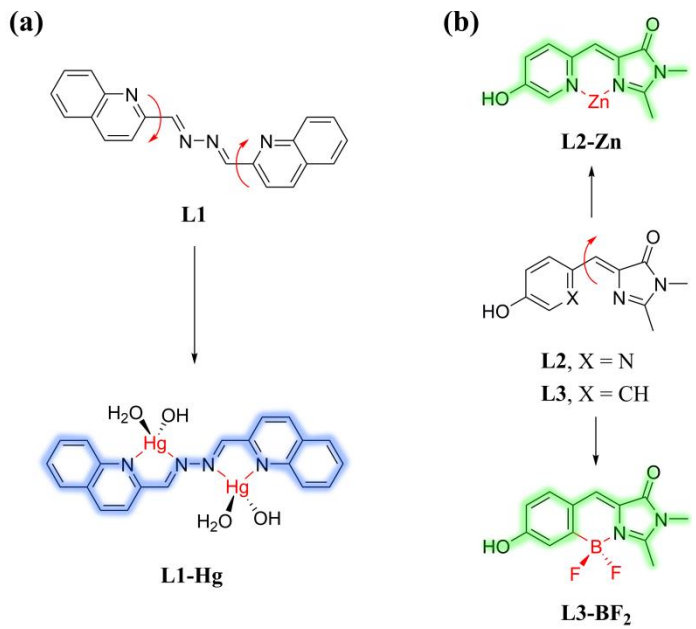

Recently, Park (Figure 1(a))[10] and You (Figure 1(b))[8b] disclosed new organic fluorophores, the photophysical properties of which can readily be controlled by substituents that are introduced in the last step of synthesis via direct C–H activation. In such systems, substituents significantly affect the intramolecular charge transfer (ICT). It is noteworthy that they have prepared a collection of fluorophores having tunable emission properties over a wide spectral range and such properties

could be rationalized by the molecular structure. Compared to trial-and-error approach, this strategy is both atom-economical and time-saving.

Figure 1. Design and construction of biaryl fluorescent skeletons for last-stage synthetic modification to control photophysical properties.

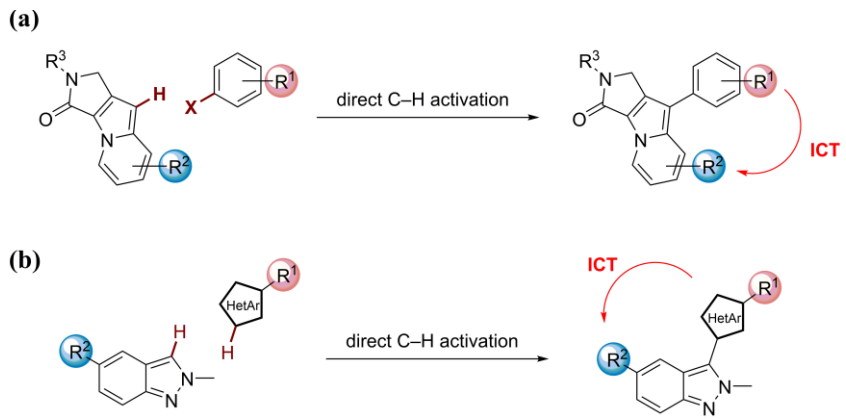

In addition, design and synthesis of organic materials that are highly emissive even in the solid state is a fundamental requirement for applications in optoelectronic devices and/or organic lasers.[11] Furthermore, those compounds are also useful in molecular sensing and imaging in living cells.[2b] Aggregation-induced emission (AIE), pioneered and refined by Tang and others, is an enhancement in fluorescence intensity upon molecular self-association.[12] AIE is becoming a powerful strategy to endow molecules with solid-state fluorescence. In this strategy, certain AIE-inducing structural motifs, such as tetraphenylethylene (TPE), are introduced to a molecule.[12a] Although this approach could be effective, it usually requires additional structural components that should have little impact on the inherent photophysical properties of the chromophore.

In this work, we have designed and synthesized benzimidazole-based fluorophores having tunable photophysical properties. Either through structural rigidification or functional group modification on a homologous set of molecules, both the fluorescence quantum yields and emission wavelengths could be controlled. With electron-donating substituents, bathochromic shifts in the emission band was observed to allow for a full coverage of the visible light region. By taking highly modular synthetic routes, we were able to construct a library of new fluorophores for which structural variations take place in the last stage of synthesis. It is noteworthy these molecules adopt essentially planar structures but display solid-state fluorescence. Results from X-ray crystallographic analysis offer a plausible explanation for this rather unusual behavior. Specifically, T-shaped molecules possessing the dipole moment lying along the "vertical axis" (of the T shape) tend to aggregate without any close π– π stacking interactions.

II. Results and Discussion

II.1. Design and Synthesis of Benzimidazole-Based Fluorophores

In order to realize high-efficiency and tunability in emission, we have designed a series of T-shaped fluorophores that are based on the benzimidazole motif. These new fluorophores are comprised of three parts: a benzimidazole core and two π-conjugated substituents that are arranged to define a T-shaped molecular architecture (Figure 2). A high modularity in our synthesis (vide infra) allows for the introduction of different functionalized π-motifs to tune the structural and photophysical properties in an orthogonal fashion. One "π-strand" in such T-shaped molecule (red part in Figure 2) was embedded with chelating motifs for sequential binding of BF_2 units to rigidify the (otherwise freely rotating) aryl–pyridyl junctions. The other (blue part in Figure 2) π-strand was introduced to modulate the photophysical properties by electronic control. In our design, such modifications can be executed in an essentially orthogonal fashion, thereby expanding the structural and functional diversity in a straightforward manner. As discussed below, we have found that such structural modifications indeed resulted in dramatic changes in fluorescence emission and other physical properties.

As a π-extended derivative of imidazole, benzimidazole is a prominent heterocyclic aromatic motif that is frequently found in nature as well as in many biologically-active synthetic molecules.[13] Due to the importance of benzimidazoles, many synthetic routes have previously been developed. Since benzimidazole has two types of nitrogen atoms (i.e. sp^3–hybridized amine and sp^2-hybridized imine) that are different in terms of reactivity, chemical reactions could take place at each position selectively.

Figure 2. (a) Chemical structures of the T-shaped fluorophores built on the benzimidazole platform. (b) Sequential and selective binding of BF_2 units.

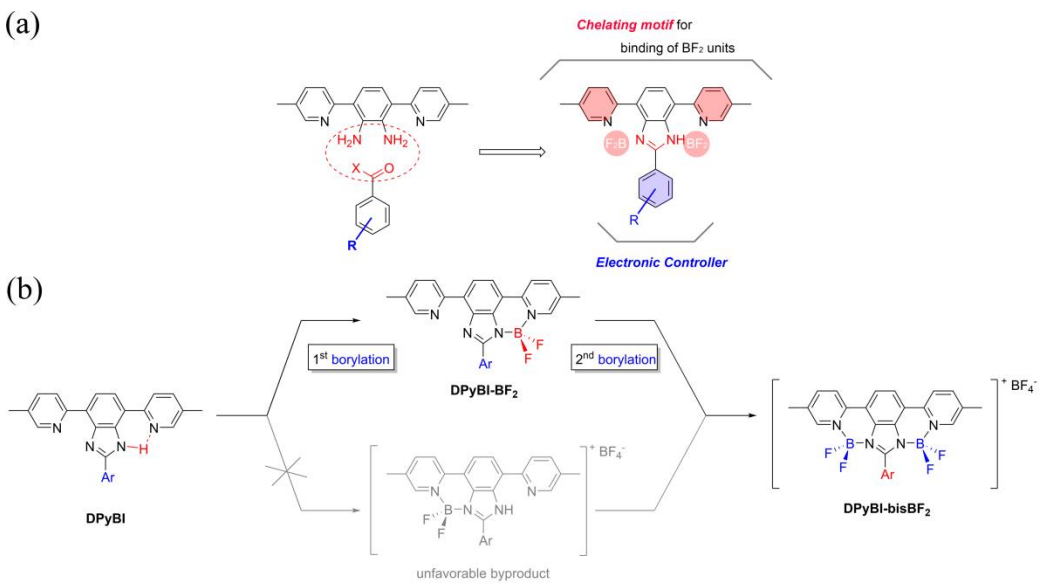

In our structure design, we wished to install two 2-pyridyl units at the 4- and 7-position of the parent benzimidazole system (Figure 2(b)). Through intramolecular hydrogen bonding, such benzimidazole-pyridyl unit would be preorganized. Moreover, the resulting $N_{\text{imidazolyl}}$, N_{pyridyl}-bidentate motif should define a six-membered chelating to capture a BF_2 unit. Since this binding process entails deprotonation of the amine N–H group of the benzimidazole, the resulting BF_2-adduct should be charge-neutral (Figure 2(b)). On the other hand, binding of the BF_2 fragment would be unfavorable for the imine nitrogen side of the benzimidazole since the resulting adduct has two sp^2-hybridized nitrogen atoms as the ligand donor to produce an overall positively-charged boron complex.

By a combination of spectroscopic and X-ray crystallographic studies (vide infra), we have confirmed that the first binding event indeed occurs at "right side" (i.e.

$N_{\text{imidazolyl amine}}$, N_{pyridyl}-bidentate), followed by the subsequent binding at the "left side" (i.e. $N_{\text{imidazolyl imine}}$, N_{pyridyl}-bidentate). Moreover, the resulting mono- and bis-BF_2 adducts (**DPyBI-BF_2** and **DPyBI-bisBF_2**, respectively) exhibited distinctively different physical properties, especially solubility and polarity, which facilitated their purification and characterization. Introduction of BF_2 units has profound impacts on the photophysical properties by changing both the positioning and energy levels of the HOMO and LUMO as well as by rigidifying the structure.

A variation of the electronic nature of the aryl substituent on the 2-position of benzimidazole core is also anticipated to lead to noticeable changes in the emissive properties. Aryl group is introduced at the ring-closing step, so that a broad range of aryl aldehydes and carboxylic acids can be employed to extend the substrate scope. Moreover, aryl aldehydes having various substituents are either commercially available or can readily be prepared.

Scheme 3 illustrates synthetic routes for the benzimidazole-based fluorophores. In this strategy, structural modifications to obtain compounds **DPyBI**, **DPyBI-BF_2**, and **DPyBI-bisBF_2** are designed to take place at the very last steps of the synthesis. Therefore, one could readily broaden the substrate scope from common synthetic intermediates **4**, which was synthesized in a three-step sequence from commercially available 2,1,3-benzothiadiazole **1**. In the first step, **1** was doubly brominated in the presence of Br_2 to generate compound **2**.[14] The horizontal axis of the T-shaped molecule was established via Stille coupling between **2** and 2-(tributylstannyl)-5-methylpyridine, which was freshly prepared before use.[15] The subsequent step was to liberate the free amine groups by reduction of **3** to produce **4**.[16] Under optimized conditions, gram-scale synthesis of **4** was achieved in high

yields. This compound is benchtop-stable, and can be stored in air for more than three months.

With large quantities of **4** in hand, we proceed to build a library of **DPyBI** derivatives by either oxidative condensation with various aldehydes[17] or by simple condensation with carboxylic acid.[18] Overall, these reactions have a high degree of tolerance to a wide range of functional groups, including both electron-withdrawing and electron-donating groups, hydroxyl groups, and pyridine rings (Scheme 3(b)). The substrate scope could be further extended by the subsequent modification, by which one or twoBF_2 units were installed to generate **DPyBI-BF_2** or **DPyBI-bisBF_2**, respectively.

Scheme 3. (a) Synthetic routes to DPyBI and its derivatives, and (b) substrate scope.

(a)

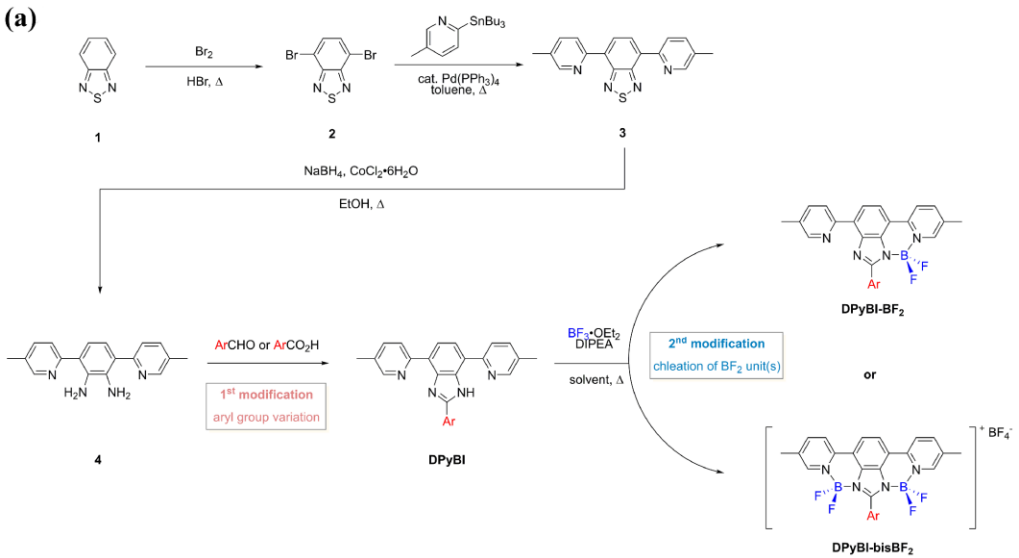

(b)

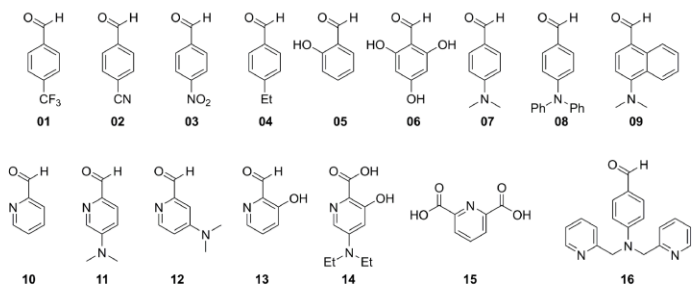

II.2. X-ray Crystallographic Studies

The chemical structures of **DPyBI-11**, **DPyBI-10-BF_2** and **DPyBI-10-bisBF_2** were unambiguously confirmed by single-crystal X-ray crystallographic analysis. Single crystals of **DPyBI-11** were obtained by slow evaporation of a dichloromethane solution of this material. Single crystals of **DPyBI-10-BF_2** suitable for X-ray analysis were obtained by vapor diffusion of Et_2O into a dichloromethane solution of this material. Single crystals of **DPyBI-10-bisBF_2** were obtained serendipitously, during washing the **DPyBI-10-bisBF_2** reaction mixtures with various solvents including hot dichloroethane, hot diethyl ether, and THF. Due to the low quality of diffraction data (i.e. poor completeness), detailed discussion cannot be made, but our results fully confirmed the chemical connectivity.

In all cases, the horizontal π-strand defined by the pyridine-benzimidazole-pyridine triad, adopts an essentially co-planar arrangement. For compounds **DPyBI-11** and **DPyBI-10-BF_2**, the pyridine ring that is not conformationally rigidified by either intramolecular hydrogen bond or BF_2 binding is slightly deviated from the perfect planarity, but with relatively small torsional angles of 12.1 ^{o} and 12.8 ^{o}, respectively. The six fused rings of **DPyBI-10-bisBF_2**, including the four rings from the triad and the additional two rings formed by BF_2 binding, lie on the same plane with little deviation of two boron atoms from the plane. With an increasing number of BF_2 units introduced to the chelating pockets, the imidazole-extended aryl group is tilted away from co-planarity. This is due to the steric hindrance imposed by the adjacent fluorine atoms.

Figure 3. (a) Face-on view, and (b) edge-on view ORTEP diagram of **DPyBI-11** with thermal ellipsoids at 50% probability, where N is blue. (c) Chemical structure of **DPyBI-11**.

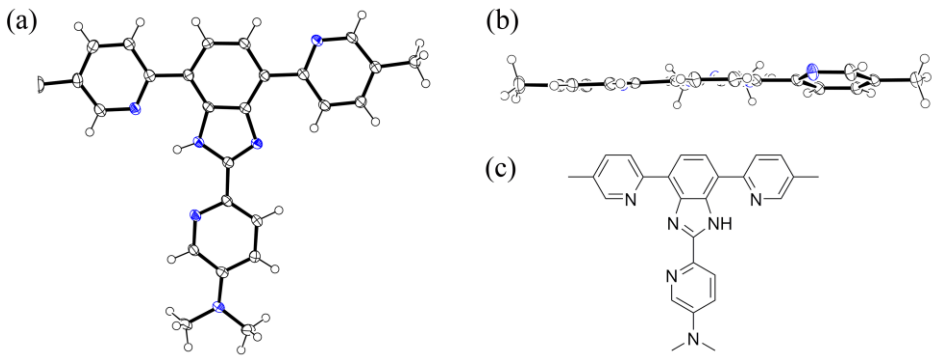

Figure 4. (a) Face-on view, and (b) edge-on view ORTEP diagram of **DPyBI-10-BF$_2$** with thermal ellipsoids at 50% probability, where N is blue, B is orange, and F is green. Two chemically equivalent but crystallographically independent molecules of DPyBI-10-BF2 were located in the asymmetric unit. Hydrogen atoms are omitted for clarity. (c) Chemical structure of **DPyBI-10-BF$_2$**.

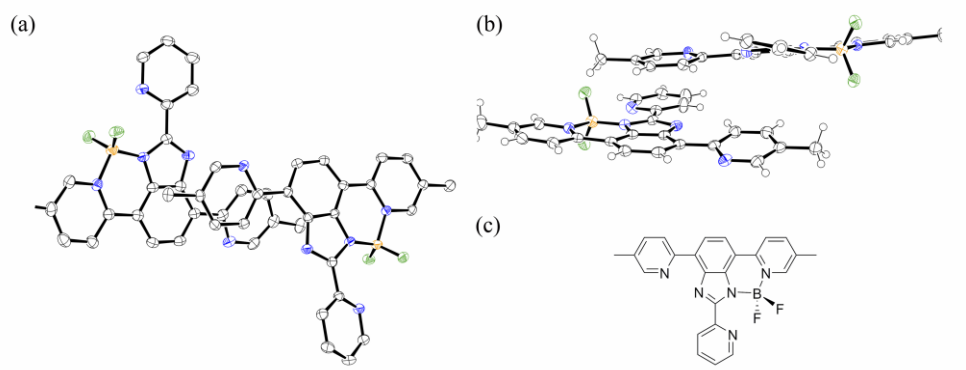

Figure 5. (a) Face-on view, and (b) edge-on view ORTEP diagram of **DPyBI-11-bisBF$_2$** with thermal ellipsoids at 50% probability, where N is blue, B is orange, and F is green. In (b), the BF_4^- counter anion has been omitted for clarity. Structural disorder exists for the imidazole-appended pyridyl group. (c) Chemical structure of **DPyBI-11-bisBF$_2$**.

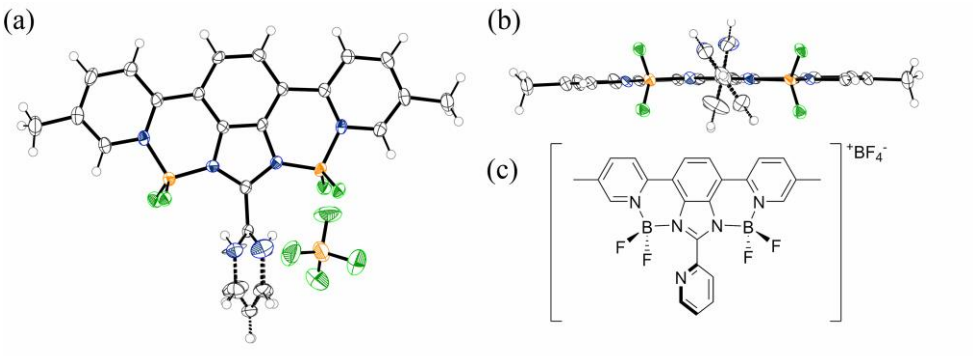

From the single-crystal diffraction data, we were able to extract valuable structural information on packing interactions in the solid-state. Single crystals of **DPyBI-11**, **DPyBI-10-BF$_2$**, and **DPyBI-10-bisBF$_2$** belong to the centrosymmetric space group of $P2_1/c$, $P\bar{1}$, and $P2_1/n$, respectively. After a careful inspection, we found that for each molecule there exists a counterpart that is aligned centrosymmetrically so that their inherent dipole moments are canceled out. At the same time, molecules tend to minimize void spaces. In order to satisfy such structural requirements, molecules need to adopt unique packing with no close π–π stacking. As a result, their inherent light-emitting properties are retained even in the solid-state.

Figure 6. (a) Crystal-packing pattern of **DPyBI-11** showing no π–π stacking between adjacent molecules. (b) A herringbone-type packing of **DPyBI-11**. Hydrogen atoms are omitted for clarity.

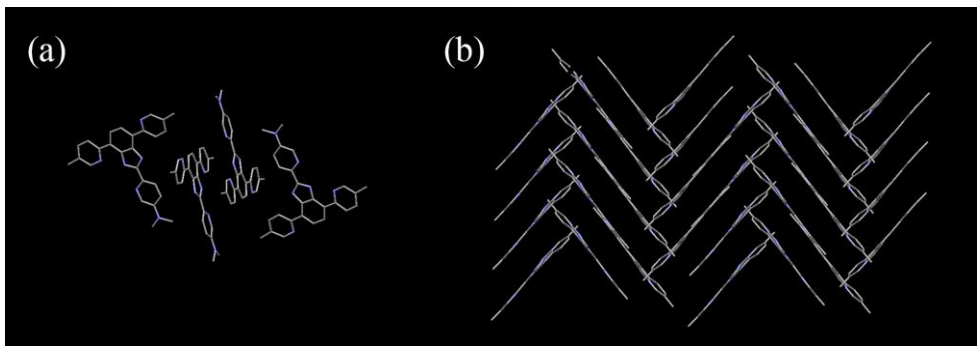

Figure 7. (a) Crystal-packing pattern of **DPyBI-10-BF_2** along the *a*-axis shows no stacking of the aromatic rings between adjacent interlayered molecules. (b) Packing diagram of **DPyBI-10-BF_2** along the *b*-axis. Hydrogen atoms are omitted for clarity.

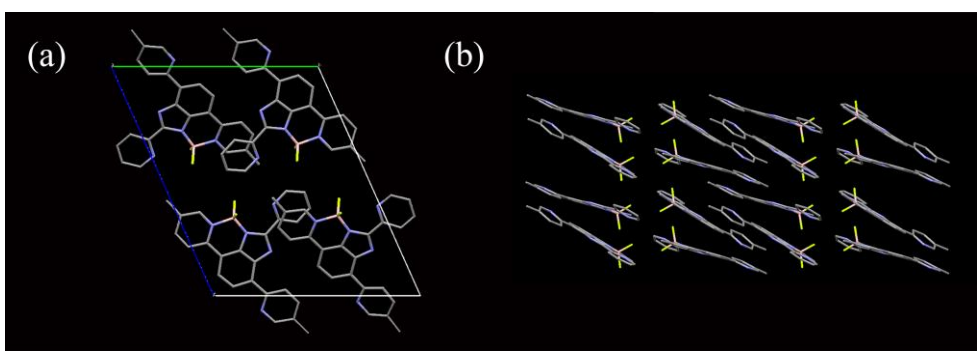

Figure 8. (a) Crystal-packing pattern of **DPyBI-10-bisBF$_2$** shows no stacking of the aromatic rings between adjacent interlayered molecules. (b) A zig-zag packing of **DPyBI-10-BF$_2$**.

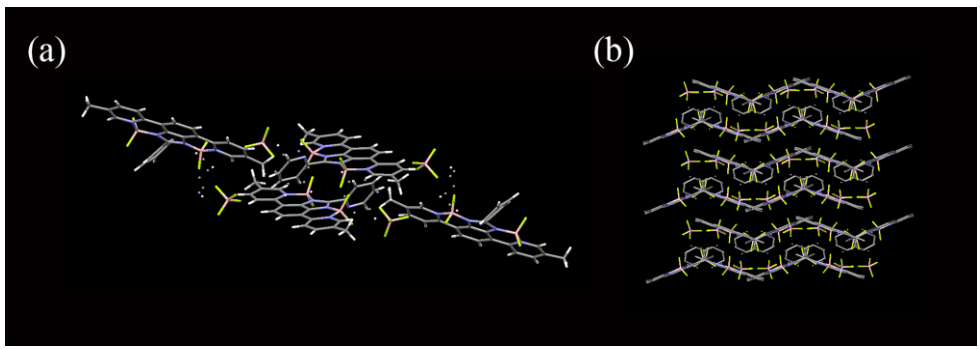

II.3. Photophysical Properties

II.3.1. Effects of BF_2 Chelation

We first investigated photophysical consequences of borylation, in which an increasing number of BF_2 fragments were introduced in a sequential fashion to a common dipyridyl-benzimidazole platform. For a direct side-by-side comparison, the 2-pyridyl-functionalized **DPyBI-10** was chosen as the reference system. Its protonated form was also studied, in which intramolecular hydrogen bonds also function as a conformational lock (Scheme 4). Photophysical properties of **DPyBI-10**, **DPyBI-10-HCl**, **DPyBI-10-BF_2**, **DPyBI-10-bisBF_2** were determined in MeCN by UV-vis and fluorescence spectroscopy. During the measurements, the sample absorbance was maintained as 0.1 to directly compare the fluorescence efficiency.

Scheme 4. Systematic rigidification of the **DPyBI-10** π-conjugation by intramolecular hydrogen bond and sequential borylation.

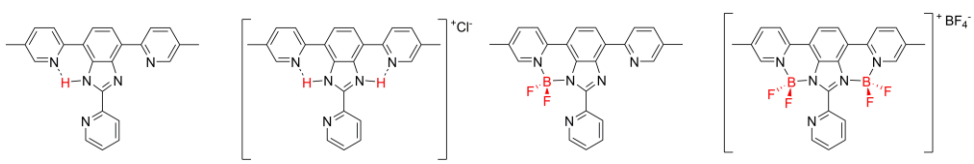

In terms of structural rigidity, the number of freely rotatable chemical bonds diminishes from left to right (Scheme 4), which is accompanied by an increase in fluorescence quantum yield and decrease in Stokes shift. It should also be noted that the BF_2 units would affect the electronic properties of compounds and accessibility of the ESIPT process. Upon photo-excitation of **DPyBI-10** or **DPyBI-10-HCl**, proton transfer could take place between the benzimidazole N–H group and the pyridine

nitrogen atom that form intramolecular hydrogen bond in the ground state (Scheme 4). Such process elicits structural rearrangement in the excited state, the geometry of which is significantly different from that of the ground state. As a result, an abnormally large Stokes shift is observed. In order for compound **DPyBI-10** to form boron complexes, deprotonation of the benzimidazole N–H is needed. Therefore, once borylation takes place, ESIPT process should not be observed. Moreover, the Lewis acidic BF_2 unit functions as a strong electron-withdrawing group, which indicates that the absorption and emission properties of the boron complexes would be quite different those of the free ligand.

The photophysical properties of **DPyBI-10** and its derivatives are summarized in Figure 9 and Table 1. First of all, an increase in the number of BF_2 units results in higher fluorescence quantum yields and smaller Stokes shifts. The shapes of the absorption/emission spectra are also dependent on the chemical structures. In the case of **DPyBI-10-bisBF$_2$**, the spectrum is sufficiently well-resolved to reveal vibronic features. In addition, dual fluorescence was observed for the protonated form of **DPyBI-10**. This dual emission might be explained by either excited-state intramolecular proton transfer (ESIPT) or ICT process.

In order to gain insights into this rather complicated phenomenon, we carried out frontier molecular orbital (FMO) analysis on the energy-minimized DFT models of **DPyBI-10** and its derivatives. As shown in Figure X, borylation results in the "relocation" of HOMO from the horizontal π-strand to the vertical π-strand. In **DPyBI-10-HCl**, HOMO is primarily localized over the horizontal π-strand, while LUMO is mostly localized on the vertical π-conjugation. This well-separated electronic structure suggests the possibility of ICT from HOMO to LUMO (Figure

9(b)). In contrast, the bis-BF_2 adduct has significantly different localization pattern of the HOMO and LUMO, along with the direction of the ICT process expected.

Figure 9. (a) Normalized UV–vis spectra (dashed lines) and fluorescence emission spectra (solid lines) in MeCN, *T* = 298 K. (b) HOMO (left) and LUMO (right) diagrams of each compound obtained from density functional theory (DFT) calculation at B3LYP/6-31G(d) level.

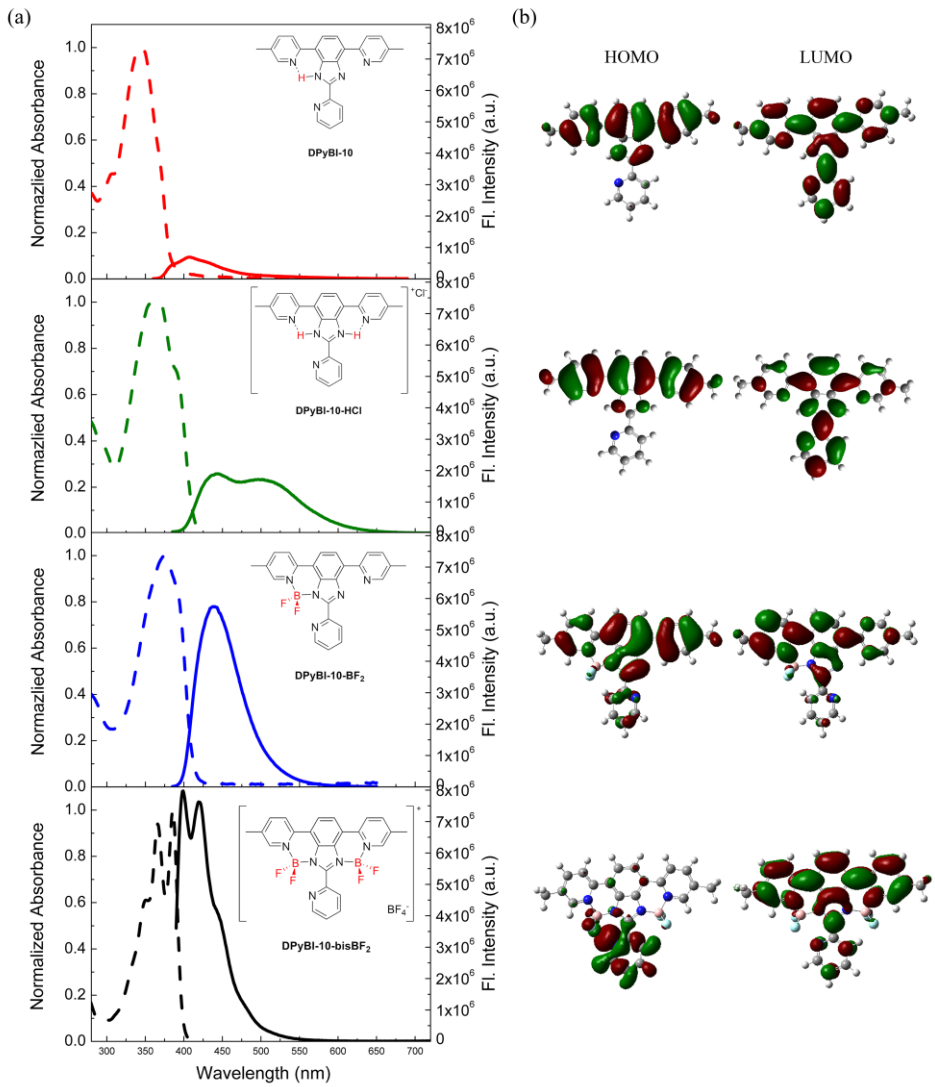

Table 1. Photophysical properties of **DPyBI-10** series. [a]Dual emission was observed for **DPyBI-10-HCl**. The value in the parentheses refers to local maximum emission wavelength. [b]Stokes shift calculated from local maximum emission wavelength.

Compound	$\lambda_{max, abs}$ (nm)	$\lambda_{max, em}$(nm)	Stokes shift (nm)	Φ_F (%)
DPyBI-10	350	408	58	10.4
DPyBI-10-HCl	375	442 (491)	67 (116)	18.2
DPyBI-10-BF2	375	437	62	77.0
DPyBI-10-bisBF2	385	399	14	84.6

Emission from ICT and ESIPT should respond sensitively to changes in solvent polarity. We thus conducted solvent-dependent measurements to probe the occurrence of CT- and/or ESIPT-type emission. The results revealed that the dual emission presumably arises from the ESIPT process. If the ICT process is responsible for the broad emission band at longer wavelength, it would be observed for **DPyBI-10-bisBF$_2$**; the spatial positioning of its HOMO and LUMO suggests that ICT process would take place with high probability. From these results, we tentatively conclude that structural modifications using the BF_2 motif fundamentally altered the photophysical properties of the molecule, including band shape, brightness, and maximum absorption/emission wavelength by (i) changing the structural rigidity and (ii) functioning as an electron-withdrawing substituent.

Figure 10. Solvent-dependent spectral changes of **DPyBI-10** and its derivatives at T = 298 K; (a) top: **DPyBI-10** (λ_{exc} = 340 nm in EtOH, 350 nm in MeCN or EA, 375 nm in DCM or chloroform), bottom: **DPyBI-10-HCl** (λ_{exc} = 340 nm in EtOH, 350 nm in EA, 375 nm in MeCN or chloroform, 380 nm in DCM); (b) top: **DPyBI-10-BF$_2$** (λ_{exc} = 375 nm in EtOH or MeCN, 380 nm in DCM or EA, 390 nm in chloroform), bottom: **DPyBI-10-bisBF$_2$** (λ_{exc} = 385 nm in EtOH or MeCN, 390 nm in DCM, chloroform, or EA). E_T(30) value of each solvent is given in the parentheses. (c) A schematic description of ESIPT process in the case of **DPyBI-10** and **DPyBI-10-HCl**.

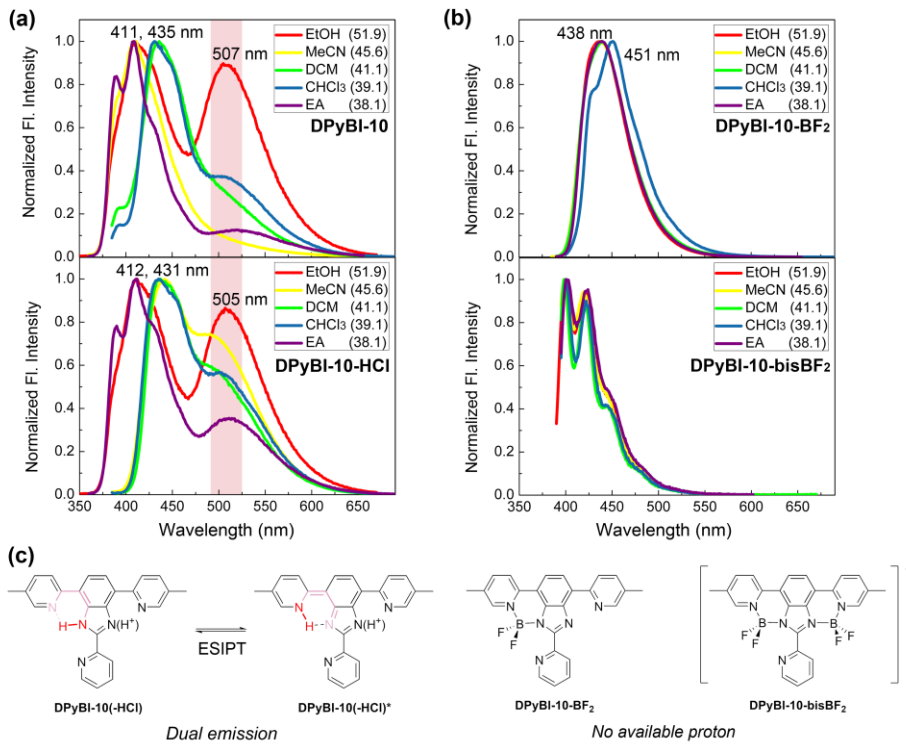

II.3.2. Eelectronic Modification of the Aryl Substituent in the "Vertical" Axis of the T-Shaped Fluorophore

The electronic properties of the aryl group in the "vertical" axis of the T-shaped molecules also impact the photophysical properties. In order to probe the structure–property relationships in detail, we systematically altered the aryl substituent on the imidazole unit but without changing the "horizontal" axis of the T-shaped molecule. The parent **DPyBI** system was employed for this purpose, which does not have the BF_2 unit. We decided to compare four molecules, which have nitro (**DPyBI-03)**, trifluoromethyl (**DPyBI-01)**, ethyl (**DPyBI-04)**, and dimethylamino substituent (**DPyBI-07)** at the *para*-position of the imidazole-appended phenyl ring. As a parameter to evaluate the structure–dependent electronic effects, Hammett sigma constant (σ) was chosen.[19] With increasing electron-withdrawing effect, the longer-wavelength emission became intensified at the expense of the shorter-wavelength emission. An increase in the fluorescence quantum yield was also observed as the functional group with more positive Hammett constant was introduced.

The mechanism of fluorescence quenching with increasing electron-donor ability of the aryl substituent might be a PET-type process. In particular, the **DPyBI-bisBF$_2$** system could be considered as a directly linked donor–acceptor dyad with the two π planes disposed essentially orthogonal to each other. As such there should be little interaction between them in the ground state. In this platform, the vertical π-strand could function an electron donor to the horizontal π-strand upon photo-excitation. Apparently, π-conjugated motifs with electron-donating substituents would be a better PET donor to induce fluorescence quenching. Based on this empirical model, we are currently working on metal- or pH-responsive sensors, in which

binding of metal or proton would decrease the donor ability to enhance the fluorescence.

Figure 11. (a) Chemical structure and fluorescence spectra of select compounds in **DPyBI** series which have different substituents at the *para*-position and (b) those of select compounds in **DPyBI-bisBF$_2$** series. Photophysical properties were measured in THF at T = 298 K. (c) Scatter plot of the relationship between Hammett substituent constant (σ_{para}) of substituent and quantum yield.

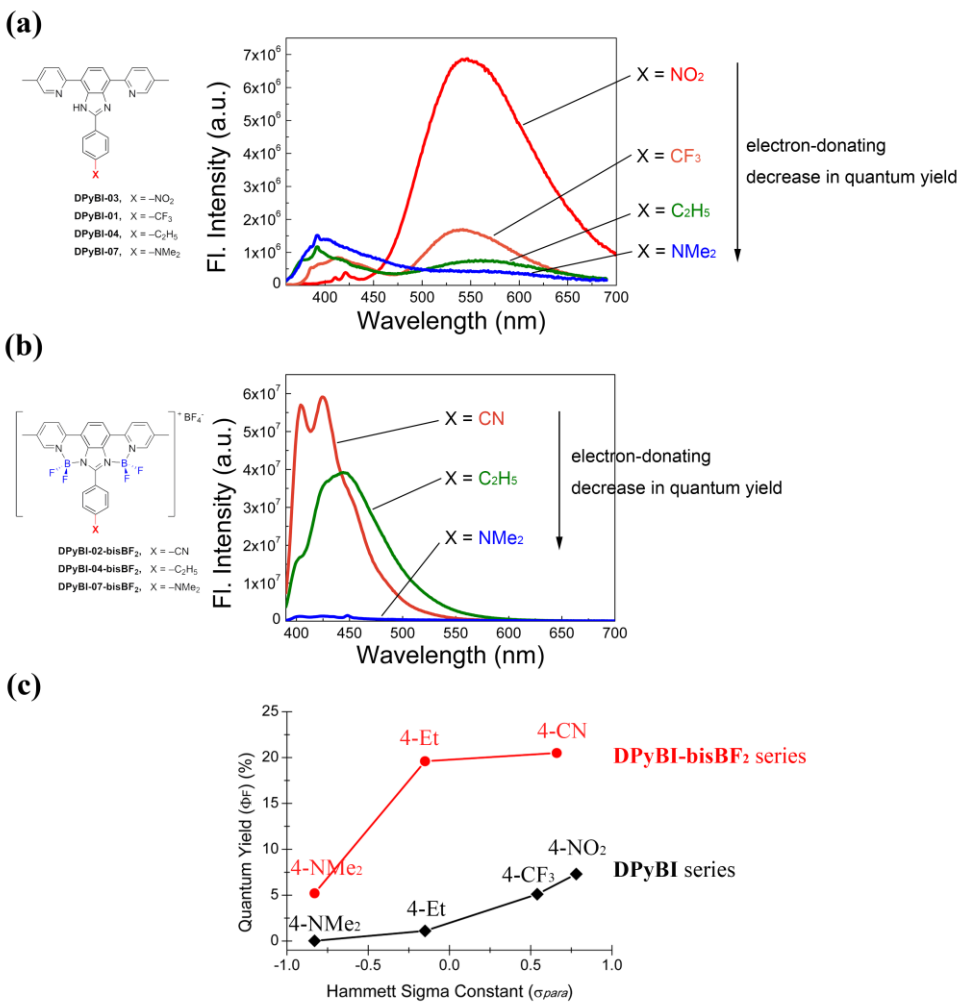

Table 2. Photophysical properties of select **DPyBI-**molecules with different substituents, and the corresponding Hammett constants.

Compound	Substituent	σ_{para}	$\lambda_{max,\ abs}$ (nm)	$\lambda_{max,\ em}$(nm)	Φ_F (%)
DPyBI-03	$-NO_2$	0.78	364	547	7.3
DPyBI-01	$-CF_3$	0.54	348	542	5.1
DPyBI-04	$-C_2H_5$	-0.15	349	392	1.1
DPyBI-07	$-NMe_2$	-0.83	352	392	0.02

Table 3. Photophysical properties of select **DPyBI-bisBF$_2$** molecules with different substituents, and the corresponding Hammett constants.

Compound	Substituent	σ_{para}	$\lambda_{max,\ abs}$ (nm)	$\lambda_{max,\ em}$(nm)	Φ_F (%)
DPyBI-02-bisBF$_2$	–CN	0.66	390	425	20.5
DPyBI-04-bisBF$_2$	$-C_2H_5$	-0.15	389	444	19.6
DPyBI-07-bisBF$_2$	$-NMe_2$	-0.83	388	448	5.2

The mechanism of fluorescence quenching with increasing electron-donor ability of the aryl substituent might be a PET-type process. In particular, the **DPyBI-bisBF$_2$** system could be considered as a directly linked donor–acceptor dyad with the two π planes disposed essentially orthogonal to each other. As such there should be little interaction between them in the ground state. In this platform, the vertical π-strand could function an electron donor to the horizontal π-strand upon photo-excitation. Apparently, π-conjugated motifs with electron-donating substituents would be a better PET donor to induce fluorescence quenching. Based on this empirical model, we are currently working on metal- or pH-responsive sensors, in which

binding of metal or proton would decrease the donor ability to enhance the fluorescence.

For pyridyl derivatives, we also investigated the effect of substitution positions. In general, blue-shifted emission with higher quantum yield is observed when comparison is made with phenyl-substituted analogues. However, introduction of electron-donating groups, such as dimethylamino substituent, rendered the molecules to become less emissive. This trend is qualitatively similar to that summarized in Table X: introduction of electron-donating group leads to decreased quantum yield. In addition, the position of the substituent is also an important factor to modulate the photophysical properties. For example, installation of the dimethylamino group at the *para*-position caused a dramatic change in fluorescence emission, in terms of both the shape and the intensity. Substitution at the *meta*-position, however, did not induce such significant change; the fluorescence intensity decreased without change in the band shape. From these results, we tentatively conclude that the positions as well as electronic properties of the substituents are crucial factors to affect the fluorescence.

Figure 12. (a) Chemical structure and fluorescence spectra of **DPyBI-10** and **DPyBI-12**, and (b) those of **DPyBI-11**. Photophysical properties were measured in THF at *T* = 298 K.

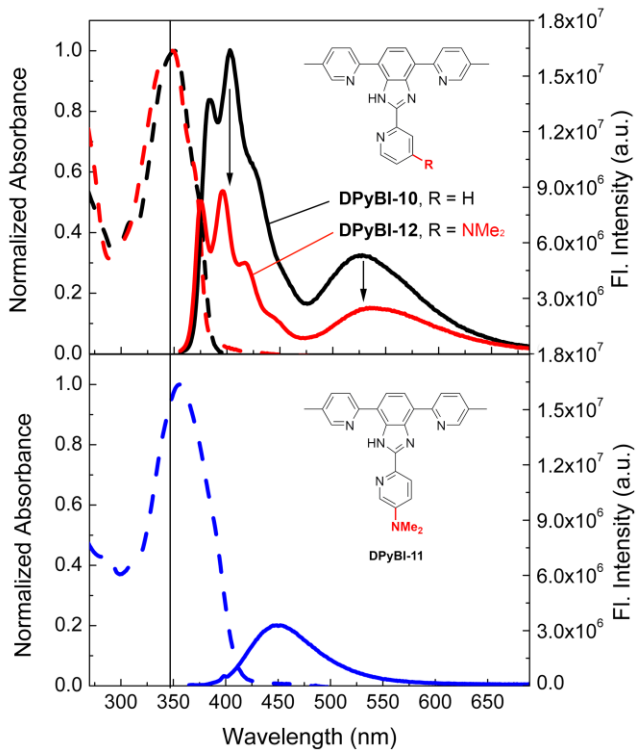

Table 4. Photophysical properties of **DPyBI-10** and dimethylamino-substituted derivatives at different position (**DPyBI-11**: para-substituted one; **DPyBI-12**: meta-substituted one), and the corresponding Hammett constants.

Compound	Substituent	σ	$\lambda_{max,\ abs}$ (nm)	$\lambda_{max,\ em}$(nm)	Φ_F (%)
DPyBI-10	None	0.00	351	407 (532)[a]	7.3
DPyBI-11	*para*-NMe_2	-0.83	356	452	5.1
DPyBI-12	*meta*-NMe_2	-0.16	348	400 (536)[a]	1.1

II.3.3. Fluorescence Studies in THF

In the previous section, we have shown that the photophysical properties of the T-shaped fluorophores can be modulated by changing either the horizontal or the vertical axis of the extended π-conjugation. Using such independent structural modifications, we could construct a library of fluorophores endowed with distinctively different emissive properties. As shown in **Figure 13**, tunable emission over a wide spectral range was achieved. Future efforts need to improve the fluorescence quantum yields of these proof-of-concept 1st-generation system.

Figure13. Normalized fluorescence intensity in THF which spans a wide range of visible light

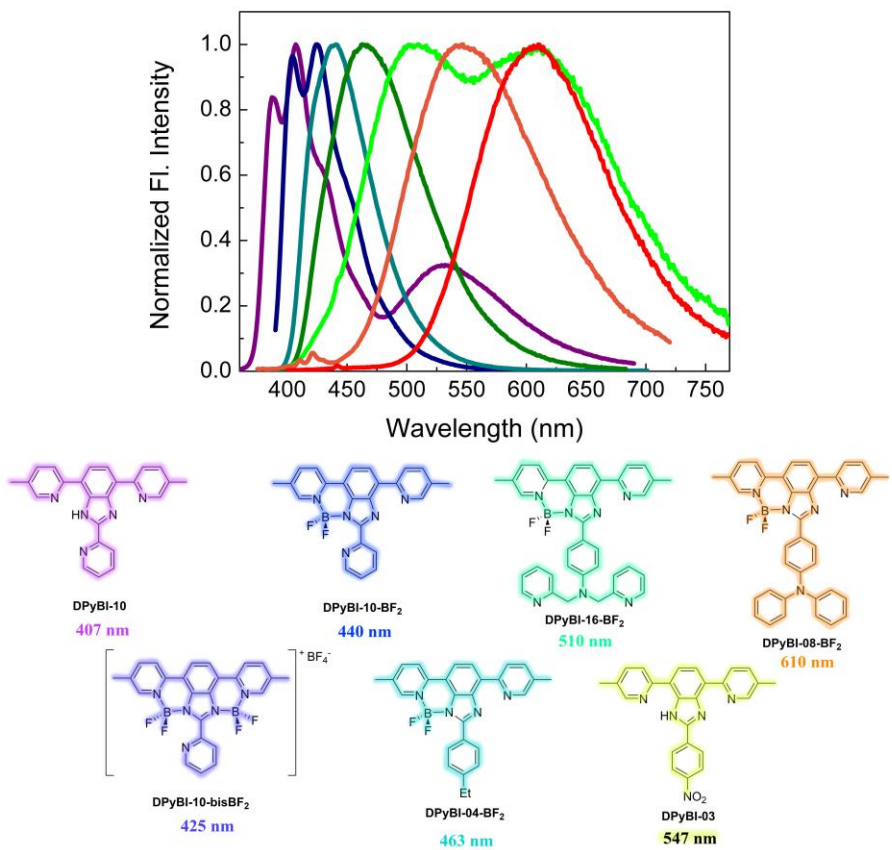

II.3.4. Fluorescence Studies on DPyBI-bisBF$_2$ Series in Aqueous Solution

The positively charged **DPyBI-bisBF$_2$** series are expected to have good solubility in water. In fact, when the imidazole-appended aryl group is sufficiently small, such as 2-pyridyl (**DPyBI-10-bisBF$_2$**) or 4-ethylphenyl (**DPyBI-04-bisBF$_2$**), the compounds show high water solubility. Compounds having bulkier substituents, such as 4-(*N*,*N*-diphenylamino)phenyl (**DPyBI-08-bisBF$_2$**) and 4-(*N*,*N*,-di(2-picolyl)amino)phenyl (**DPyBI-15-bisBF$_2$**), dissolve well in organic solvents such as dichloromethane. They also have reasonably good solubility in aqueous environment for fluorescence measurement. Fluorescence spectra were thus taken in Dulbecco's phosphate-buffered saline (DPBS) solutions (Figure xx. right) to reveal that CT-type longer-wavelength emission is essentially quenched in aqueous environment. In contrast, local excitation (LE)-type emission at shorter wavelength was still maintained. These findings suggest the potential application of these compounds as environmentally-sensitive imaging agents.

Figure 14. (a) Fluorescence spectra of select **DPyBI-bisBF$_2$** compounds in DPBS. (b)–(d) Comaparison of fluorescence spectra of each compound in THF solution (black lines) vs DPBS solution (red lines).

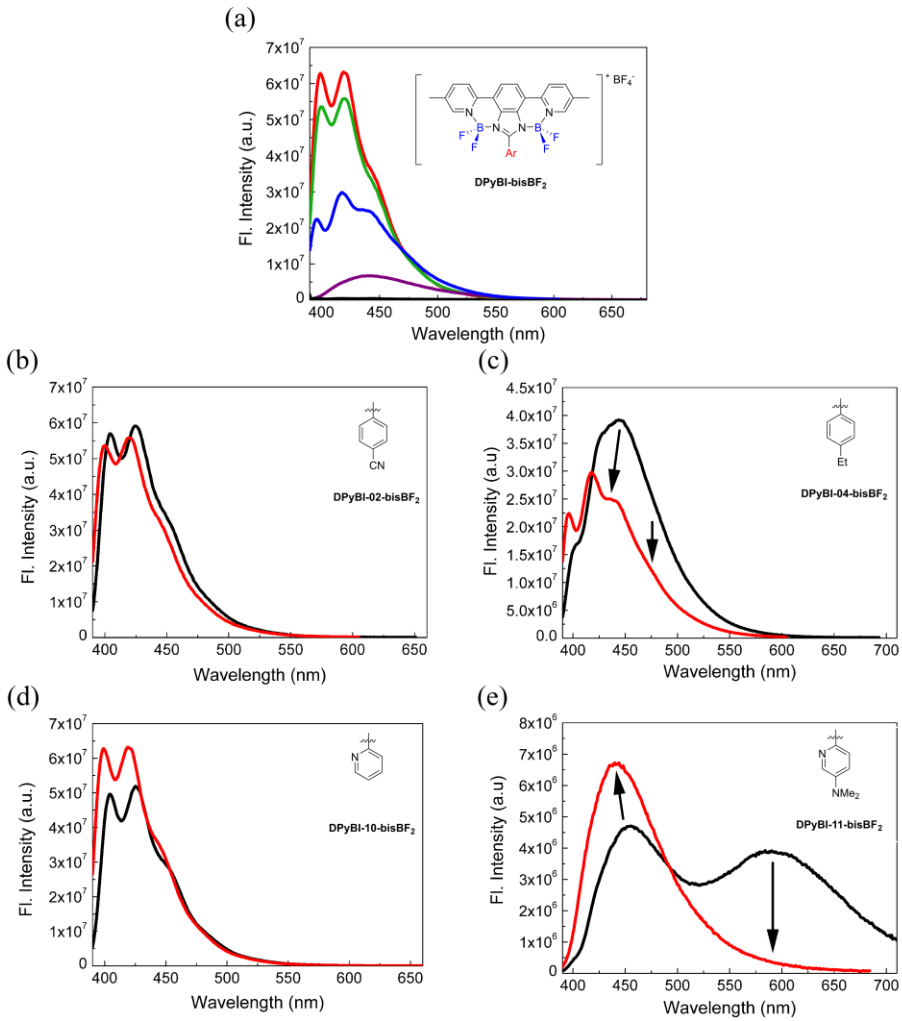

II.3.5. Solid State Fluorescence

Most of the compounds in our system emit weak to moderate fluorescence in the solid state. Similar to solution samples, emission bands of these solid samples also span a full range of visible light, as shown in Figure 15 (Φ_F = 0.026 ~ 0.193). It is noteworthy that we could observe solid-state fluorescence of molecules that adopt nearly planar structures. Conventional fluorescent dyes having disk- or rod-like shape suffer from quenching of emission when aggregated or clustered. This is because flat rigid molecules engage in intermolecular π-π stacking interactions, and the excited states of such aggregates relax back to the ground state via non-radiative channels. Therefore, in order to obtain bright fluorescence in solid state, it is crucial to suppress such interactions. Unlike existing strategies to employ AIE-inducing motifs or steric shields to prevent close contacts or to create inherently twisted shapes, the T-shaped molecules that we have created tend to avoid direct π-π stacking despite their planarity. Our findings represent an alternative strategy to realize solid-state fluorescence that does not require additional steric controller groups.

Figure 15. Normalized fluorescence intensity in solid state which spans a wide range of visible light

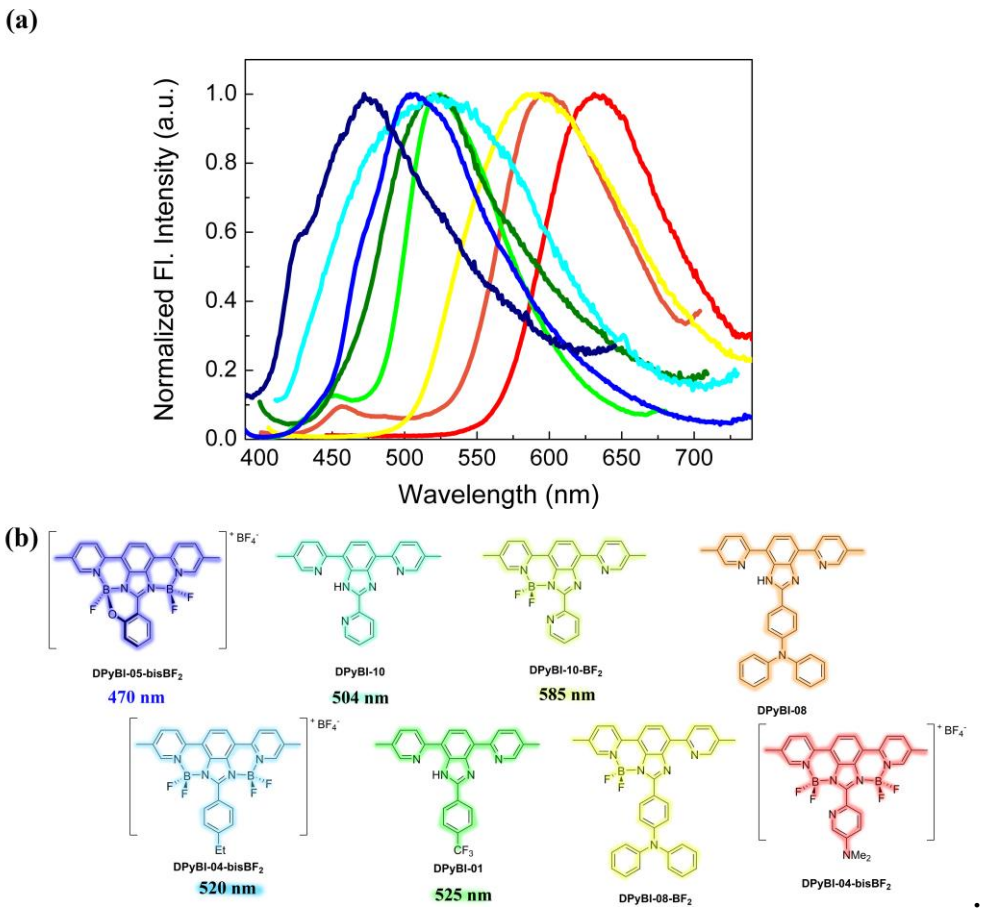

III. Summary

We have designed and prepared series of unprecedented benzidimazole-baded fluorophores **DPyBI**, **DPyBI-BF_2**, and **DPyBi-bisBF_2**. In this system, emissive properties could be modulated by means of (i) introduction of BF_2 units and (ii) change in electronic nature of aryl rings conjugated to the fluorescent core. These modifications are designed to occur at the last steps of synthesis, and this modular synthesis allowed us to readily build a collection of benzimidazole-based fluorophores. We could take advantage of X-ray crystallographic data to reveal deviation from planarity cause by introduction of BF_2 units as well as to confirm the chemical connectivity. With various compounds in hand, we scrutinized the relationship between a subtle change in the structure of fluorophore (i.e. binding of BF_2 units, alteration of substituents) and luminescent properties. These compounds display tunable emission and a broad spectral range both in solution and in solid state. Moreover, most compounds have good water solubility, which is essential for a further application. These appealing features, including accessibility of synthesis, emission wavelength tuning, and solid-state fluorescence, promise the use of this modularly accessible fluorophores in various areas, ranging from chemical sensors to light-emitting devices.

IV. Experimental Section

General Considerations

All reagents were obtained from commercial suppliers and used as received unless otherwise noted. The solvents tetrahydrofuran (THF), toluene, 1,2-dichloroethane (DCE), and dichloromethane (DCM) were saturated with argon and purified by passage through activated Al_2O_3 columns under argon (Pure Process Technology GC-SPS-4 and GC-SPS-8). Diisopropylethylamine (DIPEA) was saturated with argon and purified using the same solvent purification system before use. The compounds 4,7-dibromo-2,1,3-benzothiadiazole (**2**),[14] 2-(tributylstannyl)-5-methylpyridine[20], 2,4,6-trihydroxybenzaldehyde,[21] 4-(*N*,*N*-diphenylamino)benzaldehyde,[22] 4-(dimethyl-amino)picolinaldehyde,[23] 5-(dimethylamino)picolinaldehyde,[24] *N*,*N*-bis(pyridin-2-ylmethyl)aniline,[25] and 4-(*N*,*N*-bis(pyridin-2-ylmethyl)amino)benzaldehyde,[25] and were prepared according to literature procedures or their slight modifications. All air–sensitive manipulations were carried out under nitrogen atmosphere by standard Schlenk-line techniques.

The progress of reaction was checked on thin layer chromatography (TLC) plates (Merck silica gel 60 F_{254} or Merck aluminium oxide 60 F_{254}, neutral on aluminium foil). The spots were visualized under 254 nm UV light and/or charring after dipping the TLC plate into a vanillin solution (3.0 g of vanillin and 0.5 mL of conc H_2SO_4 in 50 mL of EtOH) or a $KMnO_4$ solution (1.0 g of $KMnO_4$, 6.7 g of K_2CO_3, and 1.7 mL of 5% NaOH solution in 100 mL of water). Flash column chromatography was performed on silica gel (SilicycleSilicaflash P60, 40–63 μm, 230–400 mesh).

Physical Measurements

^{1}H NMR and ^{13}C NMR spectra were recorded on a Bruker DPX-300 (300 MHz), an Agilent 400-MR DD2 Magnetic Resonance System (400 MHz), or a Varian/Oxford As-500 (500 MHz) spectrophotometer. For compounds having boron and fluorine, ^{11}B NMR and ^{19}F NMR spectra were also obtained on an Agilent 400-MR DD2 Magnetic Resonance System (128 MHz for the ^{11}B nucleus; 376 MHz for the ^{19}F nucleus). Chemical shifts in ^{1}H NMR spectra were reported in parts per million (ppm) on the δ scale with respect to the internal standard of tetramethylsilane (δ = 0.00 ppm) or residual solvent (δ = 2.05 ppm for acetone;δ = 5.32 ppm for CH_2Cl_2;δ = 3.31 ppm for MeOH; δ = 2.50 ppm for dimethylsulfoxide (DMSO)). Data for the ^{1}H NMR spectra were reported as follows: chemical shift, multiplicity (s = singlet, d = doublet, t = triplet, q = quartet, m = multiplet, br = broad), coupling constant in Hertz (Hz) and integration. Data for the ^{13}C NMR spectra were reported as chemical shift in ppm from the residual solvent (δ = 77.16 ppm for chloroform; δ = 29.84 ppm for acetone; δ = 53.84 ppm for CH_2Cl_2;δ = 49.00 ppm for MeOH; δ = 39.52 ppm for DMSO). ^{11}B NMR spectra were referenced to an external standard of BF_3•OEt_2 (δ = 0.00 ppm) in $CDCl_3$ prior to spectral acquisition. ^{19}F NMR spectra were referenced to $CFCl_3$ using an external standard of trifluoroacetic acid (δ = –76.55 ppm) in $CDCl_3$ prior to spectral acquisition. UV–vis spectra were recorded on an Agilent 8453 UV–vis spectrophotometer with ChemStation. Fluorescence spectra were recorded on a Photon Technology International QM-400 spectrofluorometer with FelixGX software.

Fluorescence Quantum Yield Measurements

Absolute quantum yields of solution or solid samples were measured using a 3.2-inch

K-Sphere Petite integrating sphere (PTI) and a PTI QuantaMaster™ 400 spectrofluorometer with FelixGX software. The solution sample absorbance was maintained < 0.1 to minimize internal absorption. Solid samples were prepared as follows: A transparent double-sided tape was applied to a quartz plate (2 cm × 2 cm), on which a powder sample was spread evenly.

Computational Studies

All calculations were carried out using density functional theory (DFT) with Gaussian09 program.[26]Geometry optimizations were performed with the B3LYP functional and the 6-31G(d) basis set.

Synthesis

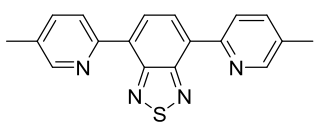

4,7-Bis(5-methylpyridin-2-yl)-2,1,3-benzothiadiazole (3). This compound was prepared in a manner similar to the literature procedure,[15] except that 2-(tributylstannyl)-5-methylpyridine[20] was used instead of 2-(tributylstannyl)pyridine. An oven-dried 250-mL 3-neck RBF was charged with **2** (6.02 g, 20.5mmol), $Pd(PPh_3)_4$ (519 mg, 0.45 mmol), and dry toluene (50 mL) under Ar. The mixture was heated at reflux. A solution of freshly prepared stannyl compound (18.35 g, 48.0 mmol) in toluene (8 mL) was added to the mixture. The resulting brown solution was stirred for 19 h at reflux. After cooling to r.t., 2 M aqueous KF solution was added to remove tin byproduct from the reaction mixture. After stirring for 30 min, the solution was filtered and the filtered solid was washed with CH_2Cl_2 until the filtrate was no

longer yellow. The filtrate was washed with saturated aqueous NH_4Cl solution. The organic layer was dried over $MgSO_4$, filtered, and concentrated under reduced pressure. The residual material was purified by flash column chromatography on SiO_2 (hexane:CH_2Cl_2:EtOAc = 8:1:1 to 1:1:1, v/v, with a few drops of Et_3N) to furnish **3** as a yellow solid (6.39 g, 20.1 mmol, yield = 98%). **3** can be further purified by recrystallization from EtOH if necessary. ^{1}H NMR (300 MHz, $CDCl_3$, 298 K): δ 8.63 (dd, *J* = 1.5, 0.7 Hz, 2H), 8.56 (d, *J* = 8.1 Hz, 2H), 8.53 (s, 2H), 7.72–7.65 (m, 2H), 2.43 (s, 6H); ^{13}C NMR (75 MHz, $CDCl_3$, 298 K) δ 153.92, 151.59, 150.38, 137.14, 132.88, 132.16, 129.31, 124.62, 18.48.

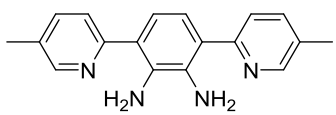

3,6-Bis(5-methylpyridin-2-yl)benzene-1,2-diamine (4). This compound was prepared by the slightly modified literature procedure.[16] A suspension of **3** (1.47 g, 4.60 mmol), $CoCl_2$•$6H_2O$ (183 mg, 0.77 mmol) in EtOH (10 mL) was stirred at 0 °C. To the yellow mixture was slowly added $NaBH_4$ (1.74 g, 46.1 mmol) over a period of 20 min. Black solid was formed and the mixture turned dark immediately. The mixture was then heated at reflux and stirred for 30 min. After cooling to r.t., H_2O was slowly added to quench the excess $NaBH_4$. The mixture was filtered through Celite 545, and the filtrate was extracted with CH_2Cl_2 three times. The combined extracts were washed with brine, dried over $MgSO_4$, filtered, and concentrated under reduced pressure. The residual material was purified by flash column chromatography on SiO_2 (hexane:EtOAc:CH_2Cl_2 = 2:1:0.5 to 1:1:0.5, v/v, with a few drops of Et_3N) to furnish **4** as a yellow solid (1.21 g, 4.18 mmol, yield = 91%). ^{1}H NMR (500 MHz, $CDCl_3$,

298 K): δ 8.49 (s, 1H), 7.63 (d, *J* = 8.2 Hz, 1H), 7.59 (d, *J* = 2.0 Hz, 1H), 7.12 (s, 1H), 5.55 (s, 2H), 2.37 (s, 3H);^{13}C NMR (125 MHz, $CDCl_3$, 298 K): δ 156.82, 148.34, 137.65, 136.37, 130.56, 123.15, 122.23, 118.87, 18.32.

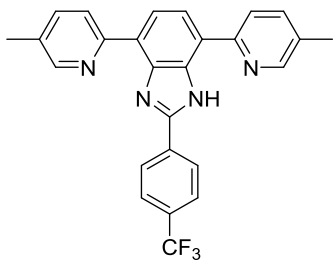

4,7-Bis(5-methylpyridin-2-yl)-2-(4-(trifluoromethyl)phenyl)-1*H*-benzimidazole (DPyBI-01). This compound was prepared by the slightly modified literature procedure.[17b] A mixture of **4** (131 mg, 0.45 mmol) and 4-(trifluoromethyl)benzaldehyde (78 mg, 0.45 mmol) in EtOH (19 mL) was stirred at reflux. After a few minutes, a solution of $Na_2S_2O_5$ (71 mg, 0.37 mmol) in H_2O (0.4 mL) was added to the mixture. Off-white solid was generated and the mixture was stirred at reflux for 15 h. The mixture was concentrated under reduced pressure to attain half of the initial volume, and then H_2O was added. The resulting solid was filtered and washed with H_2O extensively to completely remove $Na_2S_2O_5$. The solid was also washed with a small amount of MeOH to furnish **DPyBI-01** as a slightly light-green solid (180 mg, 0.41 mmol, 90%). ^{1}H NMR (300 MHz, $CDCl_3$, 298 K): δ 9.05 (d, *J* = 7.8 Hz, 1H), 8.62 (s, 2H), 8.29 (m, 3H), 7.99 (d, *J* = 8.2 Hz, 1H), 7.92 (d, *J* = 7.8 Hz, 1H), 7.80 (d, *J* = 8.2 Hz, 2H), 7.68 (t, *J* = 8.8 Hz, 2H), 2.43 (s, 6H);^{13}C NMR (75 MHz, $CDCl_3$, 298 K): δ 153.60, 152.51, 150.00, 149.42, 143.09, 137.82, 137.18, 134.53, 133.67, 131.93, 131.83, 131.50, 131.12, 127.19, 126.07, 126.02, 125.12, 122.32, 122.14, 121.69, 120.55, 119.59, 18.51.

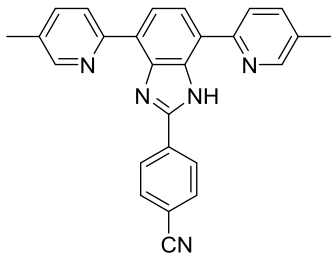

2-(4-Cyanophenyl)-4,7-bis(5-methylpyridin-2-yl)-1*H*-benzimidazole (DPyBI-02).This compound was prepared by the slightly modified literature procedure.[17a] A mixture of **4** (145 mg, 0.50 mmol) and 4-cyanobenzaldehyde (66 mg, 0.50 mmol) in $CHCl_3$ (20 mL) was stirred at r.t. for 10 min. To the mixture was added catalytic amount of $ZrCl_4$ (12 mg, 0.05 mmol). The mixture was heated at reflux and stirred for 2 days. The mixture was concentrated under reduced pressure and the residual material was purified by flash column chromatography on SiO_2(hexane:EtOAc = 1:1 to EtOAc:MeOH = 10:1)to furnish **DPyBI-02** as an off-white solid (125 mg, 0.31 mmol, 62%). ^{1}H NMR (400 MHz, $CDCl_3$, 298 K): δ 12.60 (s, 1H), 9.03 (d, *J* = 8.0 Hz, 1H), 8.59 (s, 2H), 8.27 (t, *J* = 6.9 Hz, 3H), 7.96 (d, *J* = 8.0 Hz, 1H), 7.90 (d, *J* = 8.0 Hz, 1H), 7.82–7.75 (m, 2H), 7.66 (dd, *J* = 6.9, 8.2 Hz, 2H), 2.42 (s, 7H);^{13}C NMR (100 MHz, $CDCl_3$, 298 K): δ 171.23, 152.31, 150.00, 149.31, 137.77, 137.07, 134.66, 134.34, 132.74, 132.04, 131.80, 131.16, 127.22, 124.99, 122.19, 121.65, 120.71, 119.50, 118.68, 113.16, 22.77.

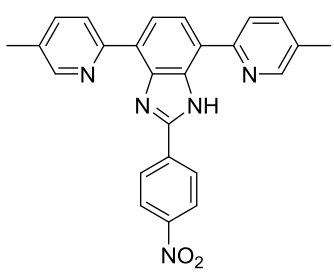

4,7-Bis(5-methylpyridin-2-yl)-2-(4-nitrophenyl)-1*H*-benzimidazole (DPyBI-03).

This compound was prepared in a manner similar to that described for **DPyBI-01**, except that 4-nitrobenzaldehyde was used instead of 4-(trifluoromethyl)benzaldehyde, and the reaction mixture was heated at reflux for 13 h prior to cooling and concentration. **DPyBI-03** was obtained as a pale-yellow solid (yield = 88%). ^{1}H NMR (400 MHz, $CDCl_3$, 298 K): δ 12.73 (s, 1H), 9.05 (d, *J* = 7.8 Hz, 1H), 8.66 (s, 1H), 8.62 (s, 1H), 8.44–8.35 (m, 4H), 8.31 (dd, *J* = 7.8, 2.0 Hz, 1H), 8.02 (d, *J* = 8.3 Hz, 1H), 7.96 (d, *J* = 8.3 Hz, 1H), 7.70 (t, *J* = 9.1 Hz, 2H), 2.44 (d, *J* = 7.0 Hz, 6H).

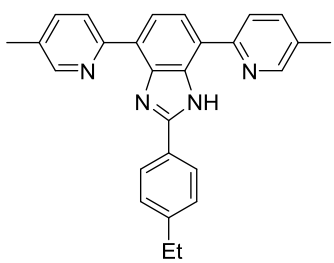

2-(4-Ethylphenyl)-4,7-bis(5-methylpyridin-2-yl)-1*H*-benzimidazole (DPyBI-04). This compound was prepared in a manner similar to that described for **DPyBI-02**, except that 4-ethylbenzaldehyde was used instead of 4-nitrobenzaldehyde, and the reaction mixture was stirred at r.t. for 24 h prior to concentration. **DPyBI-04** was obtained as a yellow solid (yield = 87%). ^{1}H NMR (300 MHz, $CDCl_3$, 298 K): δ 8.61 (s, 4H), 8.10 (dd, *J* = 7.9, 7.3 Hz, 4H), 7.67 (d, *J* = 7.9 Hz, 2H), 7.38 (d, *J* = 7.3 Hz, 2H), 2.85–2.66 (m, 2H), 2.41 (s, 6H), 1.43–1.20 (m, 3H).

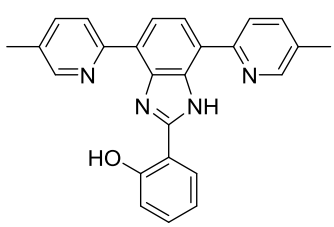

2-(4,7-Bis(5-methylpyridin-2-yl)-1*H*-benzimidazol-2-yl)phenol (DPyBI-05). This compound was prepared by the slightly modified literature procedure.[27] A mixture of **4** (87 mg, 0.30 mmol), salicylaldehyde (38 mg, 0.30 mmol), and $ZrCl_4$ (8 mg, 0.03 mmol) in MeCN (20 mL) and $CHCl_3$ (5 mL) was stirred at r.t. for 23 h. The mixture was concentrated under reduced pressure and the residual material was purified by flash column chromatography on SiO_2 (CH_2Cl_2:MeOH = 20:1, v/v) to furnish **DPyBI-05** as an off-white crystal (84 mg, 0.23mmol, 77%). ^{1}H NMR (400 MHz, $CDCl_3$, 298 K): δ 13.32 (s, 1H), 12.62 (s, 1H), 8.64 (s, 2H), 8.23 (m, 4H), 7.78 (d, *J* = 7.8 Hz, 1H), 7.68 (d, *J* = 8.1 Hz, 2H), 7.40 (dd, *J* = 8.1, 7.8 Hz, 1H), 7.15 (d, *J* = 8.3 Hz, 1H), 7.10 – 6.99 (m, 1H), 2.44 (s, 6H).

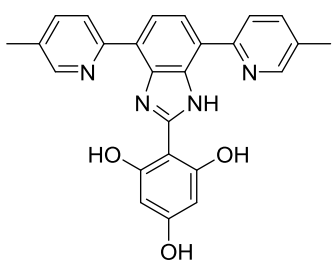

2-(4,7-Bis(5-methylpyridin-2-yl)-1*H*-benzimidazol-2-yl)benzene-1,3,5-triol (DPyBI-06).This compound was prepared in a manner similar to that described for **DPyBI-01**, except that 2,4,6-trihydroxybenzaldehyde was used instead of 4-(trifluoromethyl)benzaldehyde, and the reaction mixture was heated at reflux for 16 h prior to cooling and concentration. **DPyBI-06** was obtained as a yellow solid (yield = 72%) after filtration and washing with MeCN.

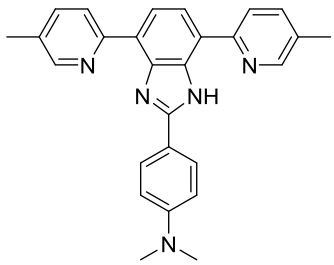

4-(4,7-Bis(5-methylpyridin-2-yl)-1*H*-benzimidazol-2-yl)-*N*,*N*-dimethylaniline (DPyBI-07). This compound was prepared in a manner similar to that described for **DPyBI-01**, except that 4-(dimethylamino)benzaldehyde was used instead of 4-(trifluoromethyl)benzaldehyde, and the reaction mixture was heated at reflux for 24 h prior to cooling and concentration. **DPyBI-07** was obtained as an orange solid (yield = 86%) after filtration and washing with H_2O. ^{1}H NMR (300 MHz, CD_2Cl_2, 298 K): δ 8.70–8.51 (m, 2H), 8.15–7.97 (m, 2H), 7.68 (d, *J* =9.0 Hz, 1H), 6.85 (d, *J* = 9.0 Hz, 1H), 3.06 (s, 3H), 2.41 (s, 3H);^{13}C NMR (75 MHz, CD_2Cl_2, 298 K): δ 153.59, 153.02, 152.14, 149.84, 137.50, 131.97, 128.24, 122.39, 120.20, 117.80, 112.20, 40.41, 18.46.

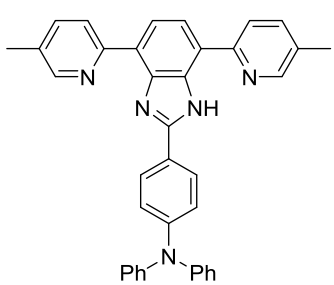

4-(4,7-Bis(5-methylpyridin-2-yl)-1*H*-benzimidazol-2-yl)-*N*,*N*-diphenylaniline (DPyBI-08). This compound was prepared in a manner similar to that described for **DPyBI-01**, except that 4-(diphenylamino)benzaldehyde was used instead of 4-(trifluoromethyl)benzaldehyde, and the reaction mixture was heated at reflux for 16 h prior to cooling and concentration. **DPyBI-08** was obtained as ayellow solid (yield = 88%) after filtration and washing with H_2O.

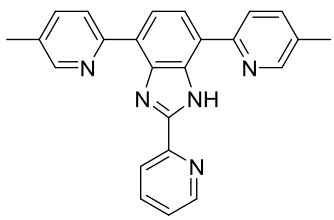

4,7-Bis(5-methylpyridin-2-yl)-2-(pyridin-2-yl)-1*H*-benzimidazole (DPyBI-10). This compound was prepared by the slightly modified literature procedure.[28] A mixture of **4** (145 mg, 0.50 mmol) and picolylaldehyde (55 mg, 0.50 mmol) in DMF (4.5 mL) and H_2O (0.5 mL) was stirred at 80 ^oC for 18 h. The mixture was concentrated under reduced pressure and the residual material was purified by flash column chromatography on SiO_2 (CH_2Cl_2:MeOH = 30:1, v/v) to furnish **DPyBI-10** as a yellow solid (167 mg, 0.44 mmol, 88%). ^1H NMR (300 MHz, $CDCl_3$, 298 K): δ 12.70 (s, 1H), 9.07 (s, 1H), 8.75–8.69 (m, 1H), 8.66 (s, 2H), 8.56 (d, *J* = 7.9 Hz, 1H), 8.02 (s, 3H), 7.86 (td, *J* = 7.7, 1.7 Hz, 1H), 7.66 (d, *J* = 7.4 Hz, 2H), 7.36 (ddd, *J* = 7.5, 4.9, 1.1 Hz, 1H), 2.42 (s, 6H);^{13}C NMR (75 MHz, $CDCl_3$, 298 K): δ 151.42, 149.89, 149.53, 148.92, 137.31, 136.90, 131.68, 124.43, 122.13, 18.49.

HCl salt of DPyBI-10 (DPyBI-10-HCl). DPyBI-10 was dissolved in CH_2Cl_2. HCl(g), generated by dehydration of conc. HCl by $CaCl_2$,[29] was bubbled into the solution. The resulting solid was filtered and washed with CH_2Cl_2. DPyBI-10-HCl was obtained as a yellow solid (quant.). ^1H NMR (300 MHz, CD_3OD, 298 K): δ9.10–8.93 (m, 4H), 8.70–8.48 (m, 5H), 8.21 (s, 2H), 8.02 (dd, *J* = 7.1, 6.0 Hz, 1H), 2.69 (s, 6H);^{13}C NMR (75 MHz, CD_3OD, 298 K): δ 150.58, 148.27, 147.52, 147.18, 145.09, 143.90, 143.65, 139.33, 139.09, 128.78, 126.99, 126.24, 125.85, 122.68, 18.39.

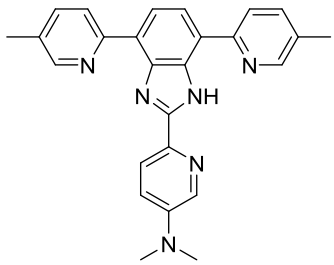

2-(4,7-Bis(5-methylpyridin-2-yl)-1*H*-benzimidazol-2-yl)-5-(*N*,*N*-dimethyamino)pyridine (DPyBI-11). This compound was prepared in a manner similar to that described for **DPyBI-05**, except that 5-(dimethylamino)picolylaldehyde was used instead of salicylaldehyde, and the reaction mixture was stirred at r.t. for 24 h prior to concentration. **DPyBI-11** was obtained as a yellow solid (yield = 46%) after filtration and washing with MeOH. ^{1}H NMR (400 MHz, $CDCl_3$, 298 K): δ 12.49 (s, br, 1H), 8.75 (s, 2H), 8.66 (s, 2H), 8.46–7.60 (m, 5H), 7.66 (s, 2H), 7.11 (s, 1H), 3.10 (s, 6H), 2.42 (s, 6H).

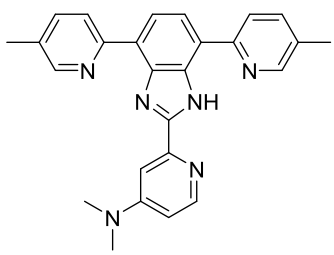

2-(4,7-Bis(5-methylpyridin-2-yl)-1*H*-benzimidazol-2-yl)-4-(*N*,*N*-dimethyamino)pyridine (DPyBI-12). This compound was prepared in a manner similar to that described for **DPyBI-05**, except that 4-(dimethylamino)picolylaldehyde was used instead of salicylaldehyde, and the reaction mixture was stirred at r.t. for 2 days prior to concentration. **DPyBI-12** was obtained as a yellow solid (yield = 32%) after flash column chromatography on SiO_2 (CH_2Cl_2:MeOH = 100:3 to 100:6, v/v, with a few drops of Et_3N) and subsequent washing with MeOH. ^{1}H NMR (400 MHz,

$CDCl_3$, 298 K): δ 12.65 (s, br, 1H), 9.03 (s, 1H), 8.66 (m, 2H), 8.36 (d, *J* = 5.9 Hz, 1H), 8.22 (s, br, 1H), 7.93 (m, 2H), 7.80 (s, 1H), 7.71–7.54 (m, 2H), 6.58 (dd, *J* = 5.9, 2.7 Hz, 1H), 3.15 (s, 6H), 2.42 (s, 6H).

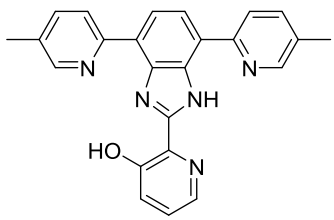

2-(4,7-Bis(5-methylpyridin-2-yl)-1*H*-benzimidazol-2-yl)pyridin-3-ol (DPyBI-13). This compound was prepared by the slightly modified literature procedure.[18] A mixture of **4** (58 mg, 0.20mmol), 3-hydroxypicolinic acid (28 mg, 0.20 mmol), and PPA was stirred at 200 ^{o}C for 10 h under Ar. The mixture was poured into ice-cooled water (100 mL), resulting in yellow solid. The mixture was neutralized with 10% (w/v) aqueous Na_2CO_3 solution, and then, the solid was filtered and washed with H_2O. The solid was dissolved in CH_2Cl_2 and the mixture was washed with brine, dried over $MgSO_4$, filtered, and concentrated under reduced pressure to furnish **DPyBI-13** as a yellow crystal (29 mg, 0.07 mmol, yield = 36%). ^{1}H NMR (300 MHz, $CDCl_3$, 298 K): δ 12.90 (s, 1H), 12.75 (s, 1H), 8.73 (s, 1H), 8.64 (s, 1H), 8.49 (d, *J* = 8.2 Hz, 1H), 8.29 (dd, *J* = 4.4, 1.3 Hz, 1H), 8.17 (d, *J* = 8.1 Hz, 1H), 7.97 (dd, *J* = 8.0, 6.2 Hz, 2H), 7.68 (t, *J* = 9.6 Hz, 2H), 7.43 (dd, *J* = 8.4, 1.3 Hz, 1H), 7.32 (dd, *J* = 8.4, 4.4 Hz, 1H), 2.44 (s, 6H).

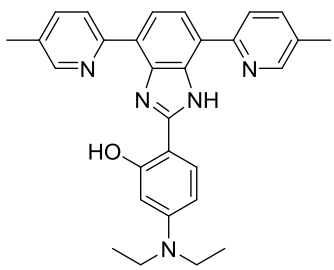

2-(4,7-Bis(5-methylpyridin-2-yl)-1*H*-benzimidazol-2-yl)-5-(diethylamino)phenol (DPyBI-14). This compound was prepared in a manner similar to that described for **DPyBI-05**, except that 4-(diethylamino)-2-hydroxybenzaldehyde was used instead of salicylaldehyde, and the reaction mixture was stirred at r.t. for 21 h prior to concentration. **DPyBI-14** was obtained as a yellow solid (yield = 13%).

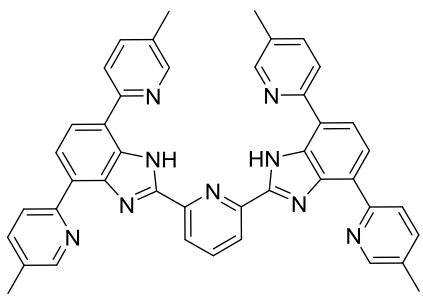

2,6-Bis(4,7-bis(5-methylpyridin-2-yl)-1*H*-benzimidazol-2-yl)pyridine (DPyBI-15). This compound was prepared by the slightly modified literature procedure.[18] A mixture of **4** (125 mg, 0.43 mmol), pyridine-2,6-dicarboxylic acid (33 mg, 0.20 mmol), and PPA was stirred at 200 ^{o}C for 12 h under Ar. The mixture was poured into ice-cooled water (100 mL), resulting in yellow solid. The mixture was neutralized with 10% (w/v) aqueous Na_2CO_3 solution, and then, the solid was filtered and washed with H_2O. The solid was dissolved in CH_2Cl_2 and the mixture was washed with brine, dried over $MgSO_4$, filtered, and concentrated under reduced pressure to furnish **DPyBI-15** as a pale-yellow crystal (109 mg, 0.16mmol, yield = 81%). ^{1}H NMR (400

MHz, $CDCl_3$, 298 K): δ 12.89 (s, 2H), 9.11 (d, *J* = 7.4 Hz, 2H), 8.64 (s, 2H), 8.45 (d, *J* = 7.6 Hz, 2H), 8.35–8.21 (m, 4H), 7.92 (d, *J* = 6.4 Hz, 5H), 7.73 (s, 2H), 7.52 (s, 2H), 2.46 (s, 6H), 2.09 (s, 6H).

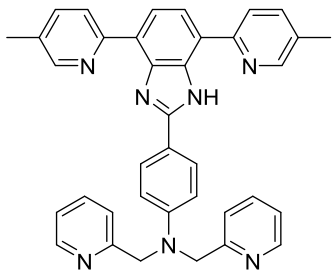

4-(4,7-Bis(5-methylpyridin-2-yl)-1*H*-benzimidazol-2-yl)-*N*,*N*-bis(pyridin-2-ylmethyl)aniline (DPyBI-16). This compound was prepared in a manner similar to that described for **DPyBI-01**, except that 4-(bis(pyridin-2-ylmethyl)amino)benzaldehyde was used instead of 4-(trifluoromethyl)benzaldehyde, and the reaction mixture was heated at reflux for 24 h prior to cooling and concentration. **DPyBI-16** was obtained as a pale-yellow solid (yield = 90%) after filtration and washing with H_2O. ^{1}H NMR (300 MHz, $CDCl_3$, 298 K): δ 12.21 (s, br, 1H), 9.07 (s,br, 1H), 8.66–8.60 (m, 2H), 8.56 (s, 2H), 8.30–7.75 (m, 5H), 7.71–7.55 (m, 4H), 7.29 (d, *J* = 7.9 Hz, 4H), 7.21 (dd, *J* = 7.4, 5.0 Hz, 2H), 6.86 (d, *J* = 8.9 Hz, 2H), 4.93 (s, 4H), 2.40 (s, 6H);^{13}C NMR (75 MHz, $CDCl_3$, 298 K): δ 158.35, 152.48, 149.99, 149.72, 149.55, 137.35, 137.08, 131.45, 128.37, 122.39, 120.98, 119.25, 112.77, 57.53, 18.47.

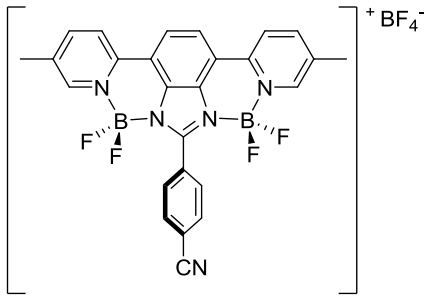

DPyBI-02-bisBF$_2$.A 50-mL 3-neck RBF was charged with **DPyBI-02** (125 mg, 0.31 mmol) under Ar. DCE (10 mL) and DIPEA (0.2 mL) were added and the mixture was heated at reflux. To the mixture was slowly added BF_3•OEt_2 (0.2 mL) over a period of 30 min. The resulting red mixture was stirred at reflux for 19 h. After cooling to r.t., the resulting pale-brown solid was filtered and washed with CH_2Cl_2 extensively to furnish **DPyBI-02-bisBF$_2$** (94 mg, 0.19mmol, yield = 61%). ^{1}H NMR (400 MHz, DMSO, 298 K): δ 9.04 (s, 4H), 8.82 (d, *J* = 2.3 Hz, 2H), 8.63 (d, *J* = 8.1 Hz, 2H), 8.28 (m, 4H), 2.60 (s, 6H).

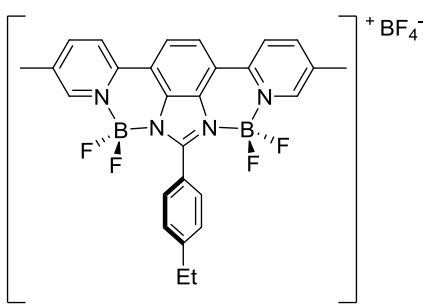

DPyBI-04-bisBF$_2$. This compound was prepared in a manner similar to that described for **DPyBI-02-bisBF$_2$**, except that **DPyBI-04** was used instead of **DPyBI-02**. **DPyBI-04-bisBF$_2$** (yield = 62%) was obtained as a pale-yellow solid by filtration and subsequent washing with CH_2Cl_2, $CHCl_3$, EtOAc, acetone, and MeCN.^{1}H NMR (400 MHz, DMSO, 298 K): δ 9.01 (m, 4H), 8.75 (s, 2H), 8.61 (d, *J* = 8.4 Hz, 2H), 8.03 (d,

J = 8.2 Hz, 2H), 7.61 (d, *J* = 8.4 Hz, 2H), 2.59 (s, 6H); ^{19}F NMR (376 MHz, DMSO, 298 K): δ –129.74, –148.32.

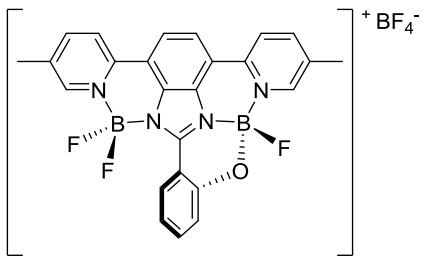

DPyBI-05-bisBF$_2$. An oven-dried 10 mL resealableSchelenk tube was charged with **DPyBI-05** (100 mg, 0.27 mmol). The reaction vessel was evacuated and backfilled with N_2 three times. DCE (4.6 mL) and DIPEA (0.2 mL) were added and the mixture was heated at reflux. To the mixture was slowly added BF_3•OEt_2 (0.2 mL) over a period of 20 min. The resulting mixture was stirred at reflux for 12 h, and off-white precipitation was observed. After cooling to r.t., the solid was filtered, washed with cold DCE, and dried overnight to furnish **DPyBI-05-bisBF$_2$** (119 mg, 0.21 mmol, yield = 78%) as an off-white solid. ^{1}H NMR (400 MHz,$(CD_3)_2CO$, 298 K): δ 9.07 (s, 1H), 8.87 (s, 1H), 8.57 (d, *J* = 8.4 Hz, 1H), 8.49 (d, *J* = 8.4 Hz, 1H), 8.38 (t, *J* = 8.7 Hz, 1H), 8.28 (m, 2H), 8.10 (d, *J* = 7.8 Hz, 1H), 7.71 (d, *J* = 7.8 Hz, 1H), 7.62 (t, *J* = 7.8 Hz, 1H), 7.20–6.98 (m, 2H), 2.71 (s, 6H), 2.61 (s, 6H);^{13}C NMR (100 MHz, $(CD_3)_2CO$, 298 K): δ 158.57, 152.99, 148.56, 146.69, 146.31, 144.72, 144.27, 143.43, 138.69, 138.38, 136.45, 132.82, 131.86, 129.45, 128.82, 128.71, 128.62, 128.53, 124.99, 122.46, 122.17, 120.82, 120.51, 117.06, 110.74, 45.31, 18.31; ^{11}B NMR (128 MHz, $(CD_3)_2CO$, 298 K): δ 1.87, 0.48, –0.90; ^{19}F NMR (376 MHz, $(CD_3)_2CO$, 298 K): δ–131.30, –137.48, –151.17

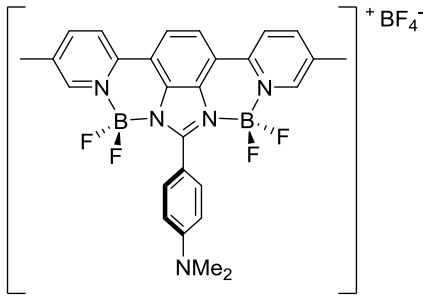

DPyBI-07-bisBF$_2$. This compound was prepared in a manner similar to that described for **DPyBI-02-bisBF$_2$**, except that **DPyBI-07** was used instead of **DPyBI-02**. **DPyBI-04-bisBF$_2$** (yield = 78%) was obtained as anorange solid by filtration and subsequent washing with CH_2Cl_2. ^{1}H NMR (400 MHz, DMSO, 298 K): δ 9.03 (s, 2H), 8.97 (d, *J* = 8.5 Hz, 2H), 8.66 (s, 2H), 8.59 (d, *J* = 8.2 Hz, 2H), 8.09 (d, *J* = 8.8 Hz, 2H), 6.97 (d, *J* = 8.9 Hz, 2H), 3.12 (s, 6H), 2.60 (s, 6H).

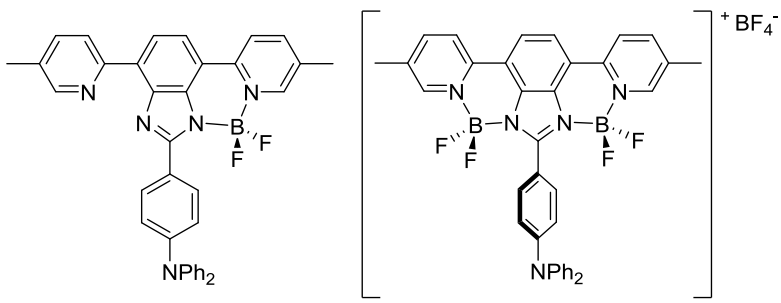

DPyBI-08-BF$_2$and **DPyBI-08-bisBF$_2$.**A 50-mL 3-neck RBF was charged with **DPyBI-08** (163 mg, 0.30 mmol) under Ar. DCE (8 mL) and DIPEA (0.4 mL) were added and the mixture was heated at reflux. To the mixture was slowly added BF_3•OEt_2 (0.4 mL) over a period of 20 min. The resulting red mixture was stirred at reflux for 12 h. After cooling to r.t., H_2O was added to the mixture, which was subsequently extracted with CH_2Cl_2. The combined extracts were dried over $MgSO_4$, filtered, and concentrated under the reduced pressure. The residual materials were

purified by flash column chromatography on SiO_2 (CH_2Cl_2:MeOH = 200:1 to 10:1, v/v) to furnish **DPyBI-08-BF_2** (33 mg, 0.06 mmol, yield = 19%) as an orange solid and **DPyBI-08-bisBF_2** (155 mg, 0.21 mmol, yield = 71%) as a red solid.

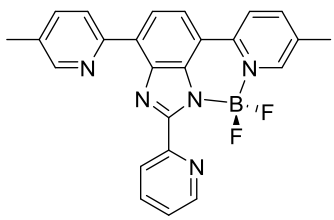

DPyBI-10-BF_2. An oven-dried 50-mL 3-neck RBF was charged with **DPyBI-10** (133 mg, 0.35 mmol) under Ar. Toluene (14 mL) and DIPEA (0.3 mL) were added and the mixture was heated at reflux. To the mixture was slowly added BF_3•OEt_2 (0.1 mL) over a period of 30 min. The resulting mixture was stirred at reflux for 12 h. After cooling to r.t., the mixture was concentrated under reduced pressure. Flash column chromatography on SiO_2 (hexane:acetone = 3:1 to 1:2, v/v) and recrystallization from acetone/pentane gave **DPyBI-10-BF_2** (122 mg, 0.29 mmol, yield =82%). ^{1}H NMR (300 MHz, $CDCl_3$, 298 K): δ 9.23 (d, *J* = 8.1 Hz, 1H), 8.96–8.88 (m, 1H), 8.74 (s, 1H), 8.65–8.53 (m, 2H), 8.35 (d, *J* = 8.2 Hz, 1H), 8.12 (d, *J* = 8.5 Hz, 1H), 7.98–7.81 (m, 3H), 7.72 (dd, *J* = 8.1, 1.6 Hz, 1H), 7.41 (ddd, *J* = 7.5, 4.8, 1.1 Hz, 1H), 2.44 (s, 6H);^{13}C NMR (75 MHz, $CDCl_3$, 298 K): δ 156.50, 151.79, 150.45, 150.06, 149.75, 146.79, 143.40, 143.22, 142.07, 137.34, 136.43, 136.35, 133.95, 133.91, 132.69, 125.81, 124.65, 124.18, 121.65, 119.77, 119.10, 113.13, 18.59;

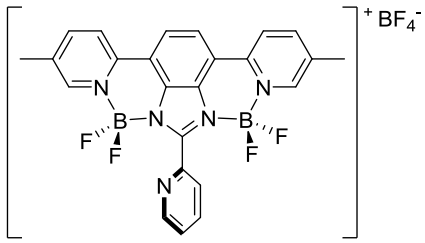

DPyBI-10-bisBF$_2$. This compound was prepared in a manner similar to that described for **DPyBI-02-bisBF$_2$**, except that **DPyBI-10** was used instead of **DPyBI-02**. **DPyBI-10-bisBF$_2$** (yield = 57%) was obtained as a yellow crystal by filtration and subsequent washing with CH_2Cl_2, $CHCl_3$, and MeCN. ^{1}H NMR (400 MHz, DMSO, 298 K): δ 9.04–8.79 (m, 5H), 8.68 (s, 2H), 8.51 (d, *J* = 8.3 Hz, 2H), 8.22–8.14 (m, 2H), 7.76 (dd, *J* = 7.2, 4.8 Hz, 1H), 2.41 (s, 6H); ^{13}C NMR (100 MHz, DMSO, 298 K): δ 150.32, 146.31, 144.43, 143.19, 142.92, 138.46, 137.61, 129.59, 127.36, 126.34, 123.62, 122.82, 118.52, 18.03; ^{19}F NMR (376 MHz, DMSO, 298 K): δ –130.79, –148.25, –148.31.

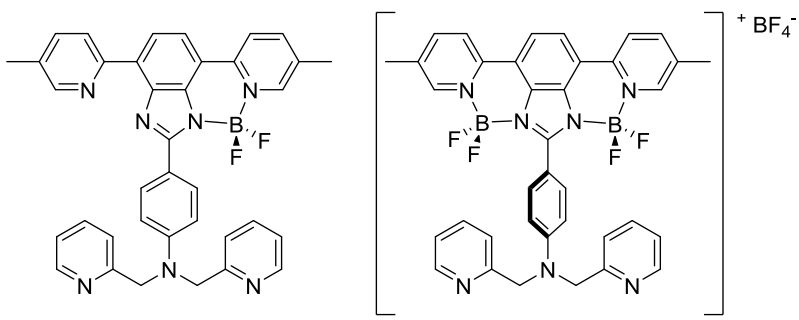

DPyBI-16-BF$_2$ and **DPyBI-16-bisBF$_2$.**This compound was prepared in a manner similar to that described for **DPyBI-08-BF$_2$**, except that **DPyBI-16** was used instead of **DPyBI-08**, and the reaction mixture was heated at reflux for 18 h prior to cooling and concentration. **DPyBI-16-BF$_2$** was isolated as anorange solid (32 mg, 0.05 mmol, yield = 25%) and **DPyBI-16-bisBF$_2$** was obtained as a dark-red solid (40 mg, 0.05

mmol, yield = 26%) after flash column chromatography on SiO_2 (CH_2Cl_2:MeOH = 100:1 to 100:7, v/v).

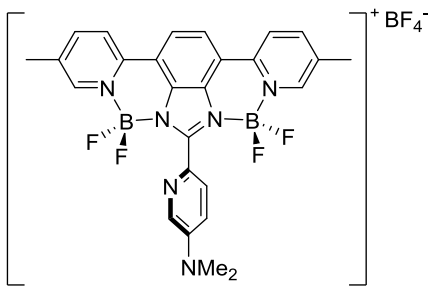

DPyBI-11-bisBF$_2$. This compound was prepared in a manner similar to that described for **DPyBI-02-bisBF$_2$**, except that **DPyBI-11** was used instead of **DPyBI-02**. **DPyBI-11-bisBF$_2$**(yield = 60%) was obtained by filtration and subsequent washing with CH_2Cl_2.

X-ray Crystallographic Studies onDPyBI-10

A yellow crystal of approximate dimensions 0.2 × 0.07 × 0.06 mm^{3}was placed on a nylon loop with paraton-N oil and mounted on a SuperNova, Dual, Cu at zero, AtlasS2 diffractometer. The data collection was carried out using Cu Kα radiation at *T* = 100 K with a frame time of 8.7 seconds and a detector distance of 5.3 cm.A randomly oriented region of reciprocal space was surveyed to achieve complete data with a redundancy of 4. Sections of frames were collected with 1^o steps in ω and φ scans. Data to a resolution of 0.80Å were considered in the reduction. Final cell constants were calculated from the xyz centroids of 3771 strong reflections from actual data collection after integration. The intensity data were corrected for absorption.

The space group $P2_1/n$ was determined based on intensity statistics and systematic absences. The structure was solved using OLEX2,[30] SHELXT[31] structure solution program (Direct Methods) and refined with the SHELXL[32]refinement package using Least Squares minimization.Data for **DPyBI-10**: a = 4.8076(1) Å , b = 33.7498(8) Å , c = 11.3550(3) Å , β = 95.966(2) °, V = 1832.44(8) Å ^{3}. The final full matrix least squares refinement converged to $R1$ = 0.0418 and $wR2$ = 0.1161 (F^2, all data).

X-ray Crystallographic Studies onDPyBI-10-BF_2

A yellow crystal of approximate dimensions 0.1 × 0.06 × 0.06 mm^3 was placed on a nylon loop with paraton-N oil and mounted on a SuperNova, Dual, Cu at zero, AtlasS2 diffractometer. The data collection was carried out using Mo Kα radiation at T = 100 K with a frame time of 40 seconds and a detector distance of 5.3 cm. A randomly oriented region of reciprocal space was surveyed to achieve complete data with a redundancy of 3. Sections of frames were collected with 1° steps in ω and φ scans. Data to a resolution of 0.84 Å were considered in the reduction. Final cell constants were calculated from the xyz centroids of 4190 strong reflections from actual data collection after integration. The intensity data were corrected for absorption.

The space group $P\bar{1}$ was determined based on intensity statistics and systematic absences. The structure was solved using OLEX2,[30] SHELXT[31] structure solution program (Direct Methods) and refined with the SHELXL[32] refinement package using Least Squares minimization. Data for **DPyBI-10-BF_2**: a = 7.8843(5) Å , b = 15.008(1) Å , c = 18.129(1) Å , α = 65.882(6) °, β = 95.966(2) °,γ = 86.629(5) °,V =

1954.3(2) Å^3. The final full matrix least squares refinement converged to $R1 = 0.0429$ and $wR2 = 0.1280$ (F^2, all data).

X-ray Crystallographic Studies onDPyBI-10-bisBF$_2$

A yellow crystal of approximate dimensions 0.2 × 0.06 × 0.06 mm^3 was placed on a nylon loop with paraton-N oil and mounted on a SuperNova, Dual, Cu at zero, AtlasS2 diffractometer. The data collection was carried out using Cu Kα radiation at T = 100 K with a frame time of 3.6 seconds and a detector distance of 5.3 cm. A randomly oriented region of reciprocal space was surveyed to achieve complete data with a redundancy of 2. Sections of frames were collected with 1^o steps in ω and φ scans. Data to a resolution of 0.80 Å were considered in the reduction. Final cell constants were calculated from the xyz centroids of 4991 strong reflections from actual data collection after integration. The intensity data were corrected for absorption.

The space group $P2_1/n$ was determined based on intensity statistics and systematic absences. The structure was solved using OLEX2,[30] SHELXT[31] structure solution program (Direct Methods) and refined with the SHELXL[32] refinement package using Least Squares minimization. Data for **DPyBI-10-bisBF$_2$**: a = 8.9382(1) Å , b = 11.9348(3) Å , c = 22.5107(4) Å , β = 93.380(2)^o, V = 2397.18(8) Å^3. The final full matrix least squares refinement converged to $R1 = 0.0482$ and $wR2 = 0.1388$ (F^2, all data).

DpyBI-10

checkCIF/PLATON report

Structure factors have been supplied for datablock(s) exp_391

THIS REPORT IS FOR GUIDANCE ONLY. IF USED AS PART OF A REVIEW PROCEDURE FOR PUBLICATION, IT SHOULD NOT REPLACE THE EXPERTISE OF AN EXPERIENCED CRYSTALLOGRAPHIC REFEREE.

No syntax errors found. CIF dictionary Interpreting this report

Datablock: exp_391

```
Bond precision:  C-C = 0.0019 A          Wavelength=1.54184

Cell:           a=4.80761(12)     b=33.7498(8)       c=11.3550(3)
                alpha=90          beta=95.966(2)     gamma=90
Temperature:    100 K

                Calculated                Reported
Volume          1832.44(8)                1832.44(8)
Space group     P 21/n                    P 1 21/n 1
Hall group      -P 2yn                    -P 2yn
Moiety formula  C24 H19 N5                C24 H19 N5
Sum formula     C24 H19 N5                C24 H19 N5
Mr              377.44                    377.44
Dx,g cm-3       1.368                     1.368
Z               4                         4
Mu (mm-1)       0.663                     0.663
F000            792.0                     792.0
F000'           794.17
h,k,lmax        6,42,14                   6,42,14
Nref            3833                      3771
Tmin,Tmax       0.944,0.964               0.917,0.970
Tmin'           0.874

Correction method= # Reported T Limits: Tmin=0.917 Tmax=0.970
AbsCorr = GAUSSIAN

Data completeness= 0.984          Theta(max)= 76.568

R(reflections)= 0.0418( 3293)     wR2(reflections)= 0.1161( 3771)

S = 1.033                 Npar= 264
```

Datablock exp_391 - ellipsoid plot

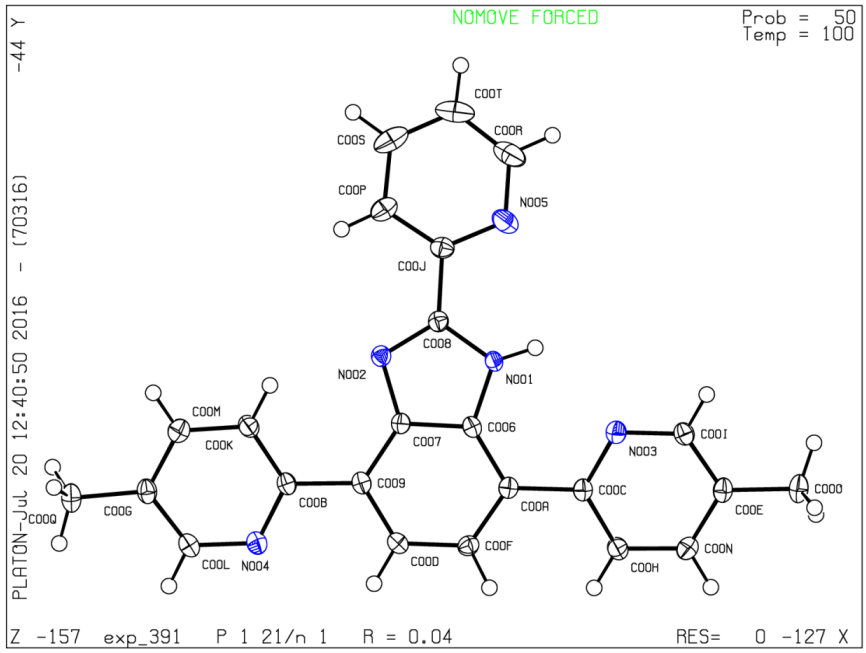

DpyBI-10-BF_2

checkCIF/PLATON report

Structure factors have been supplied for datablock(s) lbr-01-py-bf2

THIS REPORT IS FOR GUIDANCE ONLY. IF USED AS PART OF A REVIEW PROCEDURE FOR PUBLICATION, IT SHOULD NOT REPLACE THE EXPERTISE OF AN EXPERIENCED CRYSTALLOGRAPHIC REFEREE.

No syntax errors found. CIF dictionary Interpreting this report

Datablock: lbr-01-py-bf2

```
Bond precision:  C-C = 0.0048 A          Wavelength=0.71073

Cell:          a=7.8843(5)       b=15.008(1)      c=18.1293(11)
               alpha=65.882(6)   beta=89.420(5)   gamma=86.629(5)
Temperature:   100 K
```

	Calculated	Reported
Volume	1954.3(2)	1954.3(2)
Space group	P -1	P -1
Hall group	-P 1	-P 1
Moiety formula	C24 H18 B F2 N5	C24 H18 B F2 N5
Sum formula	C24 H18 B F2 N5	C24 H18 B F2 N5
Mr	425.24	425.24
Dx,g cm-3	1.445	1.445
Z	4	4
Mu (mm-1)	0.101	0.101
F000	880.0	880.0
F000'	880.38	
h,k,lmax	9,17,21	9,15,21
Nref	7064	4190
Tmin,Tmax		0.893,1.000
Tmin'		

```
Correction method= # Reported T Limits: Tmin=0.893 Tmax=1.000
AbsCorr = MULTI-SCAN

Data completeness= 0.593          Theta(max)= 25.215

R(reflections)= 0.0429( 3493)     wR2(reflections)= 0.1280( 4190)

S = 1.087                 Npar= 581
```

Datablock lbr-01-py-bf2 - ellipsoid plot

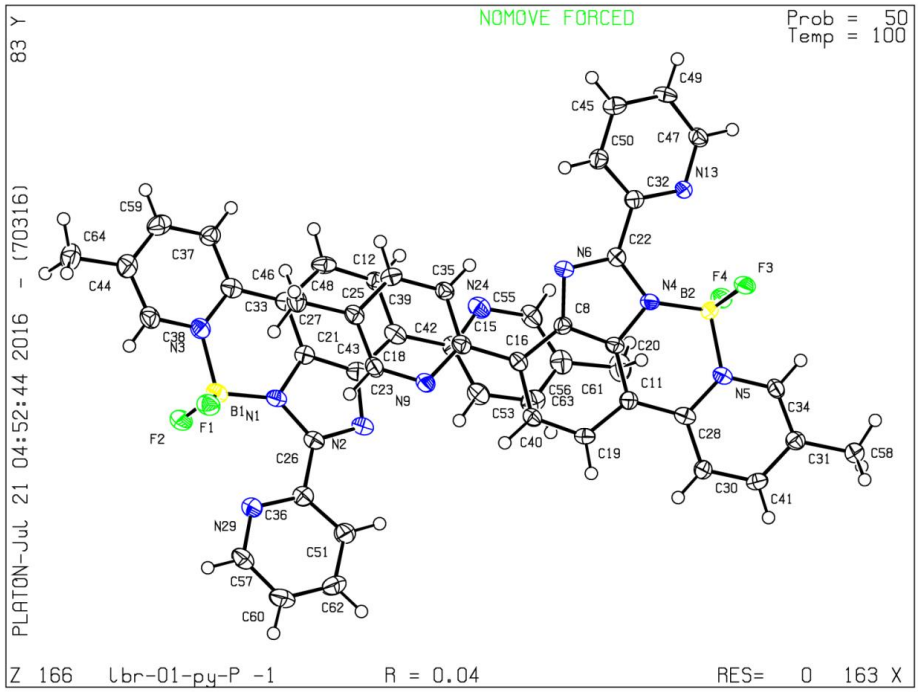

DpyBI-10-bisBF$_2$

checkCIF/PLATON report

Structure factors have been supplied for datablock(s) exp_403

THIS REPORT IS FOR GUIDANCE ONLY. IF USED AS PART OF A REVIEW PROCEDURE FOR PUBLICATION, IT SHOULD NOT REPLACE THE EXPERTISE OF AN EXPERIENCED CRYSTALLOGRAPHIC REFEREE.

No syntax errors found. CIF dictionary Interpreting this report

Datablock: exp_403

Bond precision: C-C = 0.0026 A Wavelength=1.54184

Cell: a=8.93824(14) b=11.9348(3) c=22.5107(4)
alpha=90 beta=93.3802(15) gamma=90
Temperature: 100 K

	Calculated	Reported
Volume	2397.18(8)	2397.18(8)
Space group	P 21/n	P 1 21/n 1
Hall group	-P 2yn	-P 2yn
Moiety formula	C24 H18 B2 F4 N5, B F4, H2 O	C24 H18 B2 F4 N5, B F4, H2 O
Sum formula	C24 H20 B3 F8 N5 O	C24 H20 B3 F8 N5 O
Mr	578.88	578.88
Dx,g cm-3	1.604	1.604
Z	4	4
Mu (mm-1)	1.243	1.243
F000	1176.0	1176.0
F000'	1180.76	
h,k,lmax	11,15,28	11,14,28
Nref	5036	4991
Tmin,Tmax	0.895,0.934	0.940,0.986
Tmin'	0.681	

Correction method= # Reported T Limits: Tmin=0.940 Tmax=0.986
AbsCorr = GAUSSIAN

Data completeness= 0.991 Theta(max)= 76.494

R(reflections)= 0.0482(4413) wR2(reflections)= 0.1388(4991)

S = 1.043 Npar= 412

Datablock exp_403 - ellipsoid plot

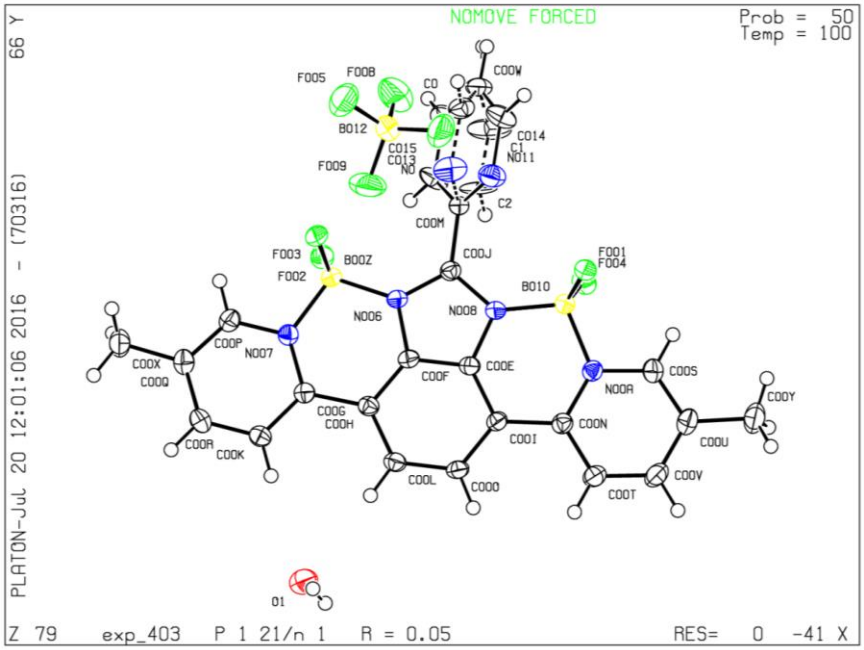

References

[1] de Silva, A. P.; Gunaratne, H. Q.; Gunnlaugsson, T.; Huxley, A. J.; M cCoy, C. P.; Rademacher, J. T.; Rice, T. E. *Chem. Rev.* **1997**, *97*, 1515 –1566.

[2] a) Hayek, A. ; Bolze, F.; Bourgogne, C.; Baldeck, P. L.; Didier, P.; Ar ntz, Y.; Mely, Y.; Nicoud, J. F., *Inorg. Chem.* **2009**, *48*, 9112–9119; b) Ding, D.; Li, K.; Liu, B.; Tang, B. Z., *Acc. Chem. Res.* **2013**, *46*, 24 41–2453; c) Kim, H. J.; Heo, C. H.; Kim, H. M., *J. Am. Chem. Soc.* **2013**, *135*, 17969–17977.

[3] a) Carter, K. P.; Young, A. M.; Palmer, A. E., *Chem. Rev.* **2014**, *114*, 4564–4601; b) Jo, J.; Lee, H. Y.; Liu, W.; Olasz, A.; Chen, C. H.; Le e, D., *J. Am. Chem. Soc.* **2012**, *134*, 16000–16007.

[4] a) Hutt, J. T.; Jo, J.; Olasz, A.; Chen, C. H.; Lee, D.; Aron, Z. D., *O rg. Lett.* **2012**, *14*, 3162–3165; b) Wang, R.; Yu, C.; Yu, F.; Chen, L.; Yu, C., *Trends Anal. Chem.* **2010**, *29*, 1004–1013; c) Han, J.; Burgess, K., *Chem. Rev.* **2010**, *110*, 2709–2728.

[5] Li, D.; Zhang, H.; Wang, Y., *Chem. Soc. Rev.* **2013**, *42*, 8416–8433.

[6] Suresh, M.; Mandal, A. K.; Saha, S.; Suresh, E.; Mandoli, A.; Di Lidd o, R.; Parnigotto, P. P.; Das, A., *Org. Lett.* **2010**, *12*, 5406–5409.

[7] Baranov, M. S. ; Lukyanov, K. A.; Borissova, A. O.; Shamir, J.; Kose nkov, D.; Slipchenko, L. V.; Tolbert, L. M.; Yampolsky, I. V.; Solntsev, K. M., *J. Am. Chem. Soc.* **2012**, *134*, 6025–6032.

[8] a) Guo, Z.; Park, S.; Yoon, J.; Shin, I., *Chem. Soc. Rev.* **2014**, *43*, 16 –29; b) Cheng, Y.; Li, G.; Liu, Y.; Shi, Y.; Gao, G.; Wu, D.; Lan, J.;

You, J., *J. Am. Chem. Soc.* **2016**, *138*, 4730–4738.

[9] Loudet, A. ; Burgess, K., *Chem. Rev.* **2007**, *107*, 4891–4932.

[10] Kim, E.; Lee, Y.; Lee, S.; Park, S. B., *Acc. Chem. Res.* **2015**, *48*, 538–547.

[11] a) Ishow, E.; Brosseau, A.; Clavier, G.; Nakatani, K.; Tauc, P.; Fiorini-Debuisschert, C.; Neveu, S.; Sandre, O.; Leaustic, A., *Chem. Mater.* **2008**, *20*, 6597–6599; b) Kamtekar, K. T.; Monkman, A. P.; Bryce, M. R., *Adv. Mater.* **2010**, *22*, 572–582.

[12] a) Zhao, Z.; Lam, J. W. Y.; Tang, B. Z., *J. Mater. Chem.* **2012**, *22*, 23726–23740; b) Mei, J.; Leung, N. L.; Kwok, R. T.; Lam, J. W.; Tang, B. Z., *Chem. Rev.* **2015**, *115*, 11718–11940.

[13] Bansal, Y.; Silakari, O., *Bioorg. Med. Chem.* **2012**, *20*, 6208–6236.

[14] Neto, B. A. D.; Lopes, A. S. A.; Ebeling, G.; Gonçalves, R. S.; Costa, V. E. U.; Quina, F. H.; Dupont, J., *Tetrahedron* **2005**, *61*, 10975–10982.

[15] Akhtaruzzaman, M.; Tomura, M.; Nishida, J.-I.; Yamashita, Y., *J. Org. Chem.* **2004**, *69*, 2953–2958.

[16] Pochorovski, I.; Milić, J.; Kolarski, D.; Gropp, C.; Schweizer, W. B.; Diederich, F., *J. Am. Chem. Soc.* **2014**, *136*, 3852–3858.

[17] a) Noujeim, N.; Zhu, K.; Vukotic, V. N.; Loeb, S. J., *Org. Lett.* **2012**, *14*, 2484–2487; b) Sando, S.; Narita, A.; Aoyama, Y., *ChemBioChem* **2007**, *8*, 1795–1803.

[18] Li, G.; Huang, J.; Zhang, M.; Zhou, Y.; Zhang, D.; Wu, Z.; Wang, S.; Weng, X.; Zhou, X.; Yang, G., *Chem. Commun.* **2008**, 4564–4566.

[19] Hansch, C.; Leo, A.; Taft, R. W., *Chem. Rev.* **1991**, *91*, 165–195.

[20] Schubert, U. S.; Eschbaumer, C.; Heller, M., *Org. Lett.* **2000**, *2*, 3373–3376.

[21] Dong, Y.; Du, N.; Li, X.; Zheng, L.; Liu, G., *Org. Lett.* **2015**, *17*, 4110–4113.

[22] Liu, T.; Huo, F.; Yin, C.; Li, J.; Chao, J.; Zhang, Y., *Dyes Pigm.* **2016**, *128*, 209–214.

[23] López-Rodríguez, R.; Ros, A.; Fernández, R.; Lassaletta, J. M., *J. Org. Chem.* **2012**, *77*, 9915–9920.

[24] Felten, A. E.; Zhu, G.; Aron, Z. D., *Org. Lett.* **2010**, *12*, 1916–1919.

[25] Peng, X.; Du, J.; Fan, J.; Wang, J.; Wu, Y.; Zhao, J.; Sun, S.; Xu, T., *J. Am. Chem. Soc.* **2007**, *129*, 1500–1501.

[26] Frisch, M. J.; Trucks, G. W.; Schlegel, H. B.; Scuseria, G. E.; Robb, M. A.; Cheeseman, J. R.; Scalmani, G.; Barone, V.; Mennucci, B.; Petersson, G. A.; Nakatsuji, H.; Caricato, M.; Li, X.; Hratchian, H. P.; Izmaylov, A. F.; Bloino, J.; Zheng, G.; Sonnenberg, J. L.; Hada, M.; Ehara, M.; Toyota, K.; Fukuda, R.; Hasegawa, J.; Ishida, M.; Nakajima, T.; Honda, Y.; Kitao, O.; Nakai, H.; Vreven, T.; Montgomery Jr., J. A.; Peralta, J. E.; Ogliaro, F.; Bearpark, M. J.; Heyd, J.; Brothers, E. N.; Kudin, K. N.; Staroverov, V. N.; Kobayashi, R.; Normand, J.; Raghavachari, K.; Rendell, A. P.; Burant, J. C.; Iyengar, S. S.; Tomasi, J.; Cossi, M.; Rega, N.; Millam, N. J.; Klene, M.; Knox, J. E.; Cross, J. B.; Bakken, V.; Adamo, C.; Jaramillo, J.; Gomperts, R.; Stratmann, R. E.; Yazyev, O.; Austin, A. J.; Cammi, R.; Pomelli, C.; Ochterski, J. W.; Mart

in, R. L.; Morokuma, K.; Zakrzewski, V. G.; Voth, G. A.; Salvador, P.; Dannenberg, J. J.; Dapprich, S.; Daniels, A. D.; Farkas, Ö.; Foresman, J. B.; Ortiz, J. V.; Cioslowski, J.; Fox, D. J., Gaussian, Inc., Wallingford, CT, USA, **2009**.

[27] Zhu, K.; Vukotic, V. N.; Noujeim, N.; Loeb, S. J., *Chem. Sci.* **2012**, *3*, 3265–3271.

[28] Lee, Y.-S.; Cho, Y.-H.; Lee, S.; Bin, J.-K.; Yang, J. H.; Chae, G.; Cheon, C.-H., *Tetrahedron* **2015**, *71*, 532–538.

[29] Arnáiz, F. J., *J. Chem. Educ.* **1995**, *72*, 1139.

[30] Dolomanov, O. V.; Bourhis, L. J.; Gildea, R. J.; Howard, J. A. K.; Puschmann, H., *J. .Appl. Crystallogr.* **2009**, *42*, 339–341.

[31] Sheldrick, G. M., *Acta Crystallogr., Sect. A* **2015**, *71*, 3–8.

[32] Linden, A., *Acta Crystallogr., Sect. C* **2015**, *71*, 1–2.

Spectra

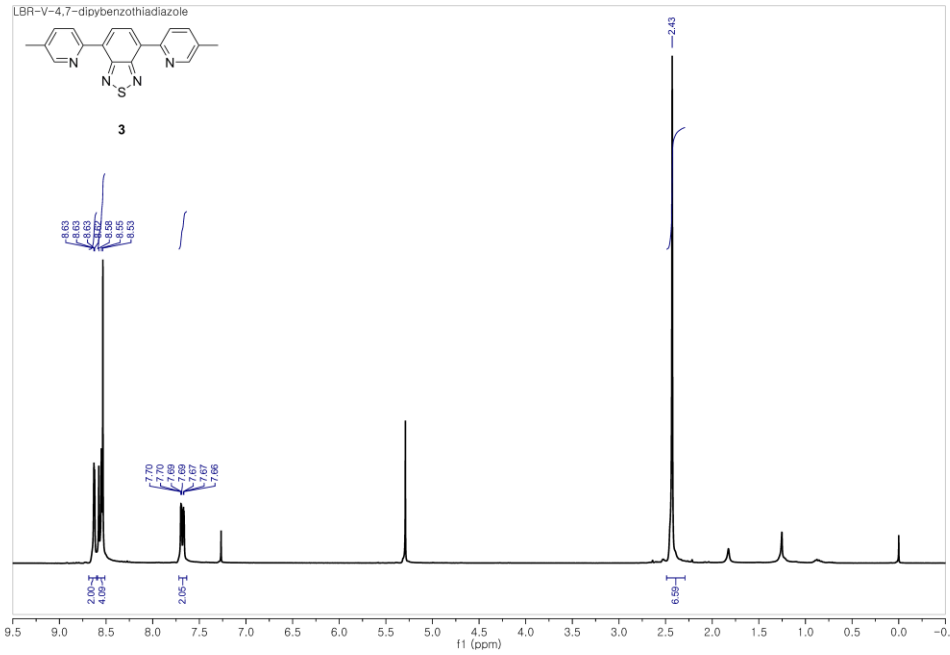
LBR-V-4,7-dipybenzothiadiazole
3
8.63
8.63
8.63
8.56
8.56
8.55
8.53
7.70
7.70
7.69
7.69
7.67
7.67
7.66
2.43
2.00
4.09
2.05
6.59
f1 (ppm)

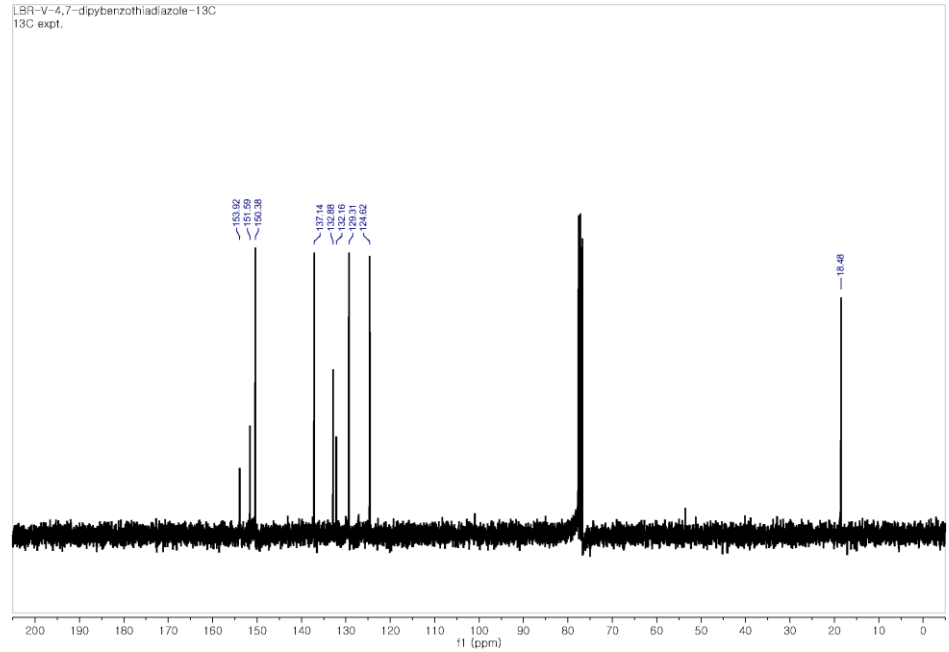
LBR-V-4,7-dipybenzothiadiazole-13C
13C expt.
153.92
151.59
150.38
137.14
132.88
132.16
129.31
124.62
18.48
f1 (ppm)

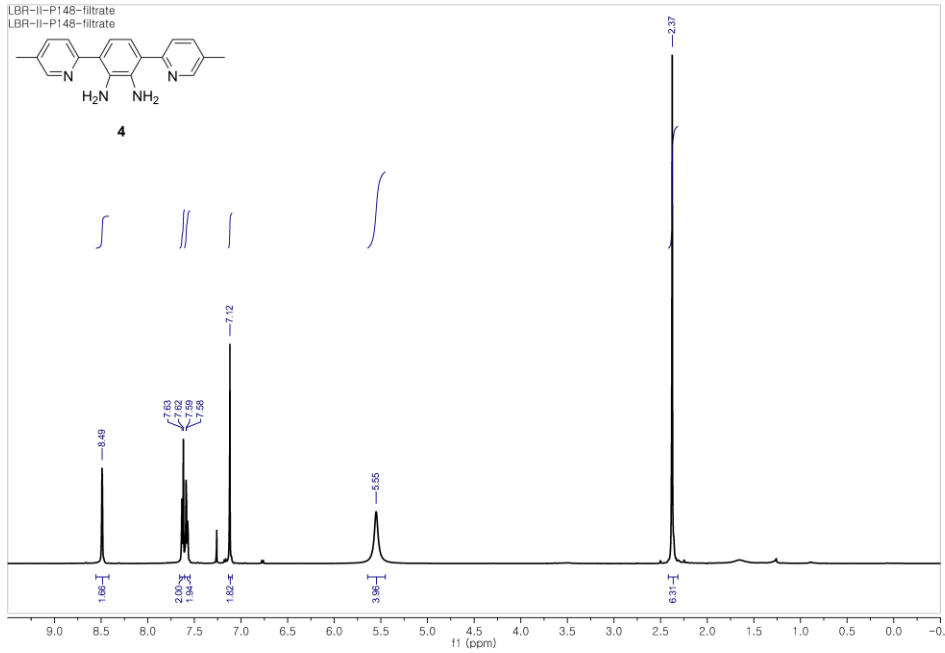
LBR-II-P148-filtrate
LBR-II-P148-filtrate
N
N
H2N
NH2
4
2.37
7.12
7.63
7.62
7.59
7.58
8.49
5.55
1.66
2.00
1.94
1.82
3.96
6.31
f1 (ppm)

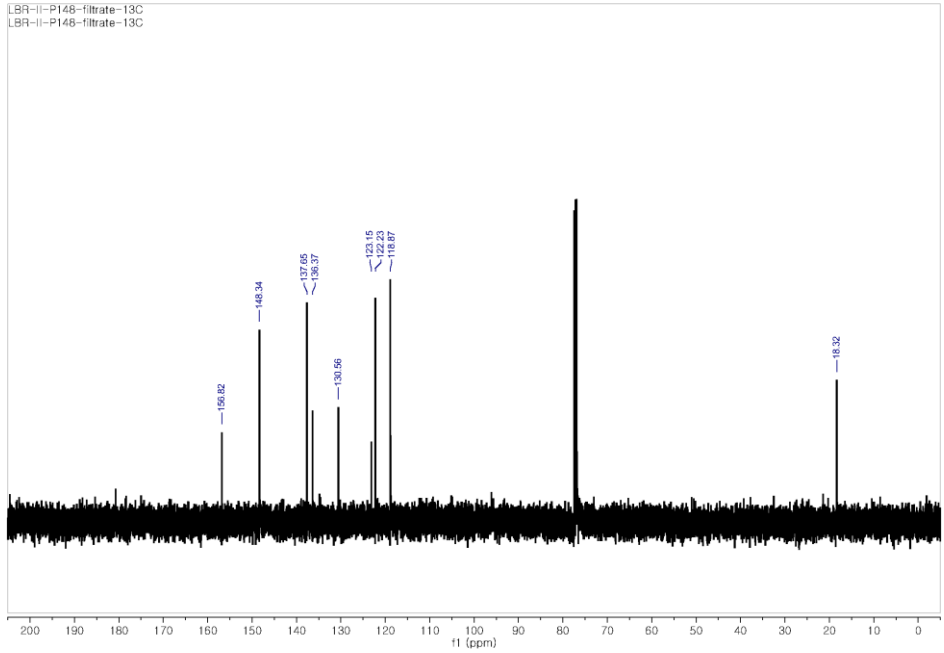
LBR-II-P148-filtrate-13C
LBR-II-P148-filtrate-13C
150.82
148.34
137.65
136.37
130.56
123.15
122.23
118.87
18.32
f1 (ppm)

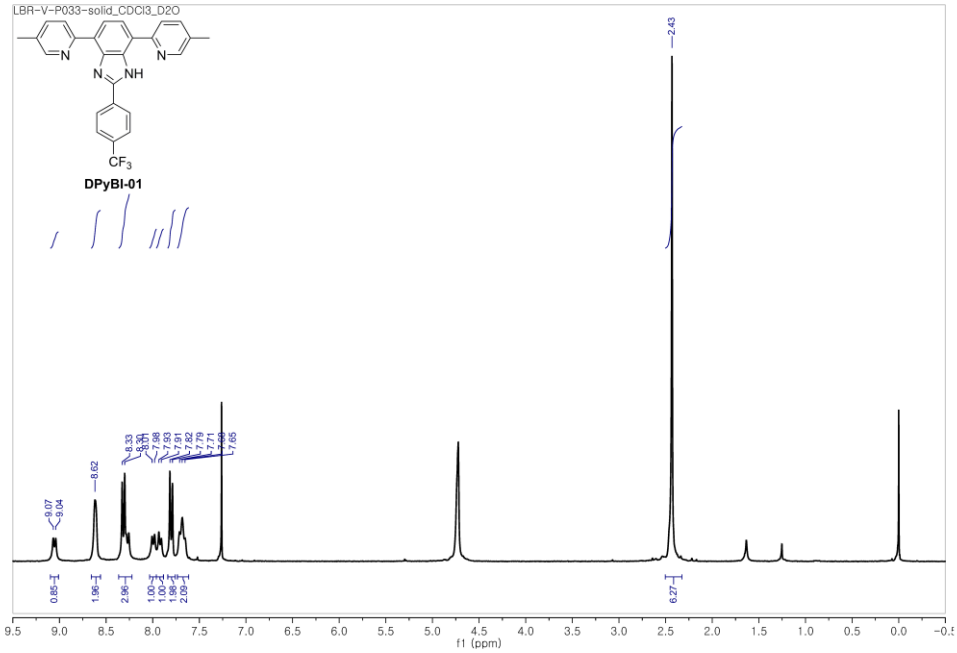
LBR-V-P033-solid_CDCl3_D2O
DPyBI-01
2.43
9.07
9.04
8.62
8.33
8.31
7.98
7.93
7.91
7.82
7.79
7.71
7.68
7.65
0.85
1.96
2.96
1.00
1.00
1.98
2.09
6.27
f1 (ppm)

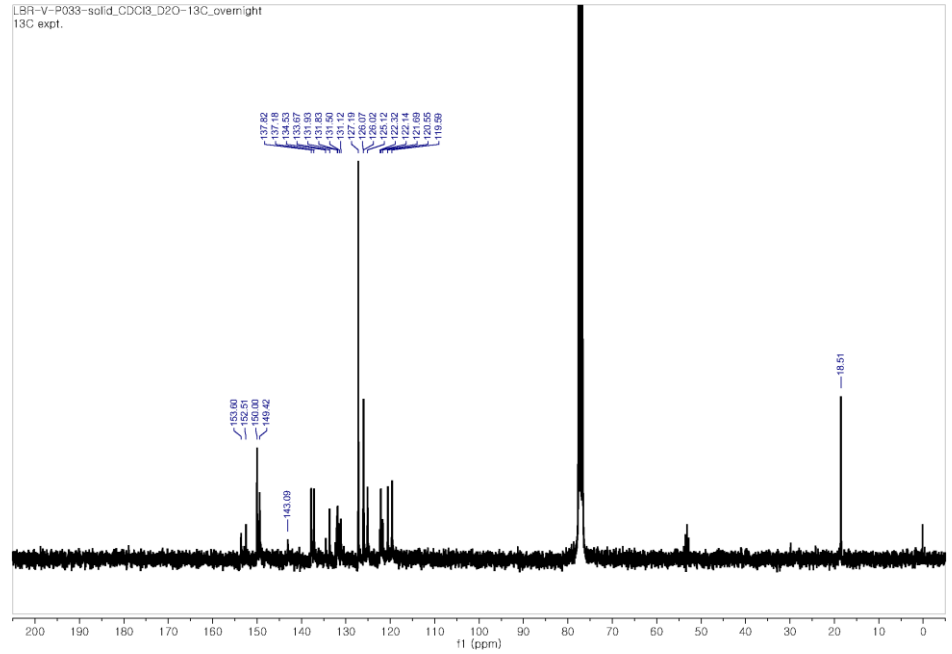
LBR-V-P033-solid_CDCl3_D2O-13C_overnight
13C expt.
137.82
137.18
134.53
133.67
131.63
131.53
131.50
131.12
127.19
126.67
126.02
125.12
122.32
121.74
121.69
120.55
119.59
153.60
152.51
150.00
149.42
143.09
18.51
f1 (ppm)

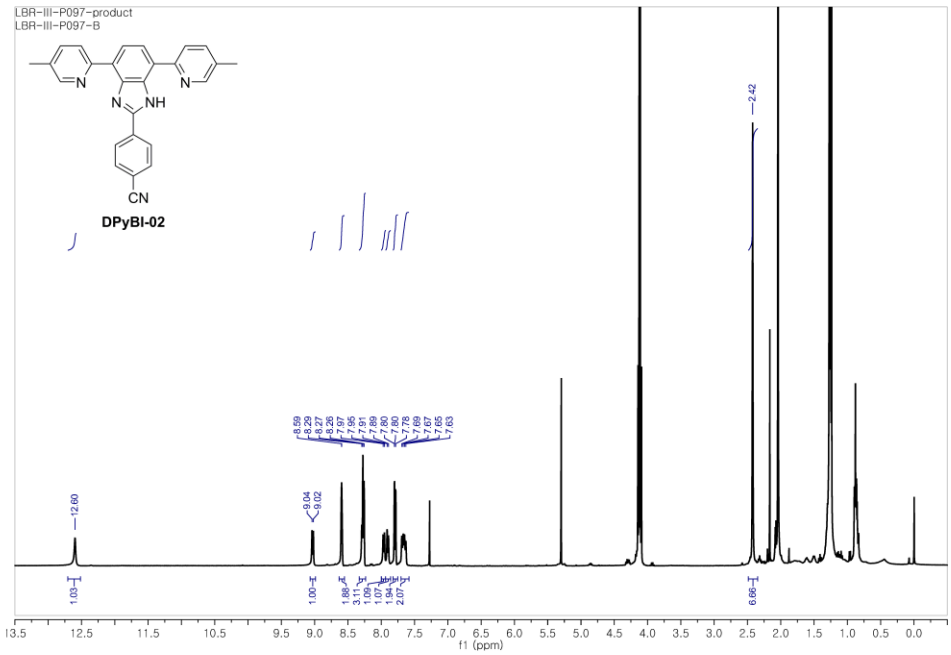
LBR-III-P097-product
LBR-III-P097-B
N
N
NH
N
CN
DPyBI-02
2.42
8.59
8.29
8.27
8.26
7.97
7.95
7.91
7.89
7.80
7.80
7.78
7.78
7.69
7.67
7.65
7.63
12.60
9.04
9.02
1.03
1.00
1.88
3.11
1.09
1.07
1.94
2.07
6.66
f1 (ppm)

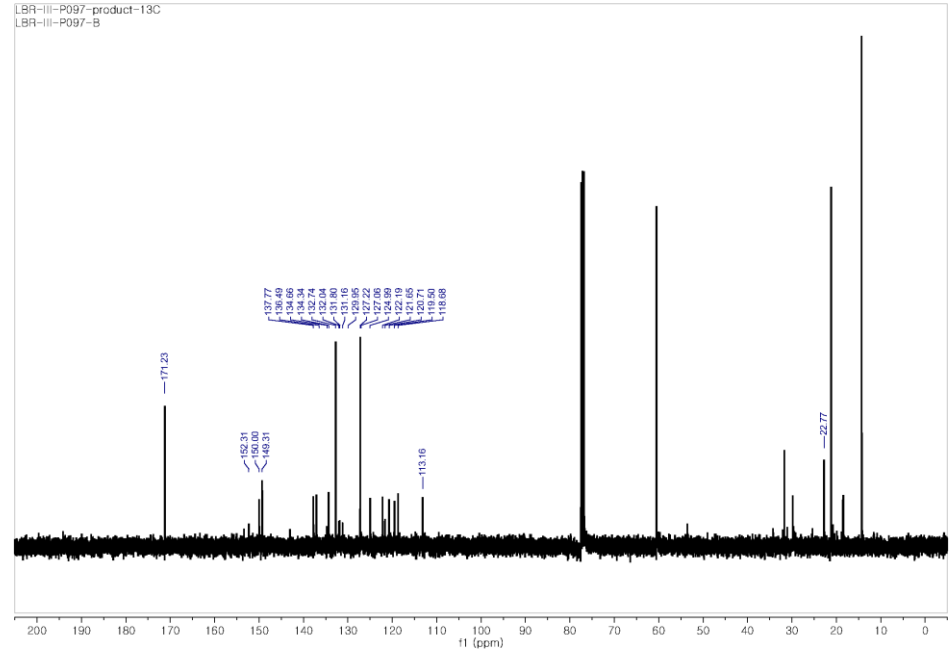
LBR-III-P097-product-13C
LBR-III-P097-B
137.77
136.49
134.66
134.34
132.74
132.64
131.80
131.16
129.95
127.22
127.08
124.99
122.19
121.65
120.71
119.50
118.68
171.23
152.31
150.00
149.31
113.16
22.77
f1 (ppm)

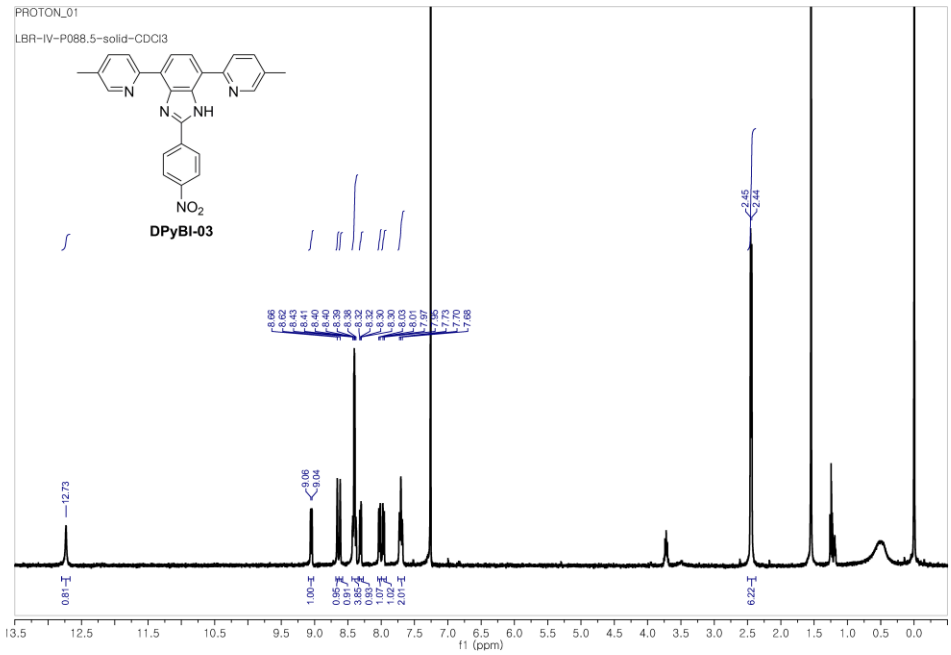
PROTON_01
LBR-IV-P088.5-solid-CDCl3
DPyBI-03
f1 (ppm)

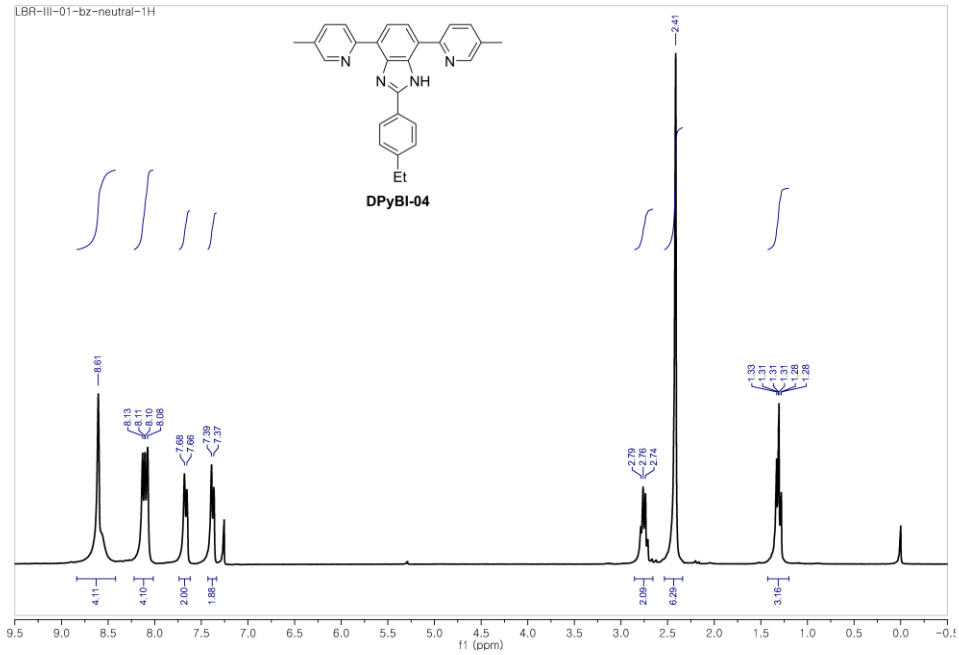
LBR-III-01-bz-neutral-1H
DPyBI-04
f1 (ppm)

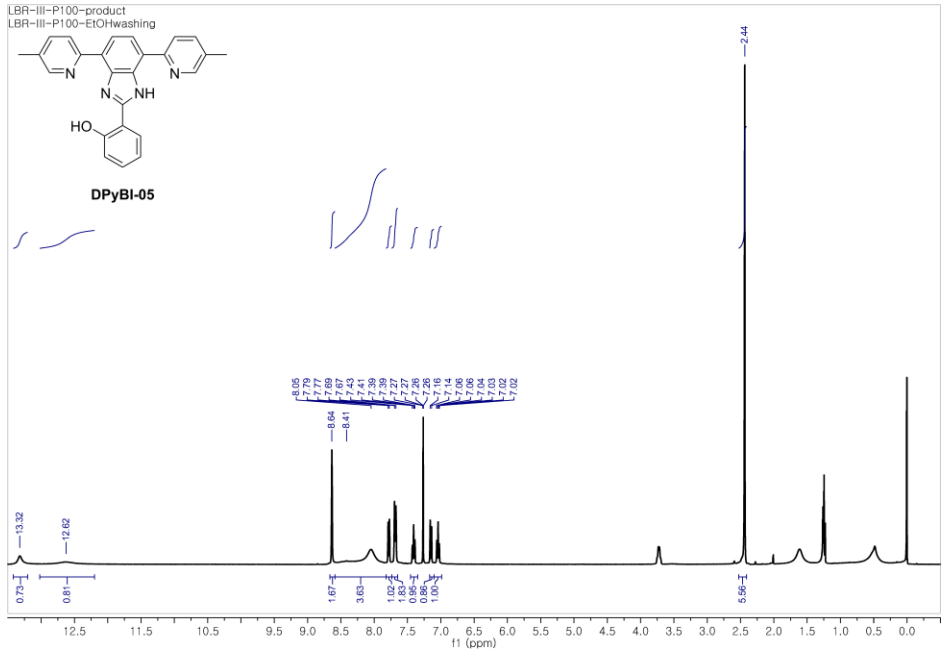
LBR-III-P100-product
LBR-III-P100-EtOHwashing
DPyBI-05
f1 (ppm)

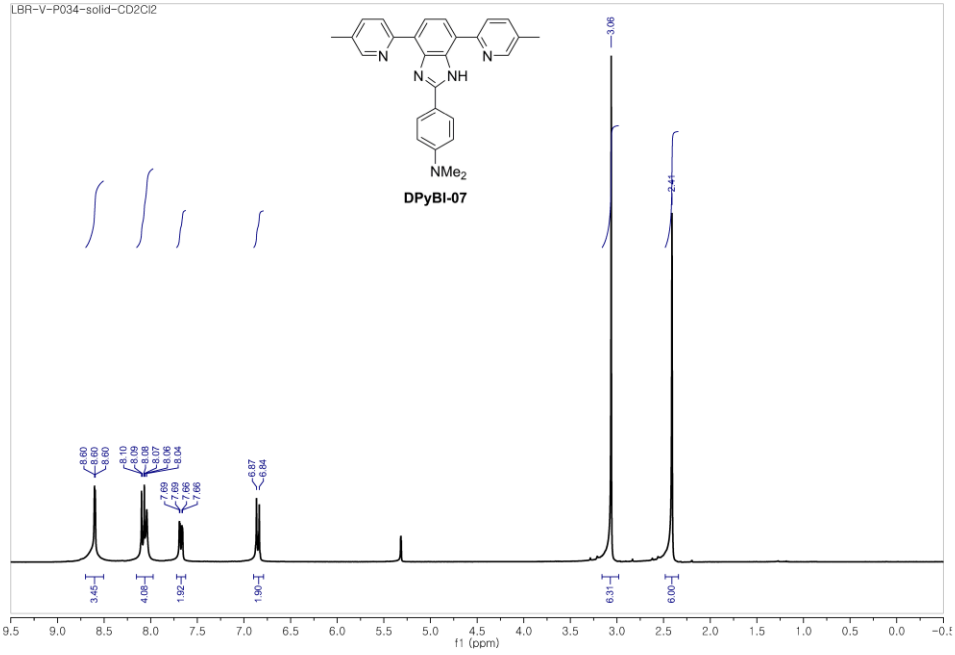
LBR-V-P034-solid-CD2Cl2
DPyBI-07
f1 (ppm)

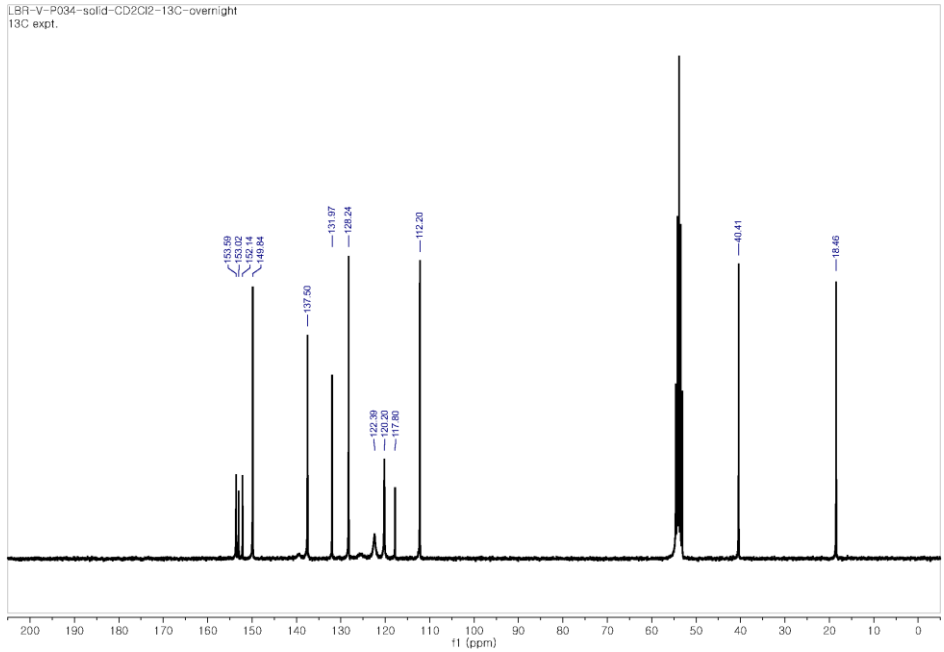
LBR-V-P034-solid-CD2Cl2-13C-overnight
13C expt.
153.59
153.02
152.14
149.84
137.50
131.97
128.24
122.39
120.33
117.80
112.20
40.41
18.46
f1 (ppm)

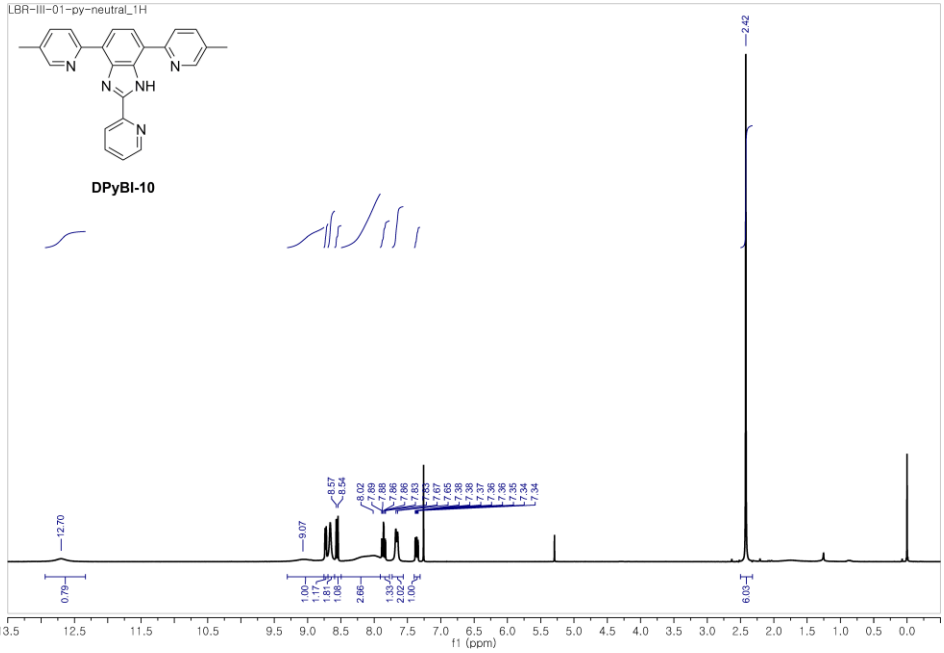
LBR-III-01-py-neutral_1H
DPyBI-10
12.70
9.07
8.57
8.54
8.02
7.88
7.88
7.86
7.86
7.83
7.83
7.67
7.65
7.38
7.38
7.37
7.36
7.36
7.35
7.34
7.34
2.42
f1 (ppm)

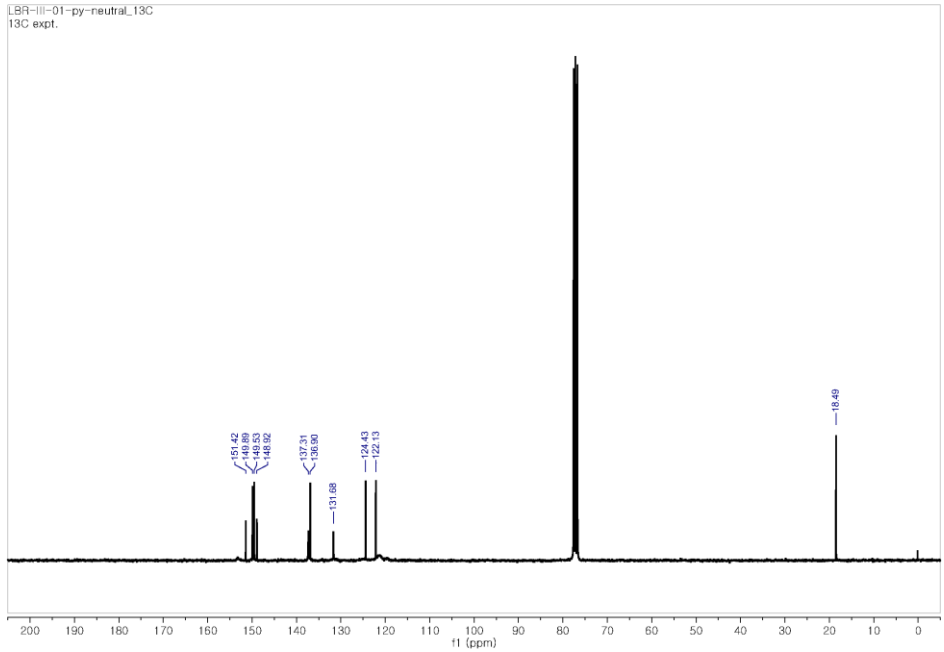
LBR-III-01-py-neutral_13C
13C expt.
151.42
149.89
149.53
148.92
137.31
136.98
131.68
124.43
122.13
18.49
f1 (ppm)

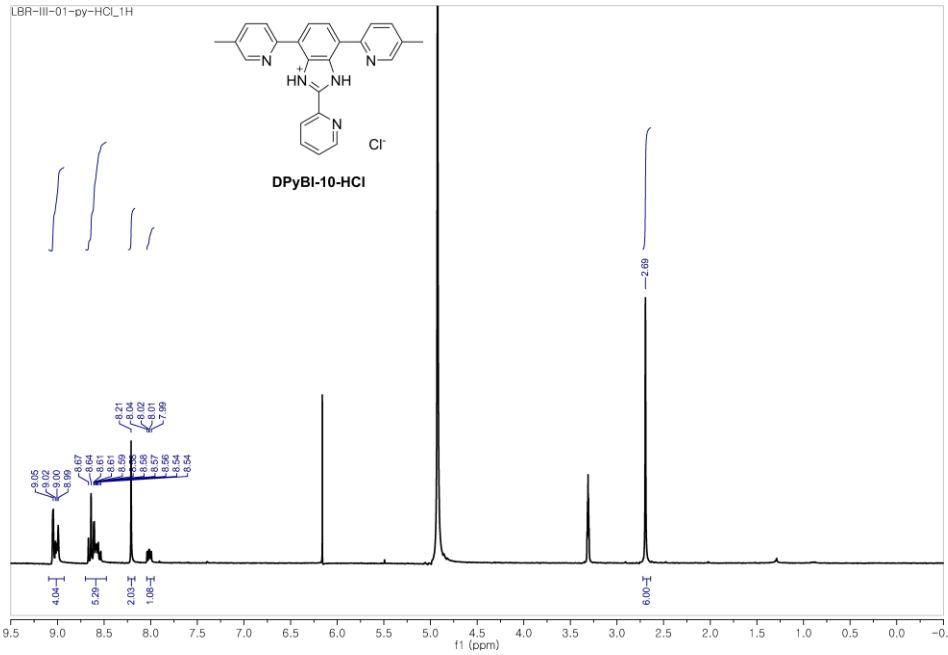
LBR-III-01-py-HCl_1H
DPyBI-10-HCl
Cl-
9.05
9.02
9.00
8.99
8.67
8.64
8.61
8.59
8.21
8.04
8.02
8.01
7.99
8.58
8.57
8.55
8.54
8.54
2.69
4.04
5.29
2.03
1.08
6.00
f1 (ppm)

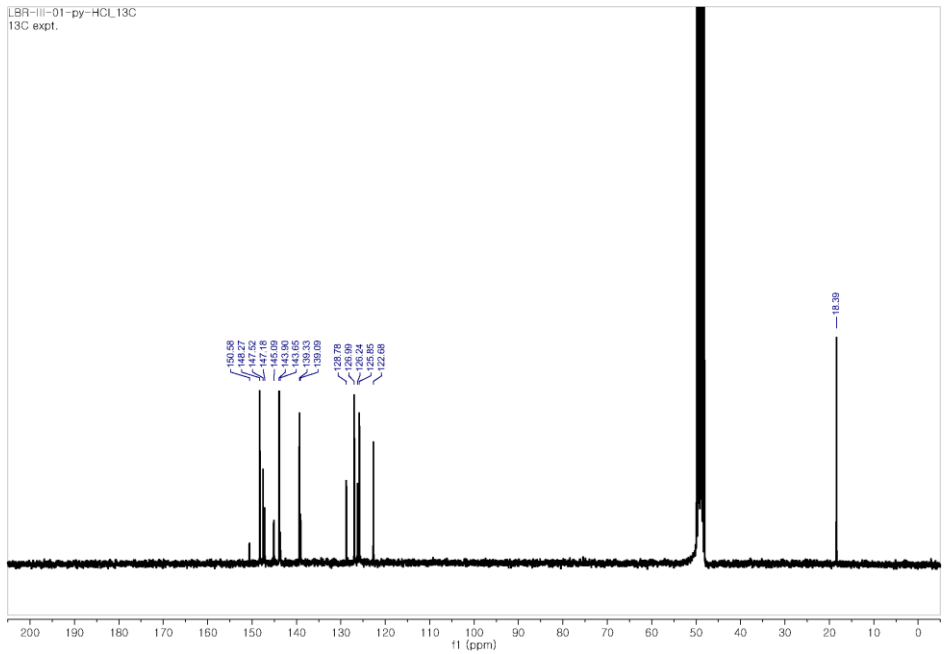
LBR-III-01-py-HCl_13C
13C expt.
150.58
148.27
147.52
147.18
145.09
143.90
143.65
139.33
139.09
128.78
126.99
126.24
125.45
122.68
18.39
f1 (ppm)

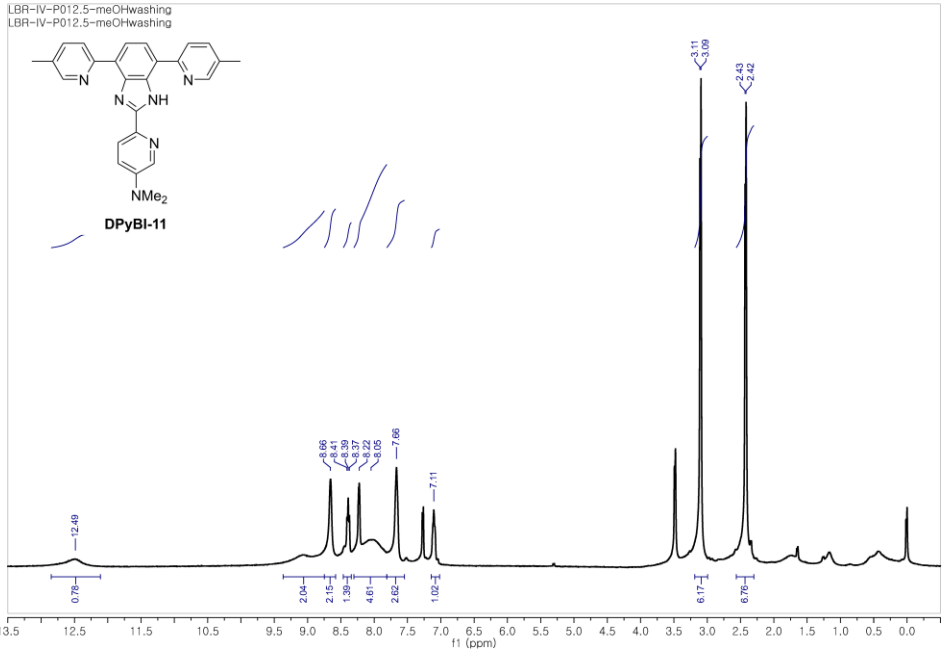
LBR-IV-P012.5-meOHwashing
LBR-IV-P012.5-meOHwashing
N
N
N
NH
N
NMe2
DPyBI-11
3.11
3.09
2.43
2.42
8.66
8.41
8.39
8.37
8.22
8.05
7.66
7.11
12.49
0.78
2.04
2.15
1.39
4.61
2.62
1.02
6.17
6.76
f1 (ppm)

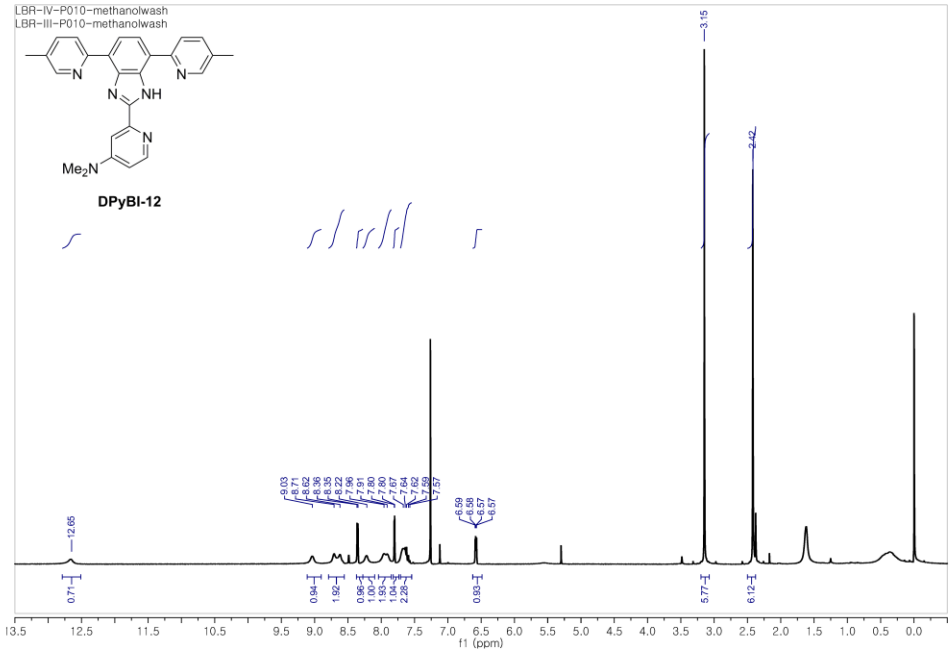
LBR-IV-P010-methanolwash
LBR-III-P010-methanolwash
DPyBI-12
f1 (ppm)

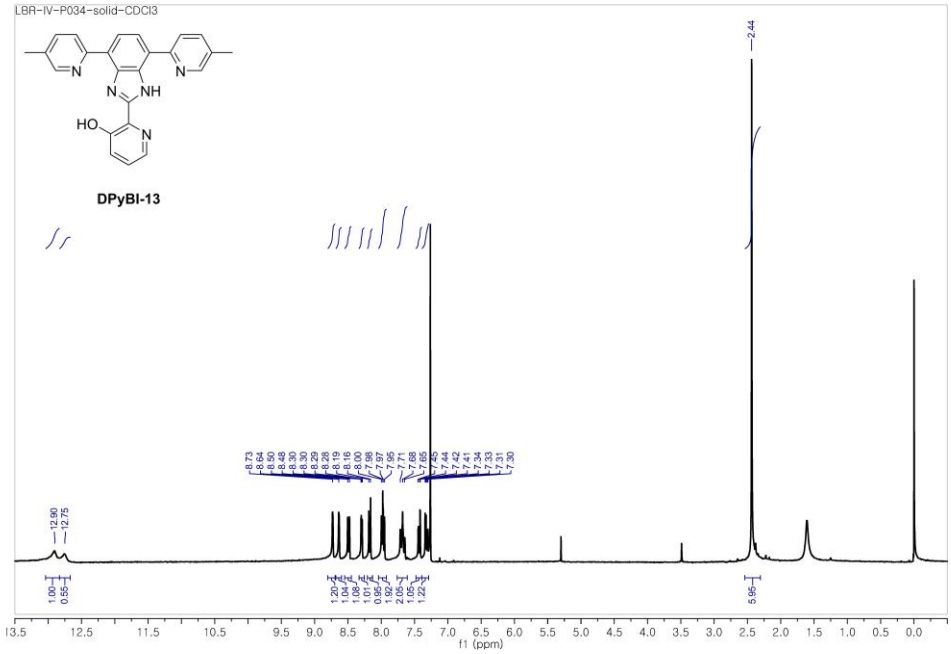
LBR-IV-P034-solid-CDCl3
DPyBI-13
f1 (ppm)

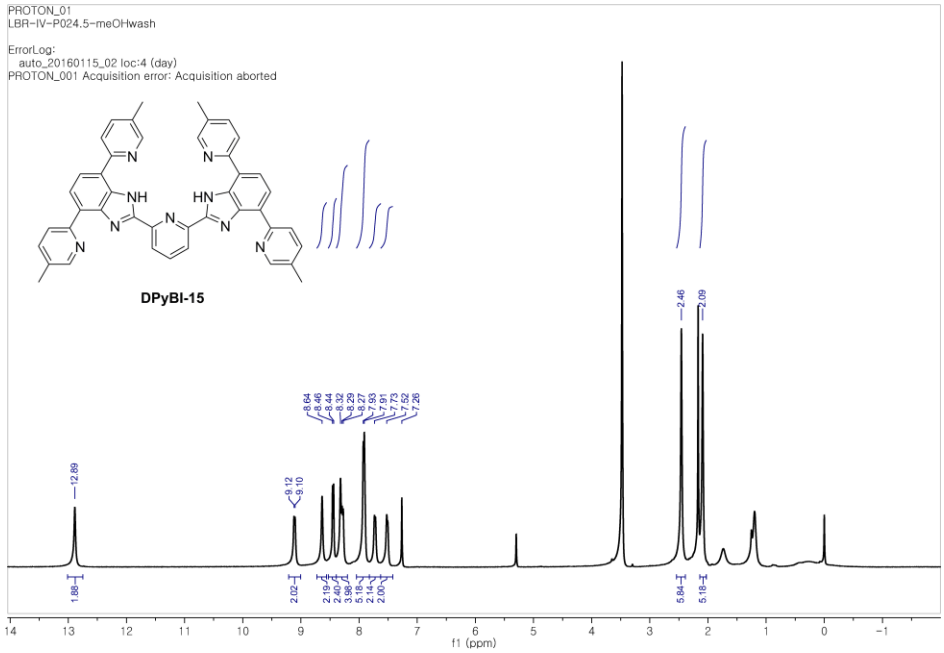
PROTON_01
LBR-IV-P024.5-meOHwash
ErrorLog:
auto_20160115_02 loc:4 (day)
PROTON_001 Acquisition error: Acquisition aborted
DPyBI-15
f1 (ppm)

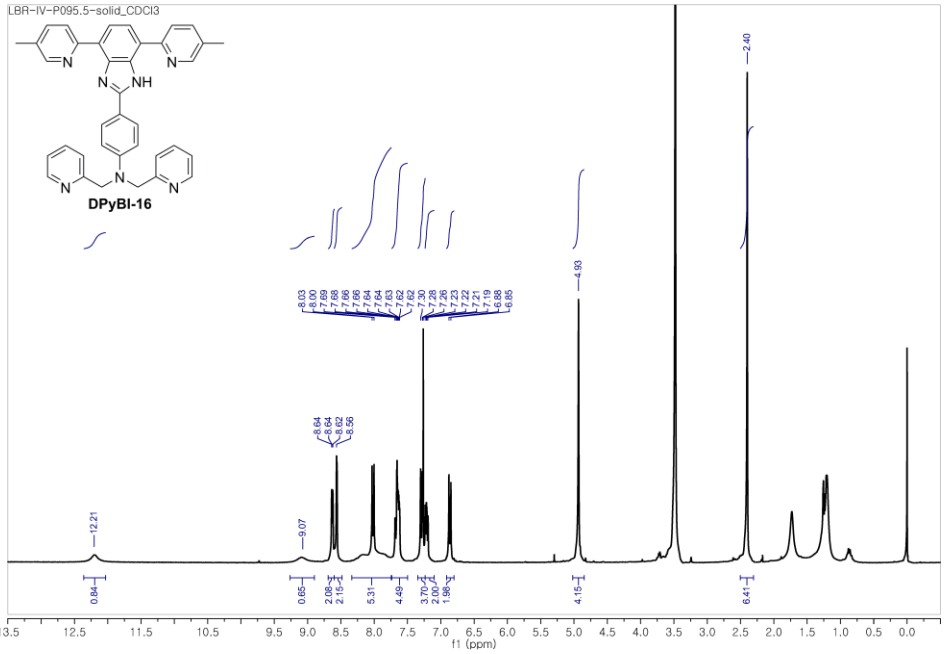
LBR-IV-P095.5-solid_CDCl3
DPyBI-16
f1 (ppm)

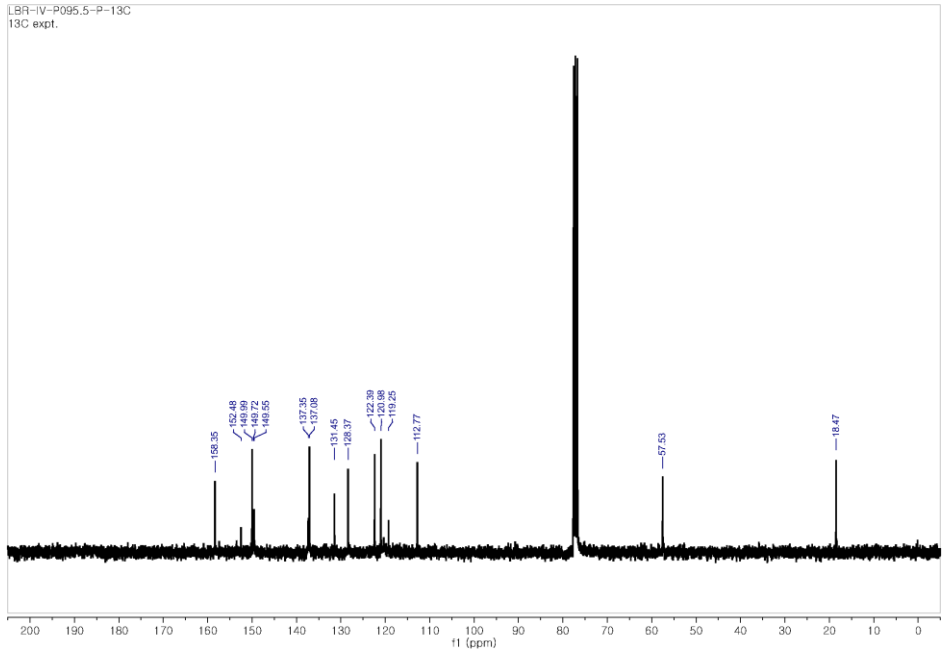
LBR-IV-P095.5-P-13C
13C expt.
158.35
152.48
149.99
149.72
149.55
137.45
137.08
131.45
128.37
122.39
120.98
119.25
112.77
57.53
18.47
f1 (ppm)

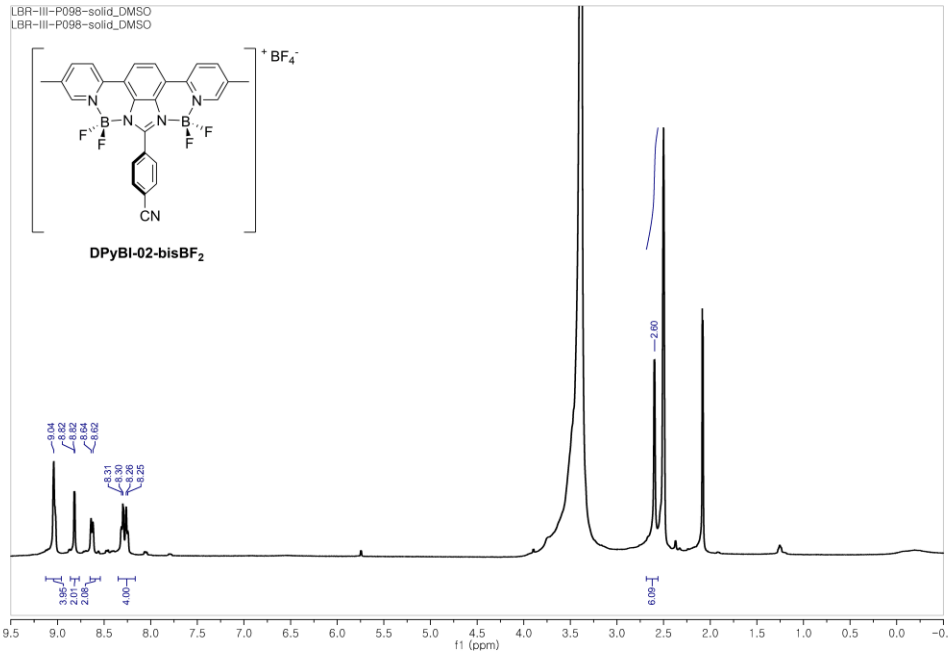
LBR-III-P098-solid_DMSO
LBR-III-P098-solid_DMSO
+ BF4-
CN
DPyBI-02-bisBF2
9.04
8.82
8.82
8.64
8.62
8.31
8.30
8.26
8.25
2.60
3.95
2.01
2.08
4.00
6.09
f1 (ppm)

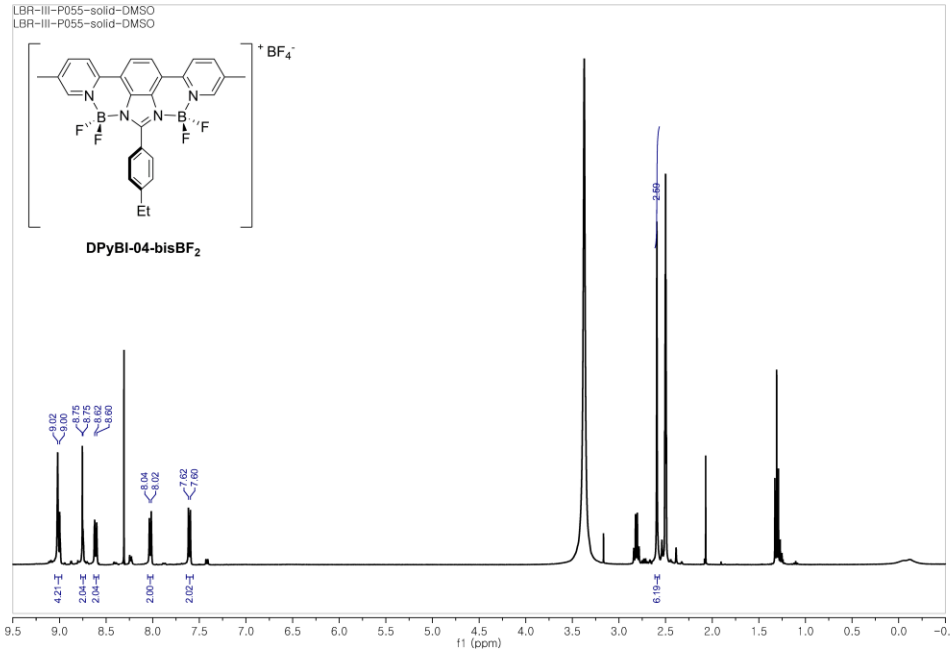
LBR-III-P055-solid-DMSO
LBR-III-P055-solid-DMSO
+ BF4-
F
B
N
N
B
F
F
F
Et
DPyBI-04-bisBF2
9.02
9.00
8.75
8.73
8.62
8.60
8.04
8.02
7.62
7.60
2.69
4.21
2.04
2.04
2.00
2.02
6.19
f1 (ppm)

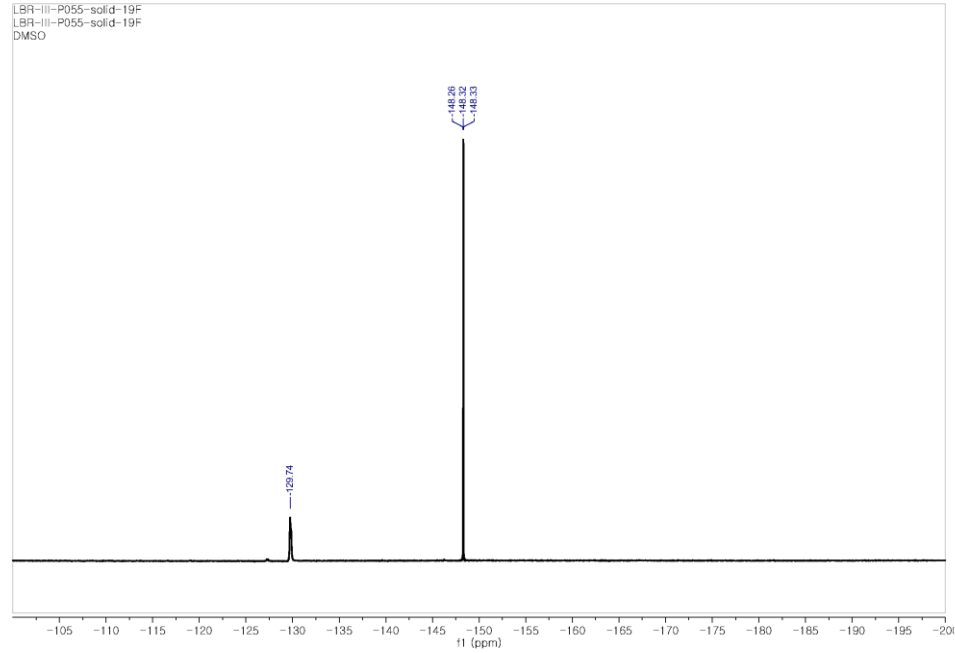
LBR-III-P055-solid-19F
LBR-III-P055-solid-19F
DMSO
-129.74
-148.26
-148.32
-148.33
f1 (ppm)

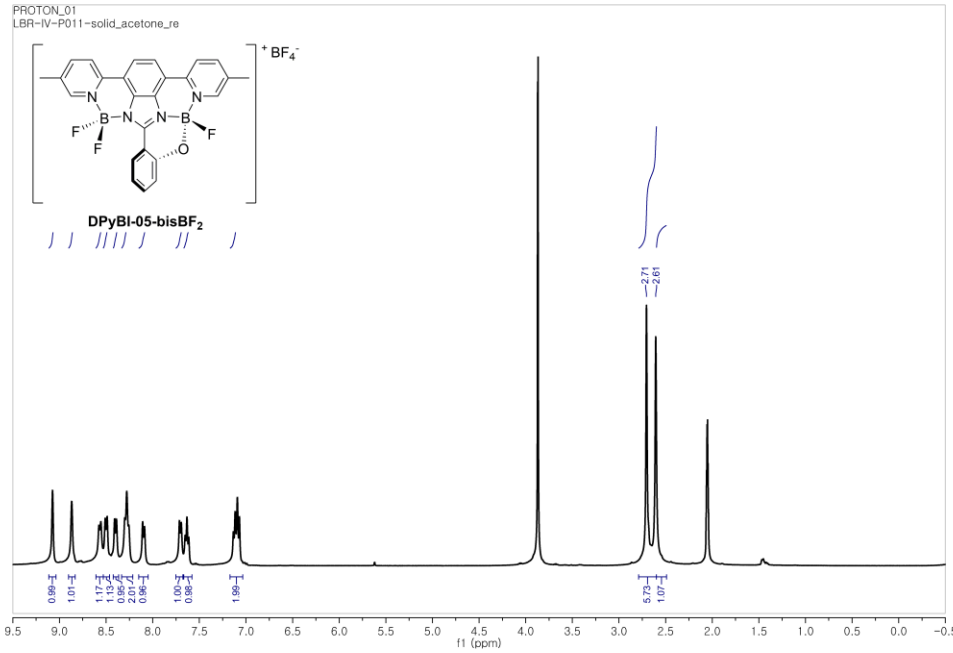
PROTON_01
LBR-IV-P011-solid_acetone_re
+ BF4-
DPyBI-05-bisBF2
2.71
2.61
0.99
1.01
1.17
1.15
0.95
2.01
0.96
1.00
0.98
1.99
5.73
1.07
f1 (ppm)

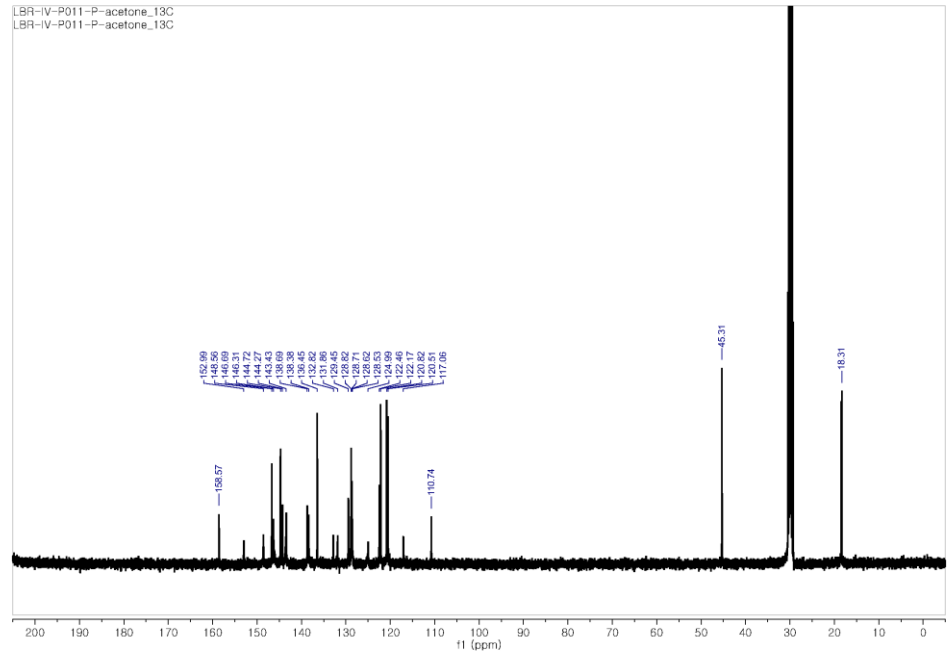
LBR-IV-P011-P-acetone_13C
LBR-IV-P011-P-acetone_13C
152.99
148.56
148.69
146.51
144.72
144.27
143.43
139.69
138.98
136.45
132.82
131.86
129.45
128.82
128.71
128.62
128.53
124.99
122.46
122.17
120.82
120.51
117.06
158.57
110.74
45.31
18.31
f1 (ppm)

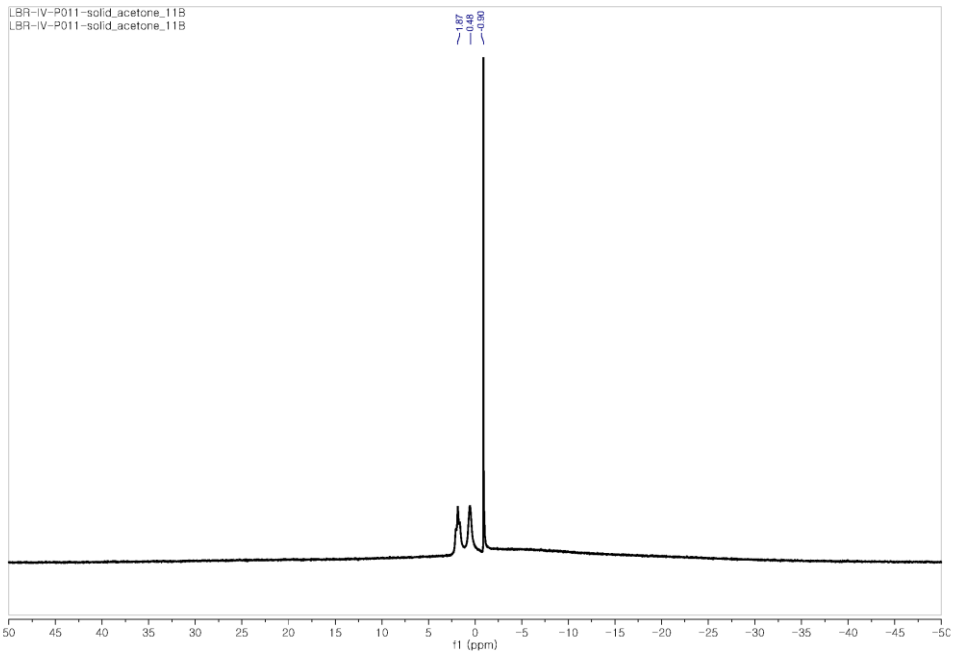
LBR-IV-P011-solid_acetone_11B
LBR-IV-P011-solid_acetone_11B
0.87
0.48
0.00
f1 (ppm)

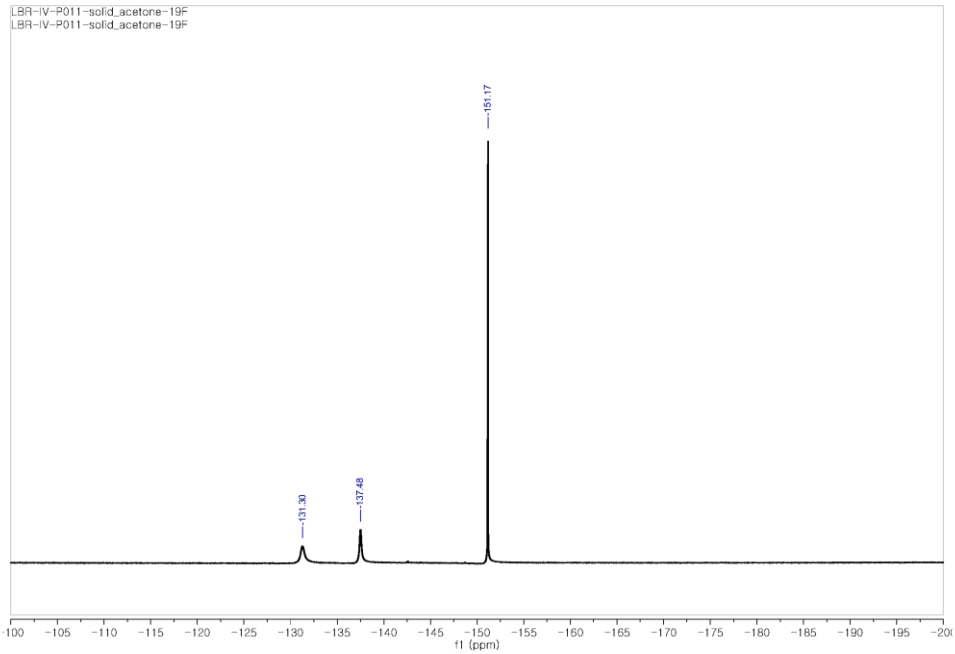
LBR-IV-P011-solid_acetone-19F
LBR-IV-P011-solid_acetone-19F
-131.30
-137.48
-151.17
f1 (ppm)

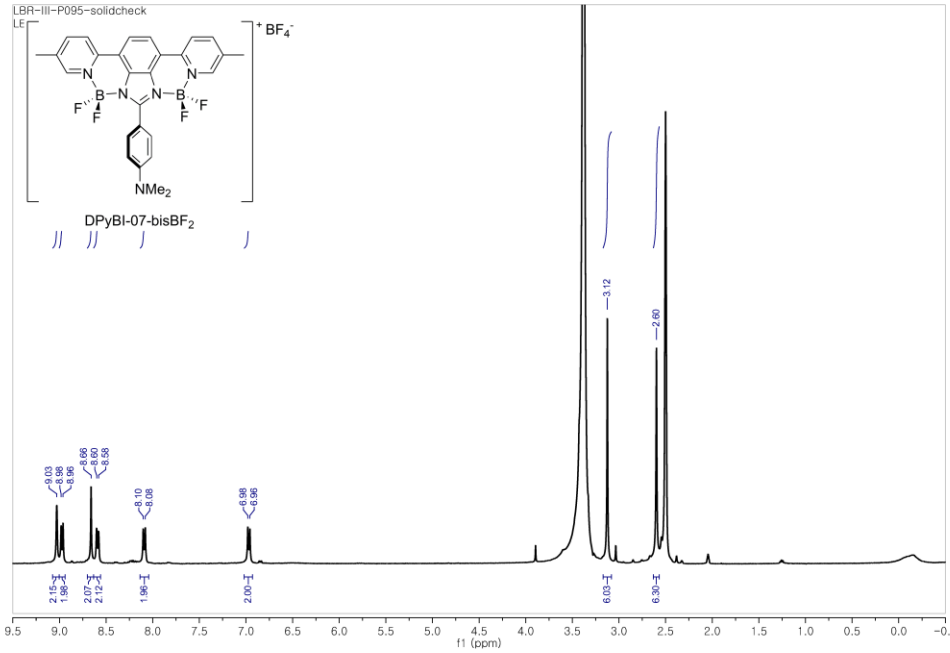
LBR-III-P095-solidcheck
DPyBI-07-bisBF2
3.12
2.60
9.03
8.98
8.96
8.66
8.60
8.59
8.10
8.08
6.98
6.96
2.15
1.98
2.07
2.12
1.96
2.00
6.03
6.30
f1 (ppm)

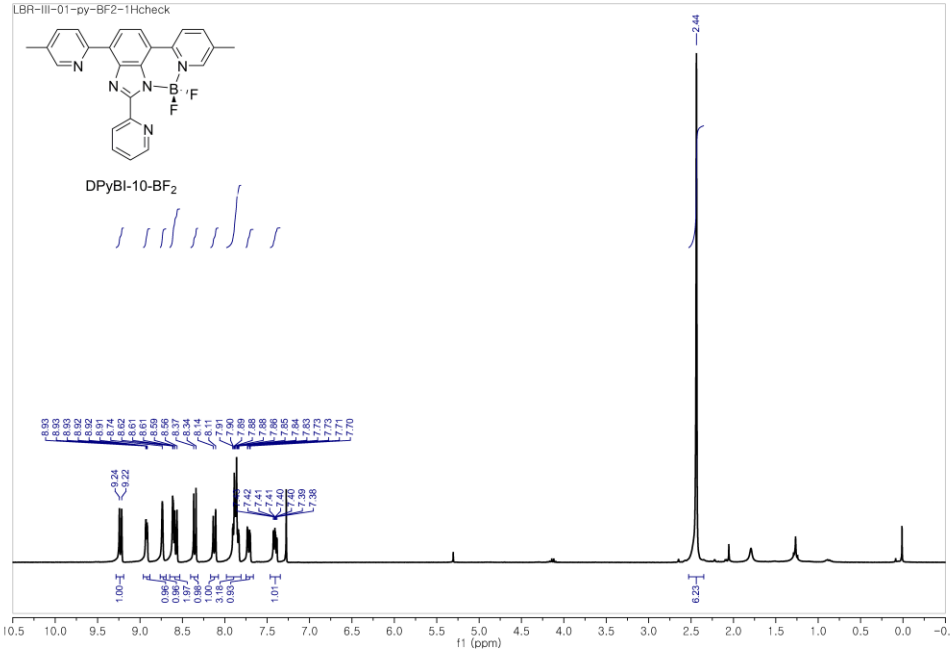
LBR-III-01-py-BF2-1Hcheck
DPyBI-10-BF2
2.44
9.24
9.22
7.42
7.41
7.40
7.39
7.38
1.00
6.23
f1 (ppm)

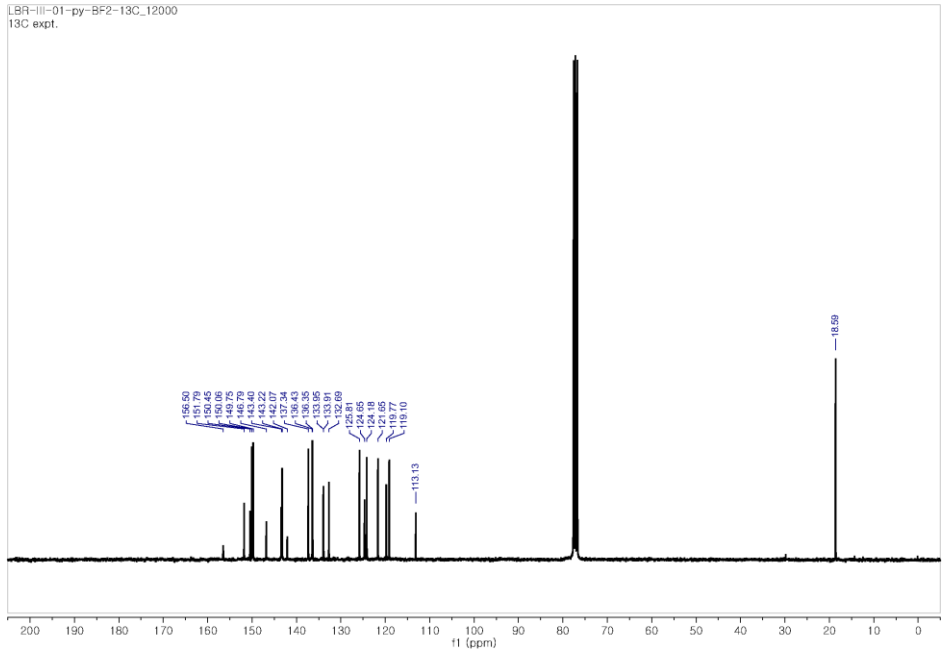
LBR-III-01-py-BF2-13C_12000
13C expt.
156.50
151.79
150.45
149.66
149.25
146.79
143.40
143.22
142.07
137.34
136.43
136.35
135.65
133.91
132.69
125.81
124.65
124.18
121.65
119.77
119.10
113.13
18.59
f1 (ppm)

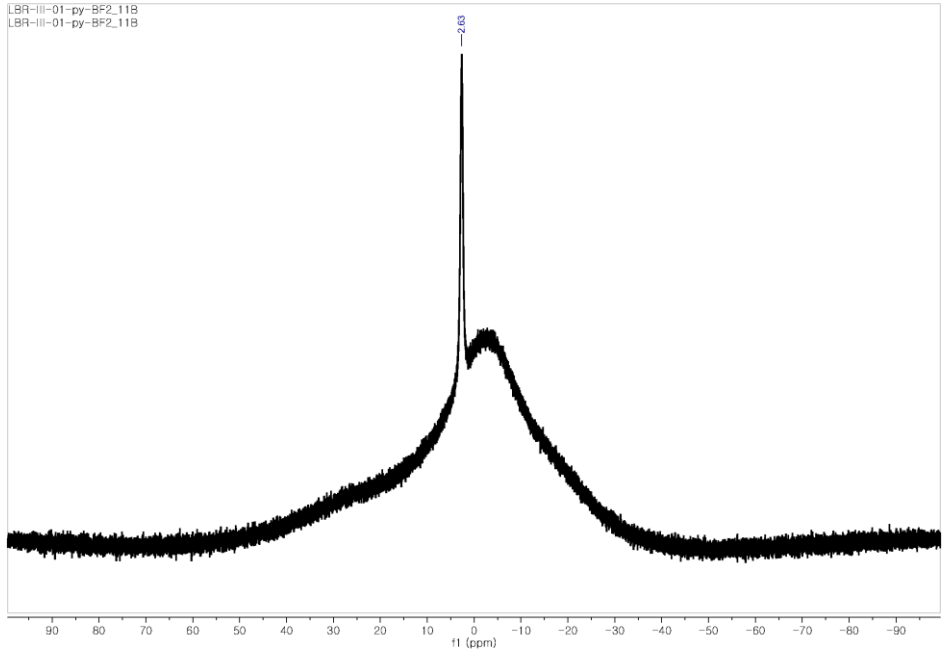
LBR-III-01-py-BF2_11B
LBR-III-01-py-BF2_11B
2.63
f1 (ppm)

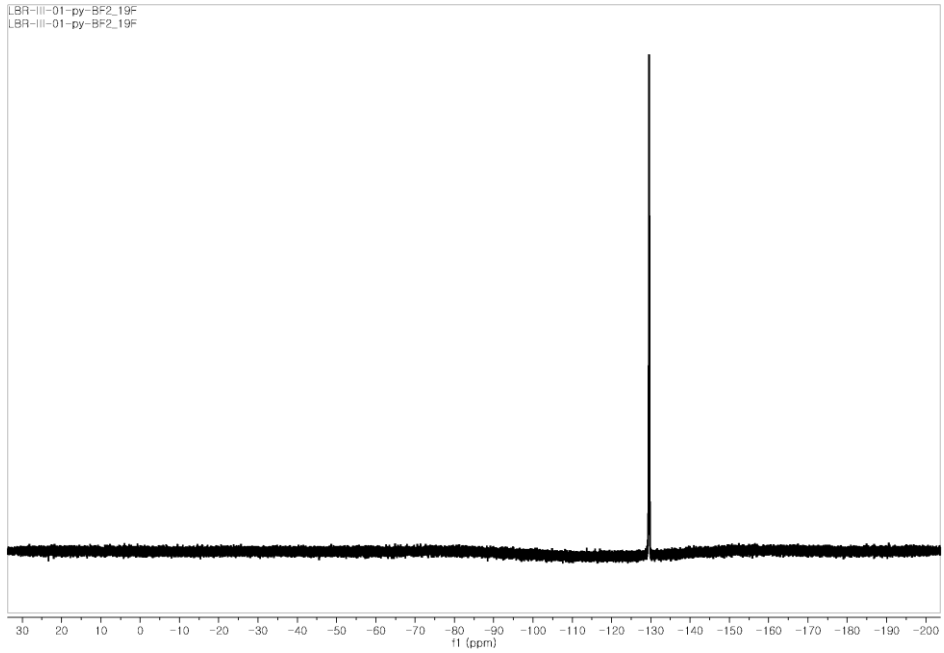
LBR-III-01-py-BF2_19F
LBR-III-01-py-BF2_19F
30 20 10 0 -10 -20 -30 -40 -50 -60 -70 -80 -90 -100 -110 -120 -130 -140 -150 -160 -170 -180 -190 -200
f1 (ppm)

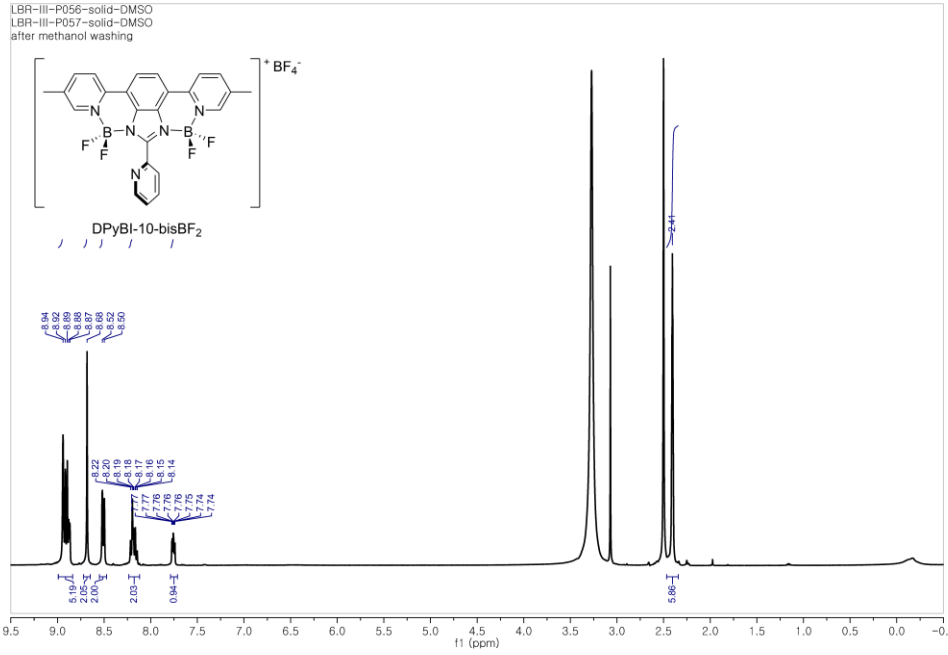
LBR-III-P056-solid-DMSO
LBR-III-P057-solid-DMSO
after methanol washing
+ BF4-
DPyBI-10-bisBF2
8.94
8.92
8.89
8.89
8.88
8.87
8.68
8.52
8.50
8.22
8.20
8.19
8.18
8.17
8.16
8.15
8.14
7.77
7.77
7.76
7.76
7.75
7.74
7.74
2.41
5.19
2.05
2.00
2.03
0.94
5.66
9.5 9.0 8.5 8.0 7.5 7.0 6.5 6.0 5.5 5.0 4.5 4.0 3.5 3.0 2.5 2.0 1.5 1.0 0.5 0.0
f1 (ppm)

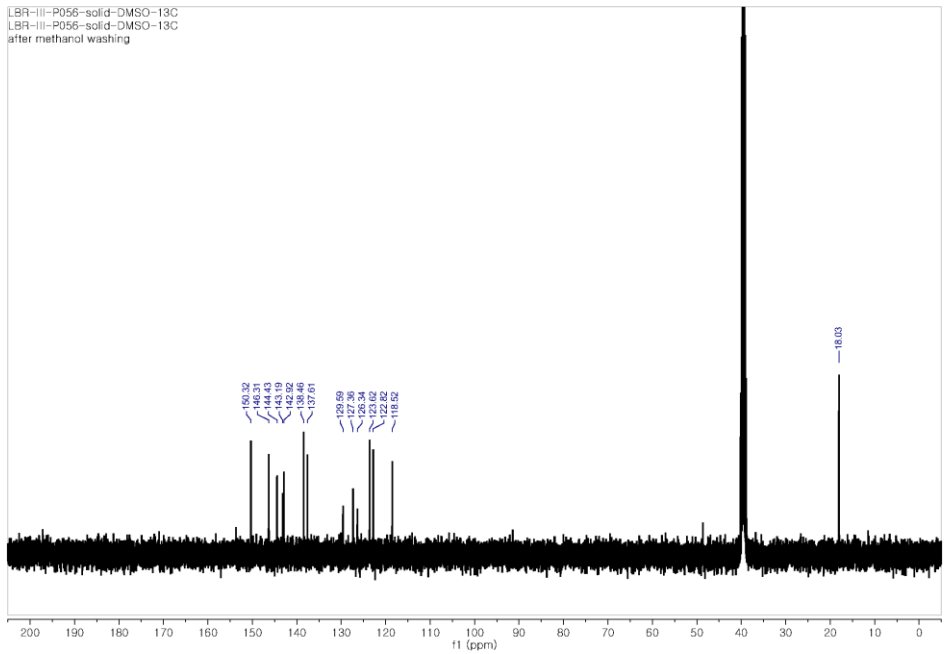
LBR-III-P056-solid-DMSO-13C
LBR-III-P056-solid-DMSO-13C
after methanol washing
160.32
146.31
144.43
143.19
142.92
138.46
137.61
129.59
127.36
126.34
123.62
122.82
118.52
18.03
f1 (ppm)

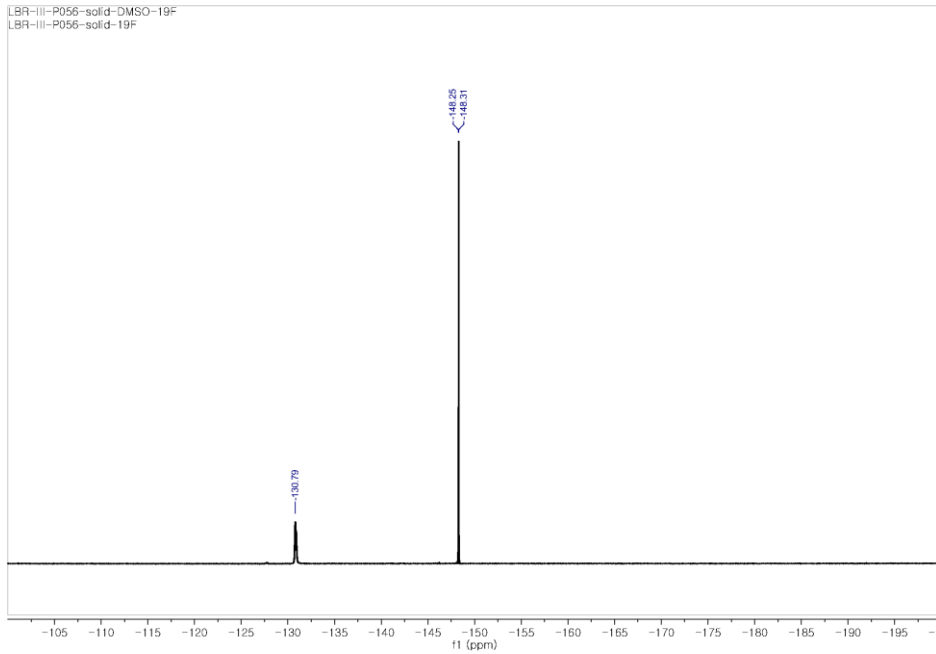
LBR-III-P056-solid-DMSO-19F
LBR-III-P056-solid-19F
-148.25
-148.31
-130.79
f1 (ppm)

Design and Synthesis of New Benzimidazole-Based Fluorophores: Tunable Emission over a Wide Spectral Range in Solution and Solid States

용액과 고체상에서 다양한 범위의 발광성을 갖는 벤지미다졸 기반 형광체의 설계와 합성

국문 초록

다양한 범위의 발광성을 갖고 고체 형광을 띄는 벤지미다졸 기반 형광체를 합성하였다. 형광 물질은 빛을 발하고 신호를 변환하는 물질로써 재료와 생리학 등 다양한 분야에서 사용되어 왔다. 그러므로 발광 특성과 물리적 특성을 조절할 수 있는 형광체를 개발하려는 연구가 많이 시도되었다. 이번 연구에서는 T 자 모양을 갖는 벤지미다졸 기반의 형광체를 설계 및 합성하였다. 이 시스템에서 벤지미다졸 중심부는 두 개의 π-시스템과 연결되어 있다. 하나의 π-시스템은 BF_2 단위체가 순차적으로 도입될 수 있는 두 개의 결합 부위를 갖고 있으며, 다른 π-시스템은 전자적인 성질을 조절하는 역할을 한다. 이 부분의 변화는 발광 파장과 형광 수율에 큰 영향을 미쳤다. 또한 이러한 변화들은 합성의 가장 마지막 단계에 일어나도록 고안되었기 때문에, 공통된 합성 중간체로부터 다양한 형광체를 쉽게 만들 수 있었다. 또한 이렇게 얻어진 물질들은 전체 가시광선 영역을 포함하는 넓은 범위의 발광 파장을 갖고 있음을 확인하였다. 또한 이들 중 대부분은 고체상태에서도 형광이 나와, OLED 와 같은 EL 소자에 응용될 가능성을 보였다. 이러한 시스템의

형광물질들은 합성의 용이함, 조절 가능한 발광 성질, 고체 형광과 같은 흥미로운 성질들 때문에 화학 센서와 전자 발광 소자와 같이 다양한 분야에 응용될 수 있을 것으로 기대된다.

핵심어: 형광을 보이는 벤지미다졸 유도체 • 조절 가능한 형광 특성 • 넓은 범위의 파장대 • 모듈 식의 합성법 • 구조–성질 관계 • 고체 형광

학 번: 2014-20309